Ultrathin 2D-oxides: A perspective on fabrication, structure, defect, transport, electron, and phonon properties

Santosh Kumar Radha, Kyle Crowley, Brian Holler, Xuan Gao, Walter Lambrecht, Halyna Volkova, Marie-Hélène Berger, Emily Pentzer, Kevin Pachuta, Alp Sehirlioglu

Ultrathin 2D-oxides: a perspective on fabrication, structure, defect, transport, electron and phonon properties

Santosh Kumar Radha, Kyle Crowley, Brian A. Holler, Xuan P. A. Gao, Walter R. L. Lambrecht
Department of Physics, Case Western Reserve University, 10900 Euclid Avenue, Cleveland, OH-44106-7079

Halyna Volkova, Marie-Hélène Berger
MINES Paris, PSL University, Centre des Matériaux, CNRS UMR 7633, BP 87 91003 Evry Cedex, France

Emily Pentzer
Texas A&M University, College Station, TX 77843-3003

Kevin G. Pachuta and Alp Sehirlioglu*
Department of Materials Science and Engineering, Case Western Reserve University, 10900 Euclid Avenue, Cleveland, OH-44106-7204

In the field of atomically thin 2D materials, oxides are relatively unexplored in spite of the large number of layered oxide structures amenable to exfoliation. There is an increasing interest in ultrathin film oxide nanostructures from applied points of view. In this perspective paper, recent progress in understanding the fundamental properties of 2D oxides is discussed. Two families of 2D oxides are considered: (1) van der Waals bonded layered materials in which the transition metal is in its highest valence state (represented by V_2O_5 and MoO_3) and (2) layered materials with ionic bonding between positive alkali cation layers and negatively charged transition metal oxide layers ($LiCoO_2$). The chemical exfoliation process and its combinaton with mechanical exfoliation are presented for the latter. Structural phase stability of the resulting nanoflakes, the role of cation size and the importance of defects in oxides are discussed. Effects of two-dimensionality on phonons, electronic band structures and electronic screening are placed in the context of what is known on other 2D materials, such as transition metal dichalcogenides. Electronic structure is discussed at the level of many-body-perturbation theory using the quasiparticle self-consistent *GW* method, the accuracy of which is critically evaluated including effects of electron-hole interactions on screening and electron-phonon coupling. The predicted occurence of a two-dimensional electron gas on Li covered surfaces of $LiCoO_2$ and its relation to topological aspects of the band structure and bonding is presented as an example of the essential role of the surface in ultrathin materials. Finally, some case studies of the electronic transport and the use of these oxides in nanoscale field effect transistors are presented.

I. INTRODUCTION: WHY 2D OXIDES?

In the rapidly growing "Flatland" [1] of 2D atomically thin materials, oxides are still newcomers. After the Nobel prize was awarded to Novoselov and Geim for the discovery of the remarkable properties of graphene,[2] several new elemental 2D materials have been studied: black phosphoros,[3] antimonene and arsenene,[4, 5] germanene and silicene[6]. Transition metal dichalcogenides (TMDC) rapidly gained interests because of their remarkable valleytronic properties[7] and the presence of a gap allowing field effect transistors[8] to be fabricated to make use of the high-mobilities encountered in 2D materials. But in spite of the large number of oxides that occur in layered crystal structures and thus might be promising candidates for exfoliation, 2D oxides have not yet been widely studied, especially from the point of view of their fundamental properties and prospects for electronic devices. Oxides constitute a broad family of materials with a wide range of potential applications, from catalysis to electronic, photonic, ferroelectric, magnetic and multiferroic functionalities. Understanding structure-property relations in free-standing, supported, and confined two-dimensional ceramics or "ceramic flatlands" has been identified as one of the challenges for future work in ceramics by a recent National Science Foundation workshop.[9]

Nonetheless, over the last decade, there have been many reviews on 2D oxides either as the main focus or as a part of a more general nano-materials focused review papers or books. One of the earlier reviews of nanosheets of oxides and hydroxides focused on synthesis, properties – especially photon-induced behavior - and their assembly, was published in 2010 by Ma *et al.* [11], followed by a second review [12] as a part of a special issue on "2D Nanomaterials beyond Graphene" in 2015. Around the same time (2011) another review by Mas-Balleste *et al.* [13] also emphasized the importance and variety of 2D oxides. A more recent focused review on 2D oxides can be found in 2019 paper of Hinterding *et al.* [14] in-

* Corresponding author: alp.sehirlioglu@case.edu

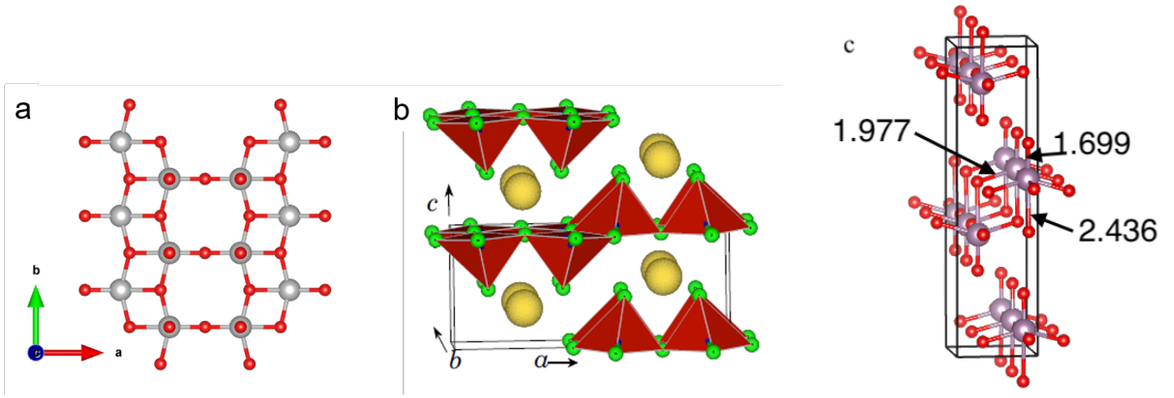

Fig. 1: a) 2D projection of V_2O_5 structure, showing the zig-zag chains within the layer, b) Side view of NaV_2O_5, showing the layered structure and the location of intercalating alkali atoms (yellow) in the corresponding bronzes, reproduced from Phys. Rev. B **92**, 125133 (2015), Copyright 2015 American Physical Society; c) Double layer structure of α-MoO_3 showing some of the Mo-O bond lengths in Å.

troducing compositions, synthesis, microstructures and applications and in a 2018 paper of Uppuluri *et al.* [15] specifically related to the soft-chemistry of exfoliation. In 2012, different morphologies of nanosheets were reviewed for Li ion storage by Liu *et al.* [16], summarizing nanoporous, sandwich-like, wave-like, flower-like nanosheets etc. Use of 2D-oxides as dielectric building blocks was reviewed by Osada *et al.* [17] in 2012. The review of liquid exfoliation of layered materials by Nicolosi *et al.* in 2013 while not focusing on oxides, included examples of exfoliation of oxides to form nanosheets.[18] A perspective on use of 2D nanosheets in hybrid systems, including oxides, was published in 2014 by Kim *et al.* [19] and was reviewed by Lee *et al.* in 2018[20]. Another review especially focused on variety of applications was published by Kalantar-zadeh[21]. Other reviews and sections of books that introduce processing, and energy conversion and storage have been published over the years by ten Elshof *et al.* [22], Tan *et al.* [23], Xiong *et al.* [24], Mahmood *et al.* [25] and Pang *et al.* [26]. There has also been a lot of recent focus on the catalytic and environmental applications as reviewed by Haque *et al.* [27], Heard *et al.* [28], Zhang *et al.* [29], Safarpour *et al.* [30]. Other applications of interest include sensors as reviewed by Shavanova *et al.* [31], Lee *et al.* [20], Dral and ten Elshhof[32]. While not specifically on oxides, as a part of the review of 2D nanomaterials some information can also be found in the review papers by Tan *et al.* [23], Jo *et al.* [33], and Yang *et al.* [34] Besides exfoliation, either mechanical or chemical, other routes to formation of 2D ultrathin films or few-layer systems have been explored using atomic layer deposition (ALD), and so on. An overview of 2D-oxdide synthesis methods and studies was recently reviewed by Yang *et al.* .[35]. Yang *et al.* [36] studied the formation of 2D oxide nanosheets of CoO with nanoparticles as intermediate step. Xiao *et al.* reviewed layered cathode oxide materials for Na based battery materials. [37] Barcaro *et al.* focused on ultrathin oxide layers grown on top of metals and their structural motifs.[38]

From the above brief overview of the review literature it is clear that most papers had an application oriented perspective. In the present perspective paper we take mostly a fundamental science point of view on the exfoliation process, the phase stability of 2D oxide nanosheets, their vibrational and electronic properties that distinguish them from their bulk layered parent materials and how the above affect their electrical transport.

While a layered structure is a good starting point for fabricating 2D-oxides, the nature of the interlayer bonding is crucial for the success of exfoliating. Two important classes of oxides can be distinguished. Oxides like V_2O_5, MoO_3 have layered crystals structures in which the layers are neutral and the interlayer interactions are weak dispersive van der Waals interactions. In these oxides, typically the transition metal is in its highest valence state and perfectly balances the oxygen ion charges. V_2O_5 has an additional interest in that 1D-chains occur inside the layers and endow the material with properties in between 1D and 2D. This is illustrated in Fig. 1. As will be detailed in Sec. VIII A 1, this leads to a high degree of in-plane anisotropy in electronic transport[39]. Successful mechanical exfoliation using the "scotch-tape" method has recently been accomplished and led to a start of the exploration of this compound in 2D form. More recently chemical exfolation as also been reported in literature and has led to atomicall thin bilayers. [40]

Orthorhombic α-MoO_3 [41] also has double layer character with oxygens bonded to a single Mo sticking out from the double layer on either side and leading to weak interlayer interactions. See Fig. 1c. However, as the distance between layers is increased, for example by inserting H_2O molecules, its properties can be modified.[41] A monoclinic form is known in which the layers are just slided slightly over each other laterally compared to the

orthorhombic form and this gives an indication that the properties could be modulated by subtle changes in the interlayer interactons. Ultrathin layers of MoO_3 have been successfully exfoliated and high mobilities have been reported by some authors.[42]

The properties of these layered materials, which in their pure form are fairly wide gap insulators, are strongly modified by defects, such as oxygen vacancies[43–45] or by intercalation with alkali or alkaline earth atoms. This leads essentially to doping of the lowest conduction bands of the insulator with electrons and turns them into n-doped semiconductors. However, this also forms the basis for novel magnetic properties. In particular in V_2O_5 intercalation with Na in the exact ratio of 1:1 forms the new compound NaV_2O_5 which is antiferromagnetic.[46] The structure of NaV_2O_5 is shown in Fig. 1b. This is because α-V_2O_5 has a narrow split-off conduction band separated from the higher conduction bands by a small gap, which becomes half-filled when doped with one Na per V_2O_5 unit.[47] This leads to the formation of a magnetic moment, splitting the band in up and down spin, and subsequently an antiferromagnetic coupling between moments along the direction of the 1D chains. Besides this antiferromagnetic structure, another phase transition, originally described as a spin-Peierls transition occurs at low temperature but may in fact, be a combination of charge disproportionation and spin-Peierls transition.[48] This system received a lot of attention in bulk form but ultrathin or monolayer thick variants of it could offer a much finer control of the Na or other intercalation content to further control and manipulate these interesting magnetic phase transitions. The intercalated forms of both V_2O_5 and MoO_3 are known as bronzes.[49, 50] These materials have multiple applications in the field of catalysis, are potential hosts for ions such as Li[51, 52] and Mg[53] in battery applications and are also electrochromic.[54] Their color and optical properties can be modified by an applied voltage.

In this perspective paper, we will use both MoO_3 and V_2O_5 as representative examples of these van der Waals bonded oxides. Their mechanical exfolation by means of the Scotch-tape method is fairly standard and does not require further discussion. We compare their phonon properties and how they are influenced by the monolayering in Sec. VI. The electronic band structure of these oxides is relatively well understood at the density functional theory level but surprisingly, many-body-theory perturbation theory such as the *GW* method which should describe their electronic structure even more accurately tends to overestimate the gaps. This is an impediment to address the change in gap in their monolayer forms because *GW* self-energy effects are known to have long-range effects in 2D materials. We discuss our progress in this respect in Sec. VII. Their transport properties are discussed in Sec. VIII.

On the other hand, many more oxides are essentially a layered arrangement of different cations in a close packed oxygen lattice, one of them a transition metal and the other a highly electropositive ion such as alkaline ions, Li, Na, K. In these materials, the nature of the bonding is such that the alkali atom donates its electron to the transition metal oxide layer. We then have electrostatic bonding between negative transition metal oxide layers and the positive Li ion layer. The prototypical examples of this type of bonding are $LiCoO_2$ and $NaCoO_2$. The former is the other main material discussed in this perspective paper. Exfoliation of these materials is not as straightforward but has recently become possible exploiting chemical ion replacement reactions. These are described in some detail in Sec. II. The stability of the resulting nanoflake materials under annealing is discussed in Sec. III. A combination of chemical and mechanical exfolation provides a promising route toward large area 2D mono or few layer thin forms of these materials.[55, 56] An important question that is not yet fully answered is how much residual compensation by alkali ions remains in operation and how it modifies the $LiCoxO_2$ nanosheet properties. In $LiCoO_2$, the additional electron supplied by the Li is precisely what is needed to give the Co a Co^{3+} formal valence state with a d^6 configuration which is stabilized by filling the lower energy t_{2g} bands in an octahedral environment leading to a low spin stable state. This illustrates the subtle interplay between structure and electronic configuration. Removing part of the Li however, now leads initially to a p-type semiconductor but with potential Co^{4+} localized ions if the Li-vacancies are ordered. The magnetic moments of this d^5 configuration now come also into play.

The extreme case of CoO_2 layers is potentially a highly interesting systems because the triangular lattice of Co spins is then highly frustrated and has been speculated to be a candidate for the elusive spin-liquid state. [57, 58] Remarkably, superconductivity has been claimed to occur in CoO_2 layers,[59] not in isolated exfoliated form, but when the layers are spaced by inserting a sufficient amount of water molecules inside the Na layer of Na_xCoO_2. To what extent such a complex system represents isolated 2D behavior of CoO_2 is not clear. However, while this provides a strong motivation to pursue exfoliation of this system, we are still a long way from perfect control over this form of CoO_2. Numerous open questions start to emerge from the exfoliation experiments carried out by our group. How much remaining Li or other alkali ions remain attached to the layers as a result of the chemical exfoliation and repricipitation route? How do they influence the properties? How stable are the layers toward annealing treatments, which may be required to make electrical contact to them? Furthermore, how are the very surfaces of CoO_2 covered with Li different from the bulk. Our initial findings on these questions are discussed in later sections. We discuss the effect of cation size on layered oxides of the $LiCoO_2$ type with different cations replacing Li in Sec. V as a way to increase the distance between the layers and approach monolayer physics. We also include H in this study because of its role in the exfoliation process. We return to the band

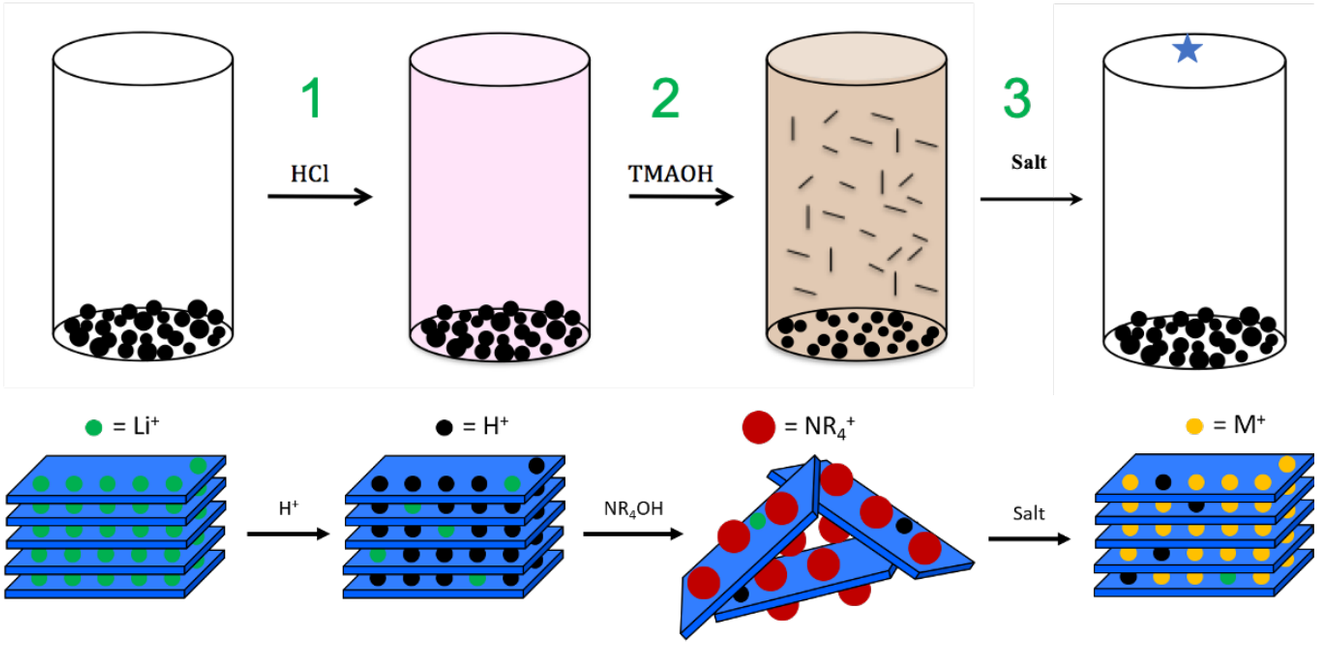

Fig. 2: Steps of chemical exfoliation of CoO_2 nanosheets.

structure of $LiCoO_2$ in Sec. VII in the context of how *GW* theory applies to it and how we currently understand its optical properties. The surprising prediction of a surface two-dimensional gas (2DEG) on $LiCoO_2$ Li terminated nanostructures is discussed in Sec. VII B and its transport properties are presented in Sec. VIII along with those of MoO_3 and V_2O_5.

II. CHEMICAL EXFOLIATION OF Li_xCoO_2 NANOSIZE FLAKES

The exfoliation of layered transition metal oxides (TMOs) has been relatively well studied, dating back to the 1990s and 2000s beginning with the exfoliation of layered titanates and manganates.[60, 61] Since then, several layered TMOs have been exfoliated using a soft-chemical exfoliation method.[11] It was not until 2009 that the exfoliation of lithium cobalt oxide (LCO) was first reported (Kim *et al.* [62]). Since then only a few groups have reported further on this topic[55, 56, 62–72] (many coming from our research group[55, 56, 63–65] leaving the exfoliation of LCO relatively underexplored.

This soft-chemical exfoliation method can be described as a two-step acid-base reaction which swells and exfoliates layered TMOs to form two-dimensional TMO nanosheets which can eventually also be reprecipitated. See Fig 2. First, the layered transition metal oxide is treated with a protic acid to replace the alkali metal ions with protons in the interlayer. Second, this protic powder is subsequently reacted with a hydroxide bearing bulky molecule (e.g. tetramethylammonium hydroxide (TMAOH), tetrabutylammonium hydroxide (TBAOH)) to swell and exfoliate the layered structure into two-dimensional transition metal oxide nanosheets. While this method can be generalized for numerous layered TMOs, many factors that promote exfoliation are inherent to the properties of the layered TMO in combination with each subsequent chemical treatment that is utilized. In consequence, it is important to investigate and understand the material at each stage of the exfoliation process.

In the case of the exfoliation of LCO, reaction with protic acid solutions differ when compared to other more well-studied transition metal oxides.[64] For instance, many layered TMOs can undergo complete alkali metal extraction and proton replacement while others, such as LCO, cannot.[62, 64, 65, 73] In other words, alkali metal and proton concentrations in the powder vary depending on the protic acid treatment applied (e.g. acid composition, reaction duration, acid concentration, solution refreshment). Moreover, when LCO is treated with high acid concentration solutions (e.g. 12 M hydrochloric acid), the powder completely dissolves into ionic species. This instability is also reported at lower concentrations (e.g. 0.1 M HCl – 3 M HCl) and plays a role in changing LCOs surface morphology, stoichiometry, cobalt and oxygen valence, and defect concentration. Due to the varying effect acid treatments have on LCO, exfoliation using a bulky hydroxide-bearing molecule (i.e. NR_4OH, where R = Methyl, Ethyl, Butyl) can have mixed results.[65] For example, the concentration of NR_4OH needed to promote the highest degree of exfoliation has been demonstrated to be dependent on acid treatment conditions. Furthermore, the degree to which exfoliation occurs is dependent on the ionic radius of the swelling molecule, with

TMAOH proving most effective. While several factors can affect the swelling and exfoliation behavior of LCO, the most important of one is proton concentration in protic LCO. If this can be effectively quantified, the swelling and exfoliation behaviors of LCO can be understood as well as other layered TMOs.

Along with the traditional soft-chemical exfoliation of LCO, other exfoliation and dispersion methods have been developed to more effectively utilize cobalt oxide nanosheets. These methods were created to avoid the destructive nature of the reagent required to promote exfoliation, TMAOH, which is highly caustic, a known etchant and developer of photoresist limiting the main applications of cobalt oxide nanosheets to electrophoretic deposition.[62] First, excess TMAOH can be removed from solution, through a solvent exchange after isolating cobalt oxide nanosheets from solution using high-speed centrifugation. The nanosheets can then be redispersed in water or another compatible solvent allowing for their use in non-aqueous applications. Second, cobalt oxide nanosheets can be precipitated/restacked from solution using salts. This opens the door, in effect, to synthesize oxide materials that are thermodynamically metastable (e.g. M_xCoO_2, where M is K, Ca, Al, etc. and found in the interstice of the layered structure). Finally, large and ultrathin cobalt oxide nanosheets in pH neutral solutions can be produced through washing the larger semi-exfoliated LCO particles (which are typically discarded as waste) initially isolated via low-speed centrifugation. These methods have allowed for a more versatile platform of the use of cobalt oxide nanosheets.

Although not statistically robust since the characterization is done using atomic force microscopy (AFM) and transmission electron microscopy (TEM), the cobalt oxide nanosheets produced using traditional exfoliation method have been demostrated to be a maximum of 0.4 μm$\times$0.4 μm in lateral size.[62, 67, 71, 72] Moreover, there is little to no detail on the structure and properties of these cobalt oxide nanosheets making the process of modeling and understanding their fundamental properties a difficult task. New exfoliation methods have increased the size of cobalt oxide nanosheets and have allowed for advanced microscopic and electrical measurements to be performed advancing our knowledge of the structure and stability of these materials.[55, 56]

III. STRUCTURAL PROPERTIES AND PHASE CHANGES UPON ANNEALING

From the many years long interest in Li_xCoO_2 as a battery material, it is well known that variations in Li content play an important role.[74–76] As the system is delithiated, at special simple fractional concentratons of Li vacancies, such as $x = 1/3$, $x = 1/2$, $x = 2/3$ ordering of the vacancies may occur.[77] Also besides the layered $R\bar{3}m$ structure other forms of $LiCoO_2$ with a disordered or partially disordered arrangement of the Li and

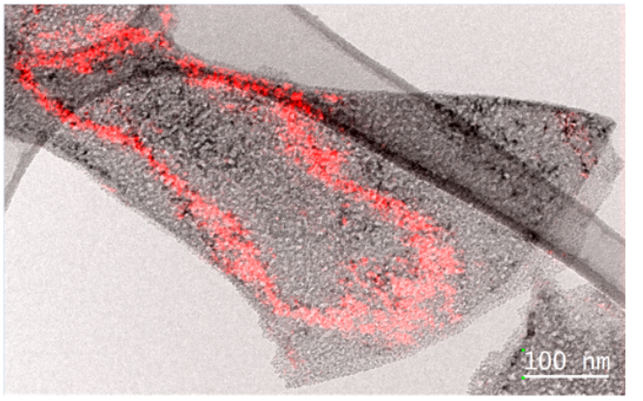

Fig. 3: Superposition of bright (grey) and dark field image (red) of a strong 220 diffraction peak characteristic of the rocksalt domains of a $LiCoO_2$ nanoflake after annearling to 350°C showing that rocksalt domains occur primarily at the rim of the flake.

Co atoms are known to occur at higher temperatures due to interdiffusion of the layers. A spinel type structure occurs with both Li and Co in octahedral sites while the tetrahedral sites can stay empty [78, 79] and a fully disordered rocksalt structure in which Li and Co randomly occupy octahedral sites has also been reported.

An important open question is to what extent the $R\bar{3}m$ structure is stable in ultrathin nanosheets as function of temperature and Li composition. A detailed electron microscopy study was recently reported by our group for Li_xCoO_2 nanosheets with $x \approx 0.37$ obtained by the chemical exfoliation route explained in Sec. II and as function of annealing temperature.[56] The important findings are that as function of increasing temperature, a gradual disordering of the Li and Co atoms occurs. Initially the structure of these nanosheets was found to consist of a mixture of $R\bar{3}m$ and $C2/m$ regions where the latter corresponds to a slight distortion of the $R\bar{3}m$ structure related to the lower Li content. Above 200°C the $P2/m$ structure related diffraction spots became evident and this indicates that around this temperature an ordering of the Li vacancies is facilitated. At even higher temperature of 250°C the spinel-type structure starts to appear, indicative of disordering of Li and Co from their layered arrangement. Eventually above 350°C, a fully disordered rocksalt structure was found.

The accompanying changes in electronic properties were investigated via electron loss spectroscopy in various energy ranges, the O-K edge, the Co-L_2/L_3 edges and the low energy interband transition range up to the plasmon energy range. These provide information on the degree of O-Co hybridization, the Co effective valence and so on. The results were interpreted with the help of first-principles simulations of these spectra. The main conclusions of this study were that in the first temperature increase, the O-2p-Co-3d hybridization is increasing but then drops precipitously as the more disordered

phases come into play. In fact, a more detailed analysis of the O-K spectra, indicated that the different shape of the spectrum at the highest temperatures could only be explained by the pure rocksalt CoO phase. This indicates a loss of Li from those regions. Subsequently, it was found that those regions were predominantly located at the edges of the nanoflake samples. This is documented here in Fig. 3. The bright domains in the dark field image taken from the strong 220 reflection locate the rocksalt domains, which are primarily found at the edges of the flake. This suggests a gradual transitions from spinel to disordered rocksalt by loss of Li from the edges of the flakes.

From the Co L_2/L_3 ratio it was concluded that the Co valence initially increased, indicative of formation of some Co^{4+} particularly near the Li-vacancies when these become ordered, but formation of Co^{2+} at the higher temperatures. The low energy loss spectra were found to be in good agreement with a direct calculation of the loss spectrum in the form of the imaginary part of the inverse of the dielectric function for small scattering vector $\mathbf{q}$ and also reproduced well the plasmon region. The lowest energy transitions near 2-3 eV correspond to transitions from the occupied t_{2g} to the empty e_g bands of Co-d electrons in their octahedral environment. The higher transitions, near 7 eV were found to come from transitions from deeper valence bands with a more dominant O-2p character to the same lowest conduction band rather than transitions from the top of the valence band to higher Co-4s or Li-2s like states, which, in fact, occur at significantly higher energy.

The changes in structure, in particular when forms of CoO with signficiant amounts of Co^{2+} are present were found to also be accompanied by a drop in conductivity. This seems reasonable because first of all disorder leads to increased scattering but secondly in those phases the low spin optimal filling of the Co-d bands for an octahedral environment are in competition with other electron configurations which carry a net magnetic moment and exhibit a strongly correlated electronic structure. In Ref. [56] this disordered paramagnetic state of CoO was modeled by means of a special quasirandom structure (SQS) model with random placement of up spin and down spin magnetic moments following the recently proposed polymorphous band structure approach [80] for such correlated systems and using the DFT+U approach. In essence this replaces the dynamic time dependent fluctuations of the spins by spatial fluctuations.

The important take-away message from this study is that at elevated temperatures, important structural changes can occur in nanoflakes, their structure does not remain uniform and significant deviations from the low spin $LiCoO_2$ band structure can occur.

IV. IMPORTANCE OF DEFECTS

The direct effect of having 2D nanosheets is the greater surface to volume ratio achieved, and since the surface can be considerably different from the bulk it affects the concentration of ions with different valence, saturation, and coordination number, as well as the structure to decrease the surface energy, all to increase the stability.[81, 82] The defect concentrations and the related formation energy can change significantly and a minor type of point defect can become a dominant one or defect complexes can take over an isolated defect.[83] In addition, within the 2D material the behavior can be heterogeneous with edges behaving differently than the surface[84–86] or due to processing steps or post-processing treatment as was introduced earlier for annealed CoO_2 nanosheets (Sec. III). Since the performance of many nanomaterials strongly depends on the defect structure (e.g., vacancies, polarons etc.), and since processing techniques strongly affect the type, quantity and the distribution of defects, their characterization and control are critical and also a challenge.

The control of defect structures and defect structures themselves are a function of processing. Top-down approaches show promise in scaling-up for future production if a wide use of these nanosheets is targeted with inexpensive processing costs, and in obtaining nanosheets with large lateral sizes with lower structural defects needed for real devices without significant fabrication challenges. Although, top-down approaches limit the number of materials and systems that can be used (to layered structures), we are still far from realizing the full potential of them. There are also more recent techniques (i.e., adaptive ionic layer epitaxy - AILE)[87] being developed to increase the lateral size of nanosheets during bottom-up processing which also opens up the material space to non-layered structures.

Even in bulk, most oxides gain function due to their defect structures and chemically doped compositions with compensating electronic and ionic defects are used, instead of chemically pure and pristine compositions.[88, 89] Such defect engineering also applies to 2D oxides. When it comes to doping, in top-down approaches, compositions are most commonly designed at the bulk form that is exfoliated, however post-processing exposure to ions and solutions can also be used to exchange ions,[90–92] while more flexibility exists for bottom-up approaches. A doped composition that retains the same layered structure can go through similar processing steps for isolation of 2D nanosheets. While such processing techniques can create similar nanosheets, doping elements can result in different defect structures. For example, Lithium cobalt oxide ($LiCoO_2$, LCO) and its relative, lithium nickel manganese cobalt oxide ($LiNi_{1/3}Mn_{1/3}Co_{1/3}O_2$, NMC), are both layered transition metal oxides (TMOs) utilized primarily as the active cathode for the Li-ion battery industry.[93, 94] NMC can also be exfoliated to form two-dimensional

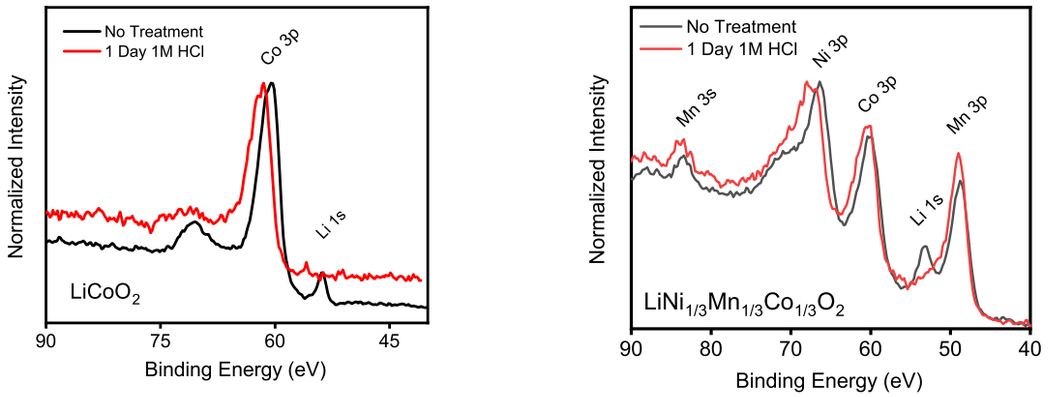

Fig. 4: (Left) XPS results for as-received $LiCoO_2$ (LCO) and 1M HCl treated LCO showing the removal of Li and the shift in Co-3p peak. (Right) XPS results for as-received Li(Ni,Mn,Co)O2 (NMC) and 1M HCl treated NMC showing the removal of Li and the shift in Ni-3p peak. Co and Mn peaks do not change with treatment.

(2D) nanosheets using the same chemical treatments as described in Sec. II. However, how the material reacts to these chemical actions may vary. For instance, observable shifts in the binding energies of the transition metals of both transition metal oxides suggest a change in the oxidation state due to acid treatment as was discussed above in detail for LCO but differences lie in the binding energy shift behavior of each transition metal within LCO and NMC. LCO consists of only one transition metal (cobalt) therefore, cobalt shifts in binding energy. On the other hand, NMC consists of three transition metals (nickel, manganese, and cobalt) of which only nickel shifts in binding energy, Fig. 4. Both cobalt and manganese remain in a similar chemical bonding state before and after acid treatment, suggesting that nickel is the primary charge balancing ion associated with NMC after this chemical treatment. This also emphasizes that the change in the oxidation state of Co does not occur in the presence of Ni.

We can categorize the defects on the nanosheets into two: (i) defects that are similar to those of the surface defects in bulk materials such as changed coordination, buckling of the bonds, or presence of unsaturated atoms etc. and (ii) defects that form during processing due to the chemistry used such as preferential etching of cations. One can consider a third category for the surface defects as exfoliated nanosheets tend to have single termination while bulk termination can vary locally. The first category can be treated as the "pristine" nanosheet, and the changes in behavior compared to bulk can be sorted under the effect of increased surface to volume ratio. For example, in pristine SnO_2, nanosheet morphology accesses a larger number of four-coordinated surface Sn and two-coordinated surface O (rather than six and three, respectively, in the bulk) which form active sites for CO adsorption and subsequent oxidation.[95] Although it should be noted that, in this case, changes to the electronic structure in the confined structure (i.e, formation of increased density of states at the valence or conduction band edge), for example in comparison to nano-particles with the same surface area to volume ratio, results in additional factors that affect the efficiency of the reaction by providing enhanced charge carrier densities and fast ionic diffusion paths. In Co_3O_4, surface Co ions have lower coordination, in a similar fashion to other oxides such as MgO and TiO_2, thus the nanosheet form accesses a larger percentage of such Co ions.[86, 96] Lowered coordination can lead to more active sites in relationship to the environment. In the nanosheet form, higher density of states near the conduction band edge and higher charge concentration occurs in comparison to the bulk form. However, increasing the surface area does not always guarantee increased performance metric, as exemplified for catalytic activity of $K_4Nb_6O_{17}$.[97]

The second category is processing specific. Even when the same technique is used (i.e., protonation and exfoliation of $LiCoO_2$ with HCl and TMAOH, respectively), the defect chemistry can change with a change in a processing parameter such as molarity of HCl. The purpose of HCl treatment is exchange of Li^+ ions with H^+. However, the solution shows the presence of Co^{2+} ions as characterized by UV-Vis. While some of that Co in the solution is due to dissolution of the formula units of $LiCoO_2$ as discussed in Sec.II, the quantification of the Li remaining in the powder and Co ions in the solution indicates leaching of Co ions into the solution beyond dissolution resulting in Co-vacancy defects in the structure to be exfoliated.[64] While the molarity and type of the acid used as well as the reaction time has an effect on the yield of exfoliation, they also vary the defect structure of the powders and thus can yield nanosheets with varying defect concentrations (here specifically Co-vacancies).[63, 64]

Many times, oxygen stoichiometry drives most performance characteristics and is generally achieved by post processing treatments of top-down processed oxide nanosheets; H_2 plasma treatment, UV radiation, and vacuum annealing.[98] In bottom-up approaches they can also be introduced during processing (e.g., sol-gel processing of TiO_{2-d})[99]. Even the difference between air and pure O_2, both of which are oxidizing atmospheres, can change the oxygen vacancy concentration both in bottom-up approaches[100] and during phase transformation of existing nanosheets.[101] As we have shown for CoO_2 nanosheets, however, as summarized in Sec. III, the changes in stoichiometry can be associated with changes in ordering as well as crystal structure. One also has to also consider that similar defects on the surface behave differently compared to bulk components. For example, in TiO_2, oxygen vacancies are compensated with two Ti^{3+} cations which are symmetrically situated around the oxygen vacancies in bulk, while an asymmetric configuration occurs on the surface due to the presence of dangling bonds. This results in formation of one and two in-gap states, respectively.[102] Similar surface sensitivity due to vacancies exist in all materials; oxides[103], selenides[104], nitrides[105], etc., however, in 2D materials the increased surface to volume ratio results in the dominant nature of the surface defects in the overall performance of the material. As noted before for SnO_2 with increasing density of states at the valence band edge in the 2D morphology, changes to the electronic structure, even if they do not have an effect in the mechanism, can have an effect on the efficiency and yield of the related reaction.[95]

The importance of the oxygen vacancies in 2D oxide nanosheets can be exemplified by observations in materials systems such as TiO_2, ZnO, Co_3O_4, In_2O_3. Formation of disorder, and presence of oxygen vacancies and Ti^{3+} cations on the surface in TiO_2 nanomaterials have been shown to increase visible and near-IR absorption, improved photocatalytic degradation of organic molecules, photoactivated reduction of CO_2, and H_2 evolution from water.[82, 106–110] Both the formation of defects and their related effects in performance are a function of crystallography, as formation energies of defects vary with the bonding environment and thus crystal planes. For example, for TiO_2, formation energy for oxygen vacancy is much lower in the {101} planes. The anisotropy of the surface energies of crystallographic planes can also affect their reactivity.[95] Reduction of TiO_2 nanoparticles to TiO_{2-d}, may result in formation of oxygen vacancies ($Vo^{\cdot\cdot}$) coupled with Ti^{3+}/Ti^{4+} with a ratio of 1 : 2. However, it is also possible that so-called Magneli phases form with formula Ti_nO_{2n-1}.[111] The presence of such vacancies results in in-gap states that increase absorption of visible light. Presence of surface oxygen vacancies can also act as trapping sites for electrons, effectively separating the photo-generated electrons and thus, limit recombination.[112] Crystallography can also play an important role in separation of photoexcited electrons and holes, as they can transfer to different facets, critical in many applications related to catalysis.[95] In ZnO, oxygen vacancies, in a similar fashion, activated CO_2 reduction by providing an electron transfer. However, it was also shown that increasing oxygen vacancy concentration increased the activity of ZnO due to the enhanced binding strength of CO_2 to the surface and not due to the increase in the number of active sites.[98] In materials such as Co_3O_4, nanosheets can have oxygens with different coordination characteristics. Thus, the vacancy formation and its effects in performance can vary based on the type of oxygen site that becomes vacant.[96] Oxygen vacancies, especially those near the surface, in In_2O_3 nanosheets result in increased DOS both near CBM and VBM which both decreases the energy needed to excite electrons (due to DOS) as well as decrease the probability of recombination before the utilization of the photoelectron (due to position).[81]

The defects can be engineered for specific applications, such as providing active sites or increasing the binding energy for certain molecules.[113] However, it can also lead to stabilization of adsorption of unwanted molecules that limit the targeted surface interactions.[114] In addition, in the case of more than one type of oxygen site (based on its coordination), one type can preferentially be recovered by different molecules over the others.[115]

V. THE ROLE OF THE CATION SIZE

An interesting question is whether the 2D properties of a metal oxide layer can be already ascertained without exfoliation but simply by spacing the layers further apart by increasing the size of the intercalation ions. Although $LiCoO_2$ is not strictly an intercalated compound because the Li constitutes an integral part of the bonding mechanism, we pursued this idea computationally by investigating the properties of $ACoO_2$ with A being Li, Na, K, Rb, Cs and H. H is included because the first step in the exfoliation process is in fact, replacing Li by H. At the same time, this study reveals some aspects of the role of the size of the intercalating A-ion in the exfoliation process.

Our initial study started from the $R\bar{3}m$ structure of $LiCoO_2$ keeping the lateral in-plane lattice constant fixed and simply replaced Li by various other ions and relaxing the interplanar distance. The densities of states resulting from this procedure are shown in Fig. 5. We can see that not much change occurs when replacing Li by Na. Even replacing Li by Na, Rb, Cs, the gap between the t_{2g} valence band and e_g conduction band remains intact. However, one may notice a new band at lower energy below the VBM and this then seems to push up the t_{2g} and O-2p derived bands. Further inspection of the partial densities of states, reveals that these are related to the K-3p, Rb-4p and Cs-5p semicore orbitals. Such a large band width for semicore orbitals is unrealistic and is due to the fact that we did not allow the in-plane lattice constant

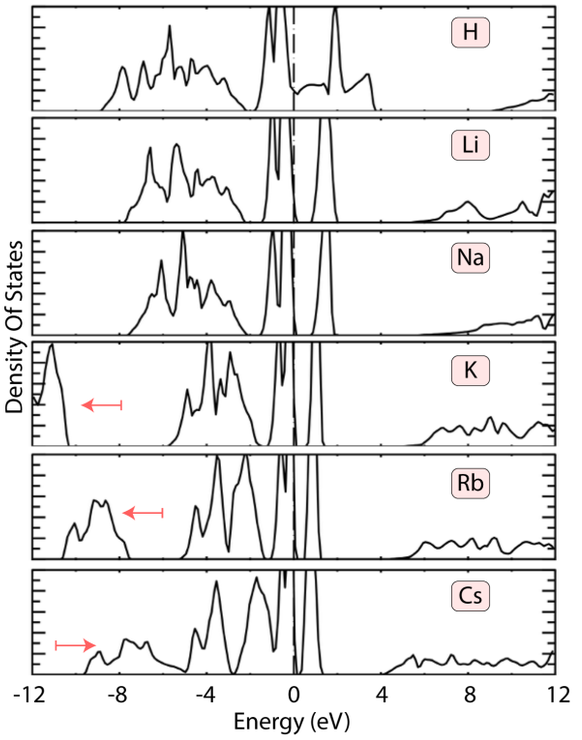

Fig. 5: Density of states in $ACoO_2$ with $A = H, Li, Na, K, Rb, Cs$ in $R\bar{3}m$ structure with in-plane lattice constant frozen at that of $LiCoO_2$ and interplaner distances relaxed. The red arrows indicate the semicore bands which are unphysically broadened and shifted up due to the unreasonable lateral proximity of the large A atoms.

to relax in this calculation. However, if we allow the in-plane lattice constant to expand, then the integrity of the CoO_2 layer becomes questionable. This suggests, that there is limitation to this procedure to expand the interlayer distance. In fact, a little bit of database search in the Materials Project (MP) database,[116] shows that for K_xCoO_2 the $R\bar{3}m$ like structure is only reported for $x = 0.5$ but not for $x = 1$.

The lowest energy structure of $KCoO_2$ has a $I\bar{4}$ space group with Co in tetrahedral coordination and the tetrahedra are connected in hexagonal rings. Another layered form with layers formed by square pyramidal CoO_2 units is found in MP[116] with space group $P4/nmm$. This structure has a significantly lower volume per formula unit and is thus a phase that could possibly be stabilized under high pressure. These various structures are illustrated in Fig.6.

For Rb and Cs, the structures are three dimensional with a $Fd\bar{3}m$ space group. Both consist of two interpenetrating diamond lattices of Rb (Cs) and CoO_4 tetrahedra. The CoO_4 tetrahedral units are corner sharing.

Subsequently, we performed fully relaxed calculations of both the $R\bar{3}m$ and $P4/nmm$ for $LiCoO_2$, and replacing Li by H, Na, K and Cs. The results in Fig. 7 show that the $R\bar{3}m$ structure has lower energy for Li and Na but the $P4/nmm$ structure has lower energy in the K and Cs case, and surprisingly also for H. According to MP,[116] the $P4/nmm$ structure itself is 0.488 eV/atom higher than the $I\bar{4}$ structure, which means 1.95 eV/formula unit. Thus the $R\bar{3}m$ structure is unstable by more than 2 eV/formula unit relative to its ground state $I\bar{4}$ structure for $KCoO_2$. The situation becomes worse for even larger alkali cations. The result for H is somewhat surprising as the $R\bar{3}m$ structure is listed as ground state structure in MP.[116] It can however by rationalized by the H forming an OH bond with just apical O of the CoO_5 pyramid instead of being shared equally between two CoO_2 layers. Other forms with more pronounced OH bonds are found in MP. As far as the process of hydrogenation in the first step of the exfoliation procedure is concerned, these calculations suggest that the process is not as simple as just replacing Li by H because then H would not have formed a simple OH bond but would be required to stay halfway in between the layers. However, Sec. VII B shows that beyond a certain distance between the layers even Li would undergo a symmetry breaking and associate with one CoO_2 layer. We may expect the same for H if the distance between the layers is kept higher perhaps because of the aqueous environment. H_2O molecules inserted between the layer may play a critical role in keeping the layers sufficiently apart so that Li and H associate with one CoO_2 layer instead of two. The critical role of the presence of H_2O is not yet fully understood but is also found in the experimental studies as function of solvent.[65]

It is thus clear that the layered $R\bar{3}m$ structure is only stable for relatively small alkali ions Li and Na. This may explain to some extent why inserting large organic TMA ions breaks the structure apart and exfoliation occurs. It also would appear that only a fraction of the Li can be replaced by TMA ions.

Finally what about the initial step of H replacement? In this case we find a metallic band structure. Essentially, the H forms energy levels within the t_{2g}-e_g gap, which broaden into a band. This can be explained by the lower energy position of the H-1s state compared to the Li-2s. In other words, H is not as electropositive.

VI. 2D EFFECTS ON PHONONS: V_2O_5 AND MoO_3

From earlier studies of 2D materials such as TMDC it is clear that the reduction in dimensionality can have important effects on phonons. First of all the acoustic modes show flexural modes which have a long wave dispersion proportional to q^2 while in 3D the phonon frequencies behave $\omega \propto q$. But optical modes in TMDC such as MoS_2 have also been found to show either red or blue shifts.[117] In this case it was found that the out-of-

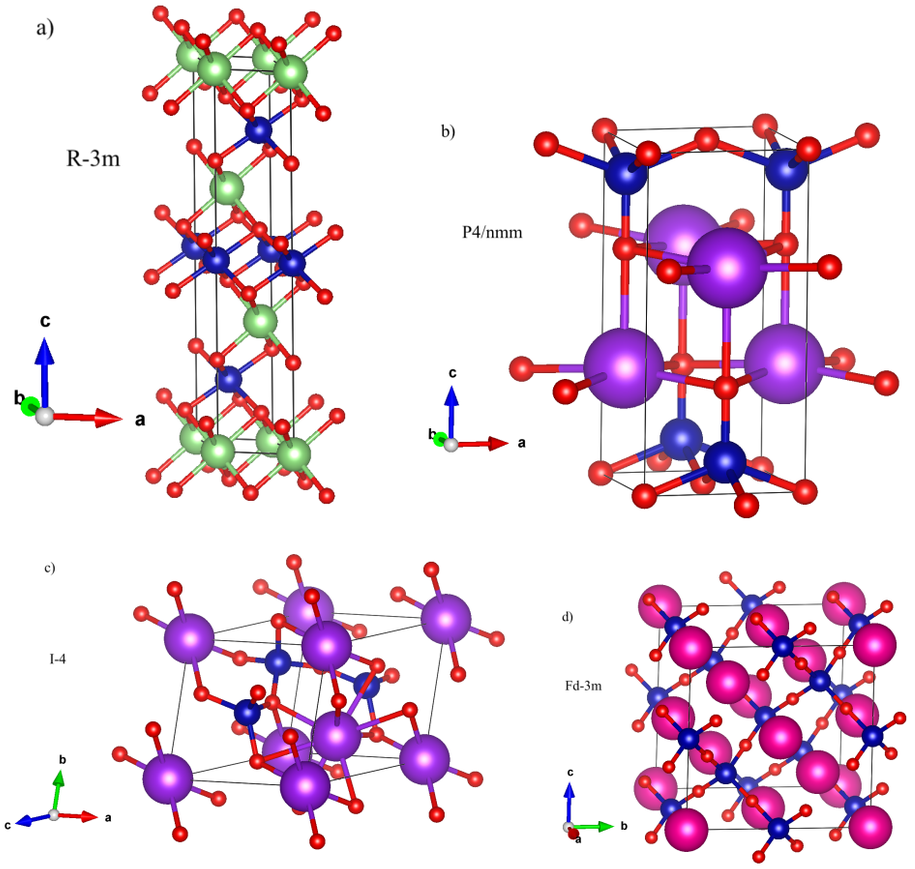

Fig. 6: Crystal structures of (a) $R\bar{3}m$ $LiCoO_2$, (b) $P4/nmm$ $KCoO_2$, (c) $I\bar{4}m$ $KCoO_2$, (d) $Fd\bar{3}m$ $RbCoO_2$, blue spheres Co, red spheres oxygen, green spheres Li, purple spheres K, magenta spheres Rb.

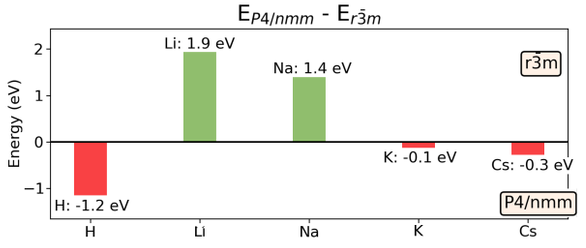

Fig. 7: Total energy difference per formula unit between pyramidal coordination $P4/nmm$ and octahdedral coordination $R\bar{3}m$ layered structures $ACoO_2$ for A being H, Li, Na, K, Cs.

plane, A_{1g}, mode, which becomes A_1 in the monolayer undergoes a red shift, while the in-plane E^1_{2g} mode which becomes E' in the monolayer undergoes a blue shift. These shifts are of the order of a 2-4 cm^{-1} or about 0.5 % of the mode frequency and have both been observed experimentally and explained theoretically. A redshift might be expected for modes normal to the plane considering that removing the interlayer interactions, however weak, should reduce the stiffness of the system and thus decrease the mode frequency. However, for an in-plane mode one would expect less of an effect of the interplanar force constants because these would be shear forces. In any case, the blue shift seemed most puzzling but was explained by the effects of reduced screening in 2D on the long-range dipolar force constants.

Similar effects have been found to occur for V_2O_5 [118] but with a more interesting twist. In fact, the out-of plane modes related to the bond stretch of the vanadyl-oxygen vanadium bond, schematically shown in Fig. 8, were found to undergo a blue shift in the monolayer compared to the bulk. Fig. 9 shows the a_{1g} and b_{1g} Raman active mode shifts from bulk to monolayer in V_2O_5. Applying a similar analysis to that of Molina-Sánchez and Wirtz [117] it was found that the applicable long-range force constant was in fact decreased instead of increased because not only the dielectric constants (shown in Fig.10) were reduced in the monolayer but also the relevant Born effective charges were reduced by a similar factor. See Fig. 11 for the Born charges, note that for the vanadyl oxygen only the zz component is large because it is bonded in the z direction while for the bridge

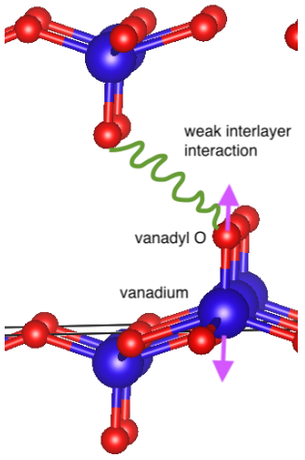

Fig. 8: Vanadyl-oxygen vibration in V_2O_5 sketch.

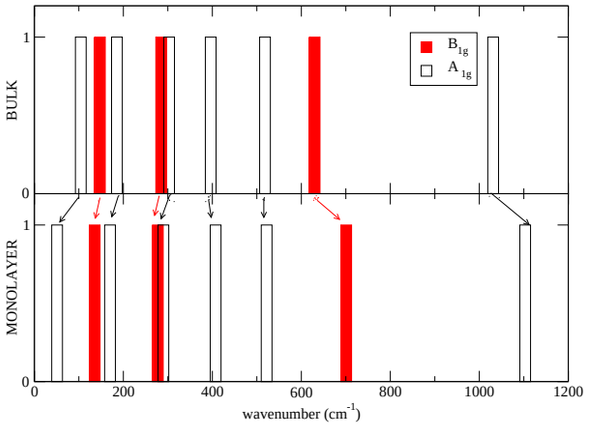

Fig. 9: Phonon mode shifts between bulk and monolayer V_2O_5. Figure reproduced with permission from Phys. Rev. B **89**, 045109 (2014). Copyright 2014, American Physical Society.

oxygen only the xx component is large because they are bonded only in the x and for the chain oxygen, both xx and yy are sizable because these oxygens are bonded in x and y directions. However, one can also see that the V xx and yy components are not much changed while the zz component is reduced by almost a factor 3. Since the dipolar force constants are proportional to the product of the Born charges of the two atoms involved in the bond stretch and inversely proportional to the in-plane dielectric constant, the long-range force constant is reduced. So, why was a blue shift obtained? The other difference with the MoS_2 case is that here a V-O bond stretch is at play rather than a Mo-Mo bond stretch in the plane.

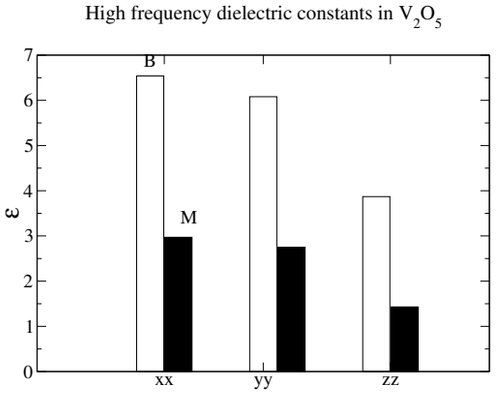

Fig. 10: High frequency dielectric constants of V_2O_5 in bulk and monolayer.

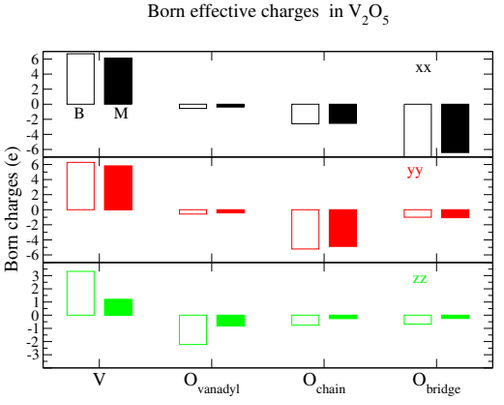

Fig. 11: Born effective charges in bulk an monolayer V_2O_5, data from [118],

Thus the Born charges have opposite sign and this results in the long-range force constant having opposite sign to the short-range force constant. The latter barely changes and so the net result of a decreased long-range force constant is less opposition to the short-range force constant. The latter then becomes dominant in the monolayer and explained the blue shift. Some other modes in V_2O_5 were also found to have red-shifts and although a detailed analytical insight is only possible for some of the simpler mode patterns, these effects still remain as predictions. Although thin V_2O_5 layers (down to about $\sim$ 10 nm or 20 layers) have been exfoliated,[39] the monolayer limit has not yet been achieved, so that these predictions remain to be confirmed by experiment. Very recently, a chemical exfolation study of V_2O_5 by Reshma *et al.* [40] reported bilayer V_2O_5. It confirms the blue shift of several vibrational modes, in particular the high-frequency A_{1g} mode, in qualitative agreement with the theoretical predictions. It also predicted a significant increas in band

gap from 2.39 eV in bulk to 3.72 eV in the bilayer to be discussed in the next section.

More recently, we have also studied such shifts on vibrational modes in MoO_3.[119] Again, the story turns out to be a bit different than in V_2O_5. The most interesting modes to analyze again involve a bond stretch of the short Mo-$O^{(2)}$ bond, which occur at about 1000 cm^{-1}. The same analysis of the dipolar force-constants apply and lead to a net but small increase of the force constant directly between Mo and the $O^{(2)}$ bonded to it. However, in contrast to V_2O_5, the geometry of the layers leads to a stronger interlayer $O^{(2)}$-$O^{(2)\prime}$ interactions between these O in adjacent layers. They just happen to be closer to each other laterally and hence there remains a larger interlayer force in bulk. This effect turns out to dominate the blue shift tendency arising from the Born charge and dielectric constant reductions, and thus, ultimately lead to a red-shift. In absolute value this shift is nonetheless larger than in MoS_2, it is about 14 cm^{-1} or 1.3 % and should thus be easy to observe by Raman spectroscopy.

In summary of this discussion, changes in screening and Born effective charges which related to the polarizability of the bonds in 2D were found in various 2D materials to lead to interesting shifts in phonon frequencies but the detailed application of these ideas is rather subtle and requires a detailed analysis of the force constants. It also shows that in the bulk of these layered materials, the interlayer forces, even when weak still affect vibrational modes.

Another general effect of the dimensionality on infrared active phonons was pointed out by Sohier *et al.* [120]. In 2D the long-range limit of the in-plane dielectric function [121] $\varepsilon_{2D}(\mathbf{q}_\parallel) = \varepsilon_m + r_{eff}|\mathbf{q}_\parallel|$ (with r_{eff} the effective screening length) becomes only the ε_m of the surrounding medium. This is a clear dimensionality effect: the field screening is dominated by the electric field lines that go through the medium outside instead of inside the 2D material. On the other hand at short distance (large $|\mathbf{q}_\parallel|$) the screening becomes proportional to $|\mathbf{q}_\parallel|$. This then affects the LO-TO splitting in a qualitative manner. First of all the Coulomb interacton in 2D is $2\pi/|\mathbf{q}_\parallel|$ instead of $4\pi/|\mathbf{q}|^2$ in 3D. Secondly the essential dependence of the screening on wave vector implies that the LO-TO splitting will go to zero for $\mathbf{q}_\parallel \to 0$. In practice, there is a small region of order $1/r_{eff}$ where the LO-TO splitting increases linearly with $|\mathbf{q}_\parallel|$. These effects may manifest themselves more strongly in 2D oxides where the ionic nature of the bonding leads to relatively low electronic (high-frequency) dielectric screening to begin with.

Apart from these specific 2D related changes in phonon modes, vibrational spectra, specifically Raman spectroscopy has been found useful as a characterization tool for 2D nanoflakes. The in-plane anisotropy of the modes can be used to determine the crystal axes of a nanoflake in cases where XRD would be difficult to carry out. This method was used for example by Sucharitakul *et al.* [39] to determine that the long axis of the rectangular nanoflakes obtained by mechanical exfoliation corresponded to the direction of the chains in the structure.

We should also point out that electron-phonon coupling has been found to play an important role in V_2O_5 and leads to the formation of self-trapped polarons.[43–45] The transport is therefore of polaron hopping nature. Finally, the anisotropy of the phonons in both V_2O_5 and MoO_3 leads to fairly wide frequency ranges where the dielectric function in the mid-infrared range is positive in one direction and negative in another. They are therefore natural hyperbolic materials in this frequency range and this holds promise for interesting optical applications.[122, 123]

VII. 2D EFFECTS ON ELECTRONIC STRUCTURE

A. Accuracy of *GW*-methods for layered oxides

Dimensional effects on electronic structure are well known to be important. The basic model of quantum confinement goes back to the quantum mechanics textbook example of a particle in a potential well. Discrete bound states occur in the well and the separation between the levels increases as the the potential well becomes narrower, essentially $\propto 1/w^2$ for an infinite square well with width w. This already formed the basis for the use of semiconductor heterostructures long before the advent of 2D materials. On the other hand, for 2D few layer materials, which are usually obtained from a weakly interacting layered material to begin with, it is not so obvious why breaking those weak interactions would strongly affect the electronic structure of the layer itself. One would expect that the confinement effects are already present in the layer even if we have a stack of such weakly interacting layers.

Yet, graphene is clearly different from graphite in the sense that the π electrons now form a Dirac cone with linear band dispersion and even bilayer graphene is essentially distinct from single layer graphene in that a gap can open. For transition metal dichalcogenides such as MoS_2 it was found early in the development of 2D materials, that the nature of the gap can change from indirect to direct when going from bulk to few layer or monolayer systems. This is because specific states in **k**-space have different deformation potential and react less or more strongly to the interlayer spacing depending on their atomic orbital composition, which may point more in-plane or out-of-plane. To discover such effects, reliable prediction of the electronic structure is a prerequisite.

It is well known that band gaps are typically underestimated by local or semilocal exchange-correlation functionals in density functional theory. The quasiparticle self-consistent *GW* method (QS*GW*),[124, 125] on the other hand provides accurate results for most materials, including all tetrahedral semiconductors. However, how well this approach works for often more strongly correlated transition metal oxides is not yet clear. We

here briefly discuss the essential concepts of the QSGW method before we discuss how it applies to the oxide materials of interestin in this paper.

In Hedin's [126, 127] GW approximation to the dynamical self-energy in many-body-perturbation theory, G stands for the one-electron Green's function and the self-energy $\Sigma(1,2) = iG(1,2)W(1+,2)$ where $1 \equiv \{\mathbf{r}_1, \sigma_1, t_1\}$ is a shorthand for position, spin and time of the particle labeled 1.

In the most prevalent implementation of the GW method, the G^0W^0 approximation, the quasiparticle excitation energy equation,

$$[H^0 - v_{xc}(\mathbf{r})]\psi_n(\mathbf{r}) + \int d^3r' \Sigma(\mathbf{r}, \mathbf{r}', E_n)\psi(\mathbf{r}') = E_n\psi_n(\mathbf{r}), \tag{1}$$

is solved by first-order perturbation theory starting from the independent particle Kohn-Sham Schrödinger equation

$$H^0\phi_n(\mathbf{r}) = \epsilon_n\phi_n(\mathbf{r}), \tag{2}$$

by assuming $\psi_n \approx \phi_n$ and calculating the one particle Green's funcion G^0 and polarizaton $P^0(1,2) = -iG^0(1,2)G^0(2,1)$ and hence screened Coulomb energy $W^0(1,2) = v(1,2) + \int d(3,4)v(1,3)P^0(3,4)W^0(3,4)$, or symbolically $W = [1 - vP]^{-1}v = \varepsilon^{-1}v$, using the Kohn-Sham ϕ_n and ϵ_n. Essentially, the self-energy $\Sigma(\mathbf{r}, \mathbf{r}', E_n)$ replaces the exchange-correlation potential $v_{xc}(\mathbf{r})$. In self-consistent GW theory, one would need so solve the equations $G = G^0 + G^0\Sigma G$, $W = v + vPW$, along with the definitions of $\Sigma = iGW$ and $P = -iGG$ consistently. Here we have dropped the variable dependencies for simplicity, which however hides that these are in fact integral equations, which in practice are solved by means of a basis set expansion and after transforming to the Bloch function $\mathbf{k}$-space and energy domain.

On the other hand, in the QSGW method, one recognizes that perturbation theory works best if the perturbation is small, in other words when the Σ is in some sense close to v_{xc}. One thus adds $\tilde{\Sigma} - v^0_{xc}$ to the H^0 Hamiltonian, with the energy-independent, Hermitian $\tilde{\Sigma}_{ij} = \frac{1}{2}\mathrm{Re}\{\Sigma_{ij}(\epsilon_i) + \Sigma_{ij}(\epsilon_j)\}$ and iterates this to self-consistency. Here the Σ is represented by a matrix in the basis of the H^0 eigenstates. The result is that the QSGW method becomes independent of the starting H^0 approximation, which is then usually taken to be the LDA or GGA. Typically QSGW slightly overestimates the gap and this has been largely attributed to the lack of electron-hole interactions in the calculation of the screened Coulomb interaction W in the standardly used random phase approximation (RPA). The upshot is that with a small and systematic correction for the underscreening, *i.e.* only including 80 % of the $\tilde{\Sigma}$, the quasiparticle energies agree typically with experiment within ~ 0.1 eV. This 80% rule or 0.8Σ approximation can be further justified[128] or avoided by including the ladder diagrams, which represent electron-hole interactions in the calculation of W within the Bethe-Salpeter-equation (BSE) approach,[129] or via a detour to time-dependent density functional theory (TDDFT) using an appropriate kernel [130, 131] but this is still significantly more computationally demanding.

Having explained the methodology briefly, and referring the reader to the literature quoted above for details, we now ask ourselves how well does this approach work for the layered oxides we are interested in and how do they work of few-layer 2D systems? Surprisingly, in V_2O_5 we found that the band gap in the more advanced QSGW method strongly overestimates the gap. While the lowest direct gap is 2.0 eV in LDA, the corresponding QSGW gap is 4.45 eV (3.96 eV in 0.8Σ), much larger than the experimental value of 2.35 eV. The direct gap at Γ is 2.30 eV and the lowest indirect gap is 1.73 eV. Given that the experimental value extracted from optical absorption most likely corresponds to the lowest direct gap, the LDA, while still underestimating, comes actually closer to the experiment than the QSGW method.

Turning now to the monolayer, we find that the LDA gap only moderately increases in the monolayer compared to the bulk by about 0.5 eV and this is mainly due to the reduced dispersion of the bands along the direction perpendicular to the layers, in other words, as expected from eliminating the interlayer hopping interactions. However, the QSGW gap increase signficantly and, moreover, was found to converge very slowly with the size of the vacuum region, separating the monolayers in the periodic boundary condition method used, even for 2D systems. In fact, the gap then converges as $1/L$ with L the size of the vacuum region and a gap as large as 7.66 eV was obtained by extrapolating to $L \to \infty$. Very recently, an increase in optical band gap measured by the Tauc method was reported for bilayer V_2O_5 compared to bulk by 1.33 eV.[40] This is larger than predicted by LDA but still significantly smaller than predicted by QSGW.

Clearly, this presents a challenging problem to our understanding of the 2D materials electronic structure because even for the bulk, there is a large discrepancy. From studies of other 2D materials,[132] it is already well known that such a large change of the gap in monolayers compared to bulk results from the long-range character of the self-energy $\Sigma(\mathbf{r}, \mathbf{r}', E)$ in insulators and again from the strong changes in screeening in 2D [121] that were already mentioned above in the context of phonons. In other words, this leads to an increase in W. However, it should be realized that these 2D effects relate to the quasiparticle gap or fundamental gap $E_g^{qp} = I - A$, defined as the difference between the ionization potential $I = E(N-1) - E(N)$ and electron affinity $A = E(N) - E(N+1)$. This type of gap is in principle measured by taking the difference between inverse photoemission (IPES), or Bremsthralung isochromat spectroscopy (BIS) and photoemission spectroscopy (PES) onsets and measures one-particle addition or removal energies. These are the excitation energies considered by many-body-theory when creating or destroying a particle from the many-electron system. However, in

optical absorption, one creates a two-particle excitation or an electron-hole pair and the interaction between the two, which is the excitonic effect can lower the excitation energy. The reduced screening in 2D compared to 3D increased W. This increases the GW self-energy and hence the one-particle gap but W also enters the exciton binding energy and hence, the exciton binding energy is increased. These two affects largely cancel each other out.

However, clearly in oxides such as V_2O_5, we need to first understand the origin of the QSGW gap overestimate in the bulk before we can attempt to understand the monolayer. So, first, inverse photoemission and photoemission experiments by Meyer *et al.* [133] show that the quasiparticle gap is about 2.8±0.5 eV. This is substantially higher than the optical absorption onset of 2.35 eV but still far from the QSGW gap. Two main reasons come to mind for the origin of this overestimate, the underscreening by the RPA or lack of electron-hole interactions or electron-phonon coupling band gap renormalization effects.

In Ref. 47 we pursued the hypothesis that electron-phonon coupling would be responsible for the discrepancy. In fact, Botti and Marques [134] had proposed that for polar materials one should take the ionic displacements or relaxation into account in the screening of W in the long-wavelength limit. They called this a lattice polarization correction (LPC). In a material with strong LO-TO splittings this substantially increases the static dielectric constant compared to the high-frequency (electron only screening) dielectric constant because of the generalized Lyddane-Sachs-Teller equation

$$\frac{\varepsilon_0(\mathbf{q}\to 0)}{\varepsilon_\infty(\mathbf{q}\to 0)} = \prod_m \left(\frac{\omega_{LO}^m}{\omega_{TO}^m}\right)^2, \tag{3}$$

which relates the dielectric screening increase to the vibrational modes m. We thus used a correction factor $\alpha = \varepsilon_\infty/\varepsilon_0$ for W and hence Σ, where we averaged in some way over the different directions. This led to an estimate of a correction factor of 0.38 which then brought the optical absorption gap down to 2.6 eV which seemed reasonable.

However, this assumed that the correction factor to apply for all wavevectors whereas according to the Botti-Marques approach it should only be applied in the $\mathbf{q}\to 0$ limit. Now in the GW method the self-energy evaluation in reciprocal space and energy rather than time domain, requires a convolution between $W(\mathbf{q},\omega)$ and the Green's function $G(\mathbf{q},\omega)$ and the singularity of $W(\mathbf{q},\omega)$ for $\mathbf{q}\to 0$ requires a special treatment of the neighborhood of $\mathbf{q}=0$. This is done by the off-set Γ method described in Refs.125, 135, and 136. Thus by replacing the macroscopic electronic-only dielectric constant by the one including lattice polarization for just $\mathbf{q}=0$, one approximately takes into account this LPC. However, the correction then depends on how large a region around $\mathbf{q}=0$ this correction represents, in other words on the integration mesh. For V_2O_5 this was reported in Bhandari's thesis[137] and showed that using a well-converged $\mathbf{k}$-mesh for which the QSGW method is converged, the correction amounted only to -0.15 eV for the indirect gap and -0.21 eV for the lowest direct gap. So, this effect cannot explain the discrepancy with experiment. Furthermore, this could still overestimate the correction. In fact, to properly apply the Botti-Marques LPC, one needs to apply it in $\mathbf{q}$-space over a region set by the inverse of the polaron length scale $a_P = \sqrt{\hbar/2\omega_{LO}m^*}$ which also involves the effective mass of the corresponding band edge.[138] This then amounts to the classical Fröhlich polaronic zero-point-motion correction apart from a factor two which arises in our model from the fact that we limited the integration of the polaron correction to $1/a_P$ whereas traditionally it is extended to infinity. This factor two is still under dispute, for example a recent paper evaluated the Fröhlich contribution more completely and arrives at estimates of this zero-point motion correction to the gap about a factor two larger than ours for various materials.[139]

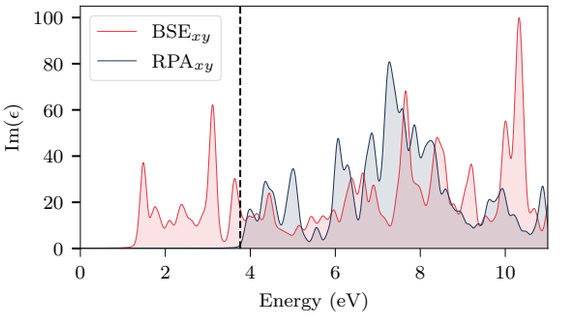

Fig. 12: Imaginary part of the dielectric function of $LiCoO_2$ calculated at the RPA and BSE levels based on QSGW(Γ)

So, at any rate, electron-phonon coupling seems not to be the primary reason for the gap overestimate in V_2O_5 by QSGW. Although polaron formation may be expected to occur given the very flat bands, this would primarily affect luminescence but not optical absorption because the polaron takes some time to form. We thus need to return to the electron-hole interactions and the BSE approach. Unfortunately, evaluating the electron-hole effects on W has still not been possible for V_2O_5 because of the demanding nature of these calculations for a system with as many as 14 atoms per unit cell.

Meanwhile we found that similar problems plague other oxides, notably $LiCoO_2$. The GGA gap in this case is found to be 0.87 eV while QSGW gives a gap of 4.125 eV. Now in this case, the smaller unit cell size allowed us to fully apply the recently developed BSE approach by Cunningham *et al.* [129]. By that we mean that the BSE is applied not only to the calculation of the macroscopic optical dielectric function, in other words in the limit $\mathbf{q}\to 0$ but at all $\mathbf{q}$ in the Brillouin zone. This allows

us, first of all, to re-evalute the QSGW gap with a modified W. We call this QS$GW(\Gamma)$ because it is equivalent to including a vertex (Γ) correction to W. This yields a quasiparticle gap of 3.76 eV. However, examining now the dielectric function in the $\mathbf{q} \to 0$ limit, we find that the lowest peaks in absorption are excitonic in nature and yield an exciton gap of only 1.4 eV in agreement with the best experimental determinations of the absorption onset (Fig. 12). Further details of this recent work can be found in Radha *et al.* [140] This clearly shows that in $LiCoO_2$ the optical absorption onset corresponds to strong Frenkel excitons and is significantly different from the quasiparticle gap. The exciton binding energy is of order 2.3 eV.

With this new insight, we expect that strong excitonic effects will also be important in V_2O_5. In terms of the bulk monolayer gap difference, we then expect, that similar to MoS_2 and other TDC materials, the monolayer effects on the optical gap will be moderate. As observed for those materials, the increase in W due to reduced screening affects both the quasiparticle gap and the exciton binding energy in a similar fashion so that ultimately they largely compensate each other.

B. Topological Surface States in $LiCoO_2$

Thus far we have focused on QSGW effects on the band gap of 2D materials related mostly to the different nature of screening in 2D. However, in some materials, 2D effects can be more profound in altering the electronic structure even at the much simpler semilocal density approximaton level. In topologically non-trivial materials the bulk-boundary connection may lead to the existence of topologically protected surface states which are partially filled and hence metallic. Needless to say for an ultrathin few-layer system, such effects are predominant because they are almost all surface.

Unexpectedly, we found this to be the case in $LiCoO_2$, although this material has not been previously recognized to be topolocially non-trivial. This is because the notion of topology has recently been signficantly expanded when considering crystalline symmetries instead of only continuous symmetries such as time reversal, or particle-hole symmetry. While such crystalline topological effects are only weakly protected, we still found them to have profound effects in the case of $LiCoO_2$ in the $R\bar{3}m$ structure.

We discovered these effects somewhat serendipitously by performing DFT calculations for a monolayer of $LiCoO_2$, inspired by the exfoliation experiments.[141] In other words, we considered a monolayer of CoO_2 consisting of the same connected CoO_6 octahedra as in the $R\bar{3}m$ structure and with Li attached to one side. Intriguingly what we found was that the Li-sp_z orbital related bands, which in bulk occur at high energy above the Fermi level, came down in energy and near Γ formed an occupied pocket below the Fermi level, which manifests itself in the formation of a two-dimensional electron gas (2DEG) with an increased electron density on the Li and floating above it, extending into the vacuum region. Even more interesting, this electron gas was found to be spin-polarized and accompanied by a corresponding hole gas on the CoO_2 layer. Further calculations of systems consisting of several layers and replacing Li by Na and in various surface locations confirmed the robustness of the effect. The surprising fact about this result is that the bonding in $LiCoO_2$ is usually assumed to be purely electrostatic with Li levels being so high that they donate their electron entirely to the CoO_2 layers. So, why would the Li levels come down in energy at the surface? The answer is that the covalent bonding between the Li hybridized sp_z orbitals and the two CoO_2 layers above and below it in the bulk phase is non-trivial in character and plays an important role.

We found that it can be related to the bonding in the quadripartite Su-Schrieffer-Heeger (SSH4) 1D chain model. To gain further insight, we modeled the CoO_2 layer as just two sites with s orbitals. Within this model, if the square of the interacton between Li and Co is stronger than the product of the interactions between Li-Li and Co-Co, the system is in a non-trivial topology, characterized by a non-zero topological winding number. This implies that if the Li-Co bond is broken at the edge, or, alternatively phrased, if the unit cell is chosen so that one of the Li-Co interactions is between one cell and the next, then a metallic (*i.e.* half filled) edge state is required. However, while the original SSH4 model has chiral or particle-hole symmetry, the energy difference between the on-site energies of Li and Co produces a gap in this edge state and would still transfer the electrons to the lower energy edge, in this case the CoO_2 layer. In other words, it is no longer topologically protected. The key to why nevertheless some electrons remained with the Li lies in the lateral interactions parallel to the surface. These are stronger for the Li than for the CoO_2 and hence the band broadening of the Li surface band allows it to overlap with the CoO_2 surface derived surface band creating a semimetallic situation with partial electron occupation on the Li surface and hole occupation on the CoO_2 surface. Crucial for this to be enabled is that the Li surface concentration is sufficiently high to allow for sufficient band width. Note that while the Li surface band center lies higher in energy than the CoO_2 one, it still is significantly lower in energy than in the bulk because the topological effect brought it down. The spin-polarization in this case results from the holes present in the CoO_2 layer, which is equivalent to reduced Li concentration in Li_xCoO_2 and, here, because of the proximity, also polarizes the Li-side 2DEG. The details of this study can be found in Radha and Lambrecht [141]

The topological effect discussed above is not limited to $LiCoO_2$ but occurs in other oxides with the $R\bar{3}m$ structure. Fig. 13 shows the Li related surface band in $LiCoO_2$, $LiFeO_2$ and $LiNiO_2$ monolayers. The bottom part of Fig. 13 shows the charge density associated

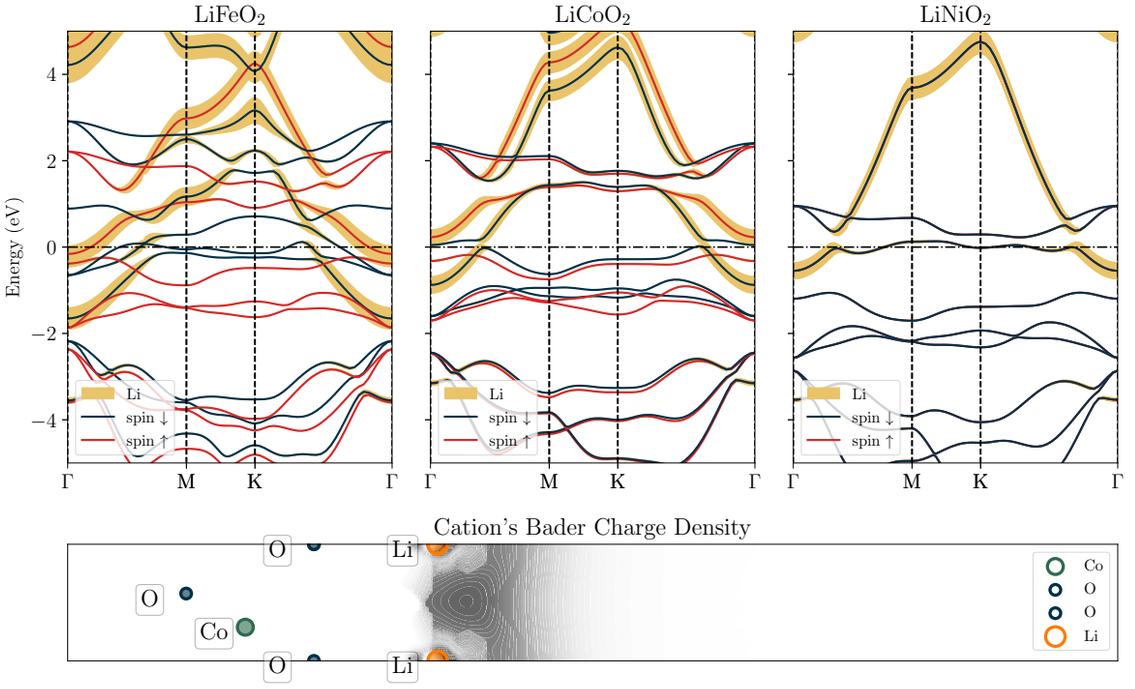

Fig. 13: Comparison of $LiCoO_2$ with $NiFeO_2$ and $LiNiO_2$ monolayers of the $R\bar{3}m$ structure. The yellow shading highlights the Li related surface states which are a result of the topological non-triviality. In both Fe and Co cases, the resulting monolayer band structure is spin-polarized (as indicated by the difference between red and black lines) while in $LiNiO_2$ it is not.

with Li in a $LiCoO_2$ monolayer using the Bader charge method.

The impact of this topology related surface 2DEG formation goes beyond the isolated 2D monolayer. We found subsequently that as the distance between CoO_2 layers is expanded in a periodic system, there is a critical transition where Li instead of staying at equal distance from the two neighboring CoO_2 layers, associates with one layer. The system at this point transforms into a set of non-interacting monolayers. Guided by the chemical exfoliation procedures, one may envision that this could be achieved by inserting large organic molecules in between the layers or by inserting H_2O molecules. As discussed in Sec. II, the role of water molecules in the process is not yet fully understood but appears to be crucial to achieve successful exfoliation. In fact, such a route to obtain essentially 2D physics within an extended periodic system has already been used in hydrated $NaCoO_2$. In this system, specifically in $Na_xCoO_2{:}yH_2O$, ($x \approx 0.35$, $y \approx 1.3$) superconductivity has been discovered at 4K.[59, 142] Remarkably we find that the required tensile strain of the interlayer distance in $NaCoO_2$ where the symmetry breaking transition to isolated monolayers occurs, is much lower in the Na than the Li case and coincides closely with the distance obtained in the hydrated layers were superconductivity occurs. We thus speculate that the superconductivity may be related to the presence of either the electron or hole electron gases in this system, which has thus far not been fully appreciated.

VIII. TRANSPORT IN 2D SYSTEMS

A. Tranport in V_2O_5

1. *Highly Anisotropic In-Plane Transport in α-V_2O_5*

The family of V-O compounds contains many species, due to vanadium's wide range of oxidation states from 2+ to 5+.[143–145] Numerous forms have found use in a range of applications, such as chemical sensors, anti-reflection coatings, and oxidation catalysts.[146–150] V_2O_5, the most stable member of the family, exists in a variety of phases. In this perspective, we are concerned with the α-phase, with all references on V_2O_5 from this point pertaining to this phase. V_2O_5 is a well-studied orthorhombic van der Waals "ladder" compound of space group $Pmmn$.[151] The reason for the name is apparent from Fig. 1, where connected double zigzag chains of V-O propagate in the **b** direction and are connected by "rungs" via a bridge oxygen in the **a** direction. Furthermore, it turns out that in NaV_2O_5 the electrons located on these V-O-V rungs in the lowest split-off conduction

band with V-d_{xy} orbital character have alternating spin orientation along the ladder direction and play a key role in its magnetic properties. There is also sufficient spacing in between layers for ionic intercalation with group-I and group-II elements, as demonstrated by Fig. 1b for sodium.

Much like MoO_3, the conductivity of V_2O_5 is largely determined by the atomic composition and stoichiometry of the crystal. In its pristine state, V_2O_5 is an insulator, becoming natively conductive only when oxygen is removed. The lattice consists of single, double, and triply coordinated oxygen species, of which the singly coordinated oxygen is most likely to leave in reducing conditions.[43, 45, 152] As oxygen bonds are broken, electrons are donated to the lowest conduction band, which is called the "split-off" band in V_2O_5, increasing n-type conductivity and mobility.[153]

The mobility increase in V_2O_5 is surprisingly anisotropic. Due to the larger orbital overlap in the V-O chains in the **b**-direction than in the **a**-direction, electrical conduction is greatly enhanced, resulting in a strongly 1D transport.[39] Similarly, phonon-polariton transport in V_2O_5 has also been found to be highly anisotropic.[123]

Recently, exfoliation experiments on V_2O_5 crystals were conducted by Sucharitakul *et al.* [39] Interestingly, the mechanical exfoliation of these crystals led mostly to rectangular nanoflakes with large aspect ratios. This is related to the presence of the above mentioned 1D chains within the layer. This means that the short side of each flake is expected to be perpendicular to these chains because these chains are connected by a bridge oxygen while the oxygen within the chain is bonded to three vanadiums. (See Fig. 1.) Confirmation of this was obtained by performing Raman spectroscopy. The A_{1g} modes near 482 cm^{-1} have a strong anisotropy in their Raman intensity which allowed us to identify the chain direction of the crystal relative to the long or short axis of the nanoflakes. Flakes with thicknesses between 10 nm and 150 nm were obtained, which is still far from a monolayer system. The c-axis of V_2O_5 perpendicular to the layers is only 4.8 Å, so even the smallest flakes are still approximately 20 layers thick. Contacts were made to flakes of μm lateral size and showed a marked anisotropy of the conductivity as measured by four probe van der Pauw method Hall measurements in addition to measuring sheet conductances. The ratio of the conductivity along the chain versus perpendicular to the chain was found to be as high as a factor of 10. Estimates of the conductivity and conductivity ratio were performed within a model based on in-plane acoustic phonon scattering using an approach previously used for MoO_3[42] and gave a satisfactory explanation of this anisotropy ratio. The large anisotropy of conductivity within the layers has previously been reported for bulk-sized samples[154] but was studied based on a variable range hopping conduction mechanism. However, the calculated conductivities were of order 306 $cm^2/(Vs)$ along the chains while actual measurements gave much lower conductivities of order 7 $cm^2/(Vs)$. The calculated theoretical limits on the mobility were comparable to those reported for MoO_3. This indicates that there is much room for improvement of the mobilities in nanoflake V_2O_5.

In V_2O_5 the conductivity is n-type and corresponds to filling of the bottom of the split-off conduction band, which primarily has dispersion along the chain direction. Nonetheless, it is not only the lower mass in this direction that plays a role in the conductivity but also the anisotropy in the deformation potentials and elastic constants in the plane. The origin of the carriers could be arising from the oxygen vacancies, such as vanadyl oxygen vacancies or could arise from intercalating impurities, such as Li and Na. The limitations in carrier concentration in V_2O_5 used in these nanoflake studies were limiting the measurements and could be overcome by intentional doping or intercalation in future studies. On the other hand, the polaronic nature of the transport as recently highlighted in Refs.44 and 45 may limit the transport mobility.

2. *P-type transport and Low Dimensional Scattering in α-$Na_{0.96}V_2O_5$*

Another way in which the conductivity of V_2O_5 may be impacted is via ionic intercalation, as in Fig. 1b. This produces what are known as bronze phases, with documented studies for species such as Li, Cs, Na, K, among others.[123, 155, 156] Li intecalation in V_2O_5 has been extensively studied in the context of Li-battery cathodes but leads to somewhat larger distortions of the lattice than Na intercalation, related to formation of the γ-form[157] of V_2O_5.[52, 158, 159] Mg-intercalated V_2O_5 in the β-form[160] has also recently been considered as a battery material.

In this perspective, we pay attention to sodium doping, which has been utilized to influence magnetic ordering and optical phonon polariton tuning. The ionic radius of sodium is small enough that it minimally impacts the lateral spacing of the crystal, only increasing the interlayer spacing in the stacking direction, while still donating electrons to the split-off band.[10, 161, 162] For this reason, sodium intercalation is a preferential candidate to examine changes to electronic transport without significantly affecting crystal symmetry. Recently, this dopant was investigated by our collaboration. P-type conduction was observed in few-layer flakes of $Na_{0.96}V_2O_5$. Using the scotch-tape mechanical exfoliation method, few-layer flakes were isolated, followed by subsequent deposition of electrical contacts in a 2-probe FET configuration. Similar thickness flakes of undoped V_2O_5 were also characterized simultaneously for comparison, as in Figure 14a. Positive/negative transconductance slopes for V_2O_5/$Na_{0.96}V_2O_5$ were observed, indicating a majority carrier of electrons/holes, respectively. Performing a linear regression, carrier mobility can be extracted.

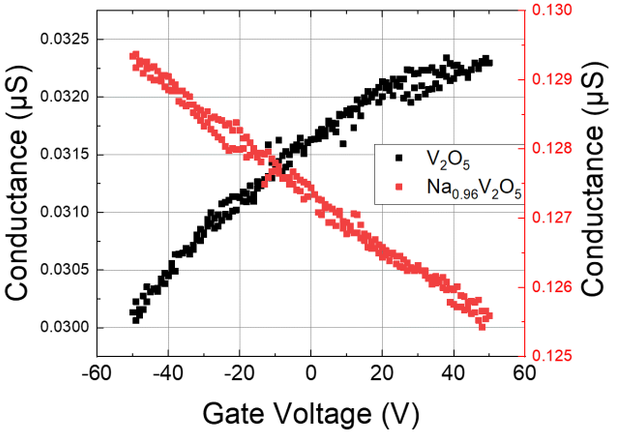

Fig. 14: Field-effect gate response for V_2O_5 and $Na_{0.96}V_2O_5$.

During our investigation, sodium-doped V_2O_5 mobility was observed to diminish in magnitude as flake thickness decreased, in contrast to our observations for undoped V_2O_5 flakes across the same thickness range. While a more thorough investigation of this behavior is required, we offer the speculation that sodium presence, or possibly absence, at the surface of the exfoliated $Na_{0.96}V_2O_5$ flakes may play a role, locally scattering charge carriers and inhibiting conduction in thinner system.

Surprisingly, of the experimental characterization which has been performed on electrical transport in NaV_2O_5 systems in the past, there is only a single mention of p-type conductivity by Carpy *et al.*[46] who obtained this result from thermoelectric measurement. However, the subject does not appear to have received attention as a focus in an experimental transport capacity as of yet.[46, 163–165] Given the contact resistance that accompanies a 2-probe configuration, the mobility extracted in our study of both systems is a few orders smaller than was observed in Sucharitakul *et al.* [39] Even so, we expect that this p-type mobility in NaV_2O_5 may be engineered to more significant magnitudes by controlling sodium stoichiometry.

Whereas oxygen deficiency in V_2O_5 donates electrons to the split-off band and leads to n-type conduction, sodium intercalation, with one Na ion per V_2O_5, leads to a splitting of the split-off band into spin-up and spin-down components, where charge donated by sodium fills the lower of these two bands. This half filling is directly linked to antiferromagnetic ordering observed in NaV_2O_5, and is examined in detail by Lambrecht and Bhandari.[10, 166] In the case of partial doping (that is, for $Na_xV_2O_5$, $x < 1.0$), the filling of the lower split-off band is incomplete, and results in a small fraction of empty acceptor states, leading to p-type transport. It follows that a greater deficit of Na should result in a greater p-type conduction, which should be limited only by the instability of the α-phase of $Na_xV_2O_5$ beyond $x < 0.7$.[161] Given the novelty of p-type transition metal oxides and their utility in the semiconducting industry, continued investigation of $Na_xV_2O_5$ at various stages of intercalation may lead to fruitful applications of this compound.

B. Transport in MoO_3

1. *Doping and Transport in MoO_3*

Transition metal oxides (TMOs) are often overlooked as candidates for the conducting component in 2D transistor applications because of their large native insulating behavior. However, these oxides offer a wide range of applications after minimal modification. MoO_3 has demonstrated its usefulness as a multifunctional material with its current uses ranging as an electrochromic material[167, 168], an optical and gas sensor[169, 170], and a hole-injection layer for organic photovoltaic cells.[171, 172] Recently MoO_3 has also been investigated for its applications in 2D field effect transistors (FETs) as both the conducting channel[173, 174] and as the gate oxide dielectric material.[175]

As mentioned in Sec. I, MoO_3 has an orthorhombic α-phase which allows for simple mechanical exfoliation. Specifically, α-MoO_3 is composed of double-layers of distorted MoO_6 octahedra bonded to adjacent layers via weak van der Waals (vdW) forces, which allows for isolation and study of 2D and few-layer systems.[176] Intrinsic α-MoO_3 has a large work function of > 6.9 eV and an even deeper ionization energy of > 9 eV which leads to a bandgap of $\sim$3eV.[177, 178]

Various methods of doping have been utilized to tune the electrical properties of α-MoO_3, enabling exploration of this oxide as a FET. For example, recently Crowley *et al.* demonstrated that exposure to H_2 gas at temperatures ranging from 275-400°C allowed for controllable reduction to a substoichiometric α-$MoO_{(3-x)}$.[174] Characteristics such as conductivity, field effect mobility, and carrier concentration increased as a function of reduction temperature, and showed consistent n-type behavior. Electron conduction in α-$MoO_{(3-x)}$ is indeed consistent with theoretical predictions,[42] despite previous accounts of hole-conduction in similar systems by other groups.[179, 180]

Recently, the creation of oxygen vacancies via hydrogen doping has been used to purposefully tune the conductivity and electron mobility of MoO_3, making it a more suitable and controllable candidate for 2D transistors.[174, 180, 181] For instance, Crowley *et al.*[174] demonstrated that exposure to H_2 gas at temperatures ranging from 275-400°C caused a reduction in the MoO_3, forming a more conductive substoichiometric $MoO_{(3-x)}$. This study revealed that the conductivity, field effect mobility, and carrier concentration increased as a function of reduction temperature, and thus reduc-

tion rate, and showed consistent n-type behavior of the modified MoO_3.

Another method of transport enhancement under recent investigation is via utilization of fluorine. Fluorination of α-MoO_3 has until recently only been examined using first-principles methods, where F is predicted to replace the doubly coordinated oxygen and facilitate Mg diffusion throughout the lattice.[182] Experimentally, F exposure via dry-etching with SF_6 plasma was found to impact n-type mobility in a similar manner as oxygen deficiency, albeit to a lesser magnitude. Interestingly, this effect was observed to be reversible upon annealing the exposed flakes in an inert atmosphere, returning the α-MoO_3 to an insulating state. F presence was observed to impact the terminal oxygen in α-MoO_3, suggesting that fluorine may provide a means of engineering n-type effects via surface interaction, without permanently impacting oxide stoichiometry.

2. *Opportunities for 2D MoO_3-based Transistors*

Since α-MoO_3 intrinsically has a band gap of $\sim$3eV, it seems natural to realize its function as a dielectric material for 2D semiconductor devices. In a recent paper, Holler *et al.*[175] demonstrated that MoO_3 can act as the top-gating material in layered 2D semiconductor FETs. This was motivated by experimental claims of thin-film MoO_3 having a large dielectric constant.[183–186] some reporting a low-frequency κ as high as $\sim$200.[183] In their study, they fabricated MoO_3 single crystal parallel-plate capacitors and measured the 90 degrees out-of-phase ac current to calculate a dielectric constant κ approximately 35 near 0Hz, (figure 15a), which is approximately ten times greater than that of SiO_2 and also greater than other comparable non-vdW high-κ oxides such as ZrO_2 and HfO_2.[187–190] This high value of the static dielectric constant differs significantly from the calculated values[119] for pure insulating α-MoO_3 including phonon contributions, which are 27, 13 and 7 along b, c, a in the standard *Pnma* setting of the spacegroup. This indicates an extrinsic origin related to the non-zero conductivity in these samples.

WSe_2/MoO_3 heterostructures were fabricated by exfoliation via the adhesive tape method and then transferred onto a 300nm Si/Si^{++} substrate. The MoO_3 was carefully stacked onto the WSe_2 via a polydimethylsiloxane (PDMS) stamp. The source and drain electrodes in addition to the top-gate were fabricated via electron-beam lithography, as seen in figure 15b. As presented in figure 15c, MoO_3 proves to be capable of properly gating the WSe_2 device, sweeping the gate voltage from -10V to +10V. The electron field effect mobility, μ_{FET}, was calculated to be 1.62 $\mathrm{cm^2V^{-1}s^{-1}}$ and can be improved by increasing the surface area coverage of of the top gate material with respect to uncovered WSe_2. The device exhibits an on/off ratio of approximately 10^3 and a subthreshold swing of approximately 2.2V/dec.

Due to its deep work function and relative band alignment, the MoO_3 top-gate was also shown to induce holes in the WSe_2 layer, allowing for another option to control and modify the properties of the conducting channel.[191, 192] This comparison was performed using the SiO_2 back-gate before and after the MoO_3 layer was stacked. The device illustrates a threshold shift $\Delta V_{\mathrm{T}} = +7$V, indicating a shift towards more p-type behavior, in addition to a clear p-type response at negative gate voltages (see figure 15d).

MoO_3 has proven itself to be an interesting candidate for many 2D transistor applications. It has been shown that hydrogen doping of MoO_3 consistently resulted in n-type semiconducting characteristics, and it was observed that MoO_3 reduces much more readily than previously reported. This was confirmed via measurements of conductivity, mobility, and carrier concentration for multiple annealing temperatures in a hydrogen forming gas. Also, the effects of fluorine doping were observed with MoO_3: it has been shown that F presence likely impacts certain oxygen species, such as replacement of the doubly coordinated oxygen, or can adsorb on the surface. Lastly, in contrast to studying its conductive properties, intrinsic, undoped MoO_3 displays a large dielectric constant at DC and low-frequency measurements and α-phase MoO_3 has been demonstrated to work as the gate oxide dielectric material for 2D semiconductor FETs. The culmination of these studies have validated that MoO_3 is worth continued research due to its expressive multi-functionality and potential applications.

C. Transport in 2D $LiCoO_2$ Nanosystems

$LiCoO_2$ (LCO) belongs to the rhombohedral space group $R\bar{3}m$ with trigonal layer symmetry, with alternately stacked LiO_6 and CoO_6 octahedra in the c-direction.[193, 194] Typically, this material is characterized in its bulk form ($>$ 0.1mm thickness) as single crystals or compressed polycrystalline pellets, due to the strong cohesion between layers from electrostatic stabilization. LCO is often studied as a processed powder, or obtained through ion replacement methods from $NaCoO_2$.[195] Delithiation studies use chemical or electrochemical (EC) methods[196–199] to examine the effects of partial lithium loss. As already mentioned in Sec. I, in its stoichiometric form, LCO is insulating, where all electrons are paired and cobalt is in the low-spin configuration of Co^{3+}.[200] As the oxide is delithiated, it loses an electron with each lithium ion, forcing the surrounding lattice to compensate the charge loss. While this is often referred to as the formation of Co^{4+} ions, it is not evident whether localized Co^{4+} ions actually form or whether the holes are distributed in extended states as in a p-type semiconductor. Wolverton and Zunger [77] noted that the net charge in a sphere around Co actually barely changes upon delithiation and the different nominal valence is rather accomodated by changes in the

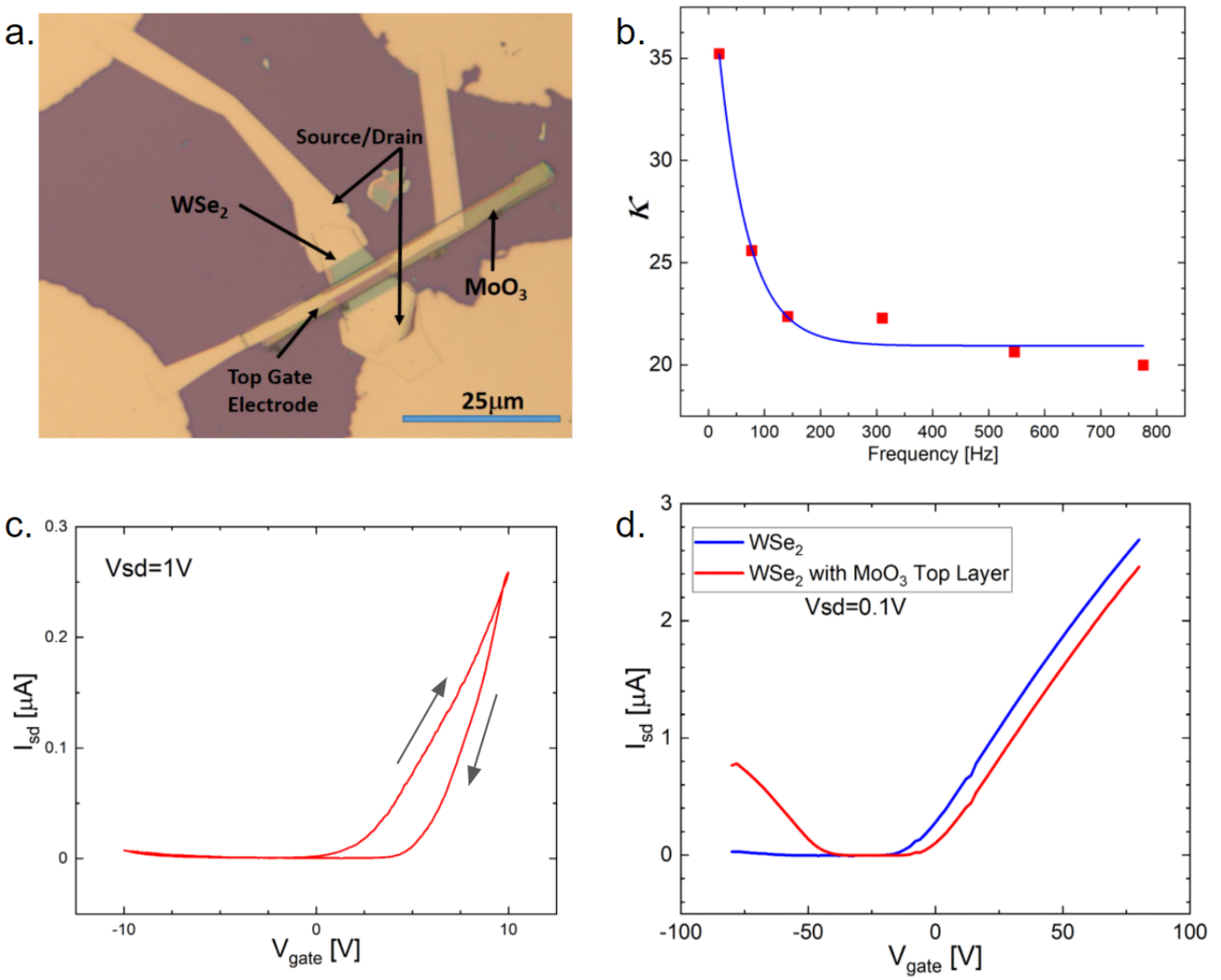

Fig. 15: a) Optical photograph of WSe_2/MoO_3 FET. b) Dielectric constant, κ, of MoO_3 ranging over low frequencies. c) Top-gate behavior of WSe_2/MoO_3 FET. d) Hole inducing behavior after exfoliated MoO_3 is layered on top of WSe_2. Parts of this Figure are Reproduced with permission from Advanced Electronic Materials **6**, 2000635 (2020). Copyright 2020 Wiley.

degree of covalency of the O-Co bonds. As mentioned in Sec. III the highest average Co valence deduced from electron loss spectroscopy of the L_2/L_3 edges is only 3.3 for $Li_{0.37}CoO_2$.[56] Thus, delithiation in Li_xCoO_2 leads to both increased p-type conductivity via thermally activated hopping conduction[201, 202] as well as the emergence of an overall magnetic moment.[151, 196, 203] As delithiation continues, conduction transitions from an insulating variable-range hopping to a classical metallic conduction, with a transition typically observed around the $x = 0.75 - 0.9$ range.[201, 203–205] However, a low carrier concentration, coupled with a variety of scattering mechanisms (such as lithium vacancies) results in low mobility and a small magnitude of current.[202]

The transition of LCO to a metallic phase is also accompanied by the phenomenon known as charge ordering, which tends to occur in strongly correlated oxides, such as magnetite and doped magnetite.[206, 207] The commonly accepted mechanism of charge ordering is such that there is a repeating alternation of oxidation states among the metal cation species in an ionic lattice, occurring at low enough temperatures where charge fluctuation due to ion diffusion is no longer energetically favorable. For LCO, as the ratio of Co^{4+}/Co^{3+} increases, charge is balanced among the surrounding Co sites for each lithium vacancy to minimize energy, achieved via localized lithium diffusion throughout the lattice. At low enough temperature, lithium diffusion is halted, and the Co network assumes a stable charge ordering. This coordination can impact macroscopic characteristics, cre-

ating anomalies or jumps in electrical resistance and magnetic susceptibility when monitoring across the transition temperature. This has been observed in many cases for LCO, with a documented transition at T_s = 150-175K, over a lithium content range of x =0.46-0.78.[75, 195, 196, 199, 201, 203, 208–211] It has been assumed that this ordering favors fractional lithium contents of $x = 2/3$ and $1/2$,[204] with calculations of another minima in energy at $x = 1/3$, though this last fraction has not been conclusively observed.[211]

Despite all of the previously detailed delithiation effects of LCO, this process is actually still not well-understood. For example, while the insulator-metal transition is commonly observed in many studies, there is no consensus on an exact value of lithium content required for this change to occur, as is evident in the broad range x reported above. Further, the charge ordering transition T_s is observed over large temperature ranges and lithium concentrations, and has proven extremely difficult to predict. In a 2012 article, Yang et al. compend anomaly observations among 12 separate studies, comparing forms of LCO and the deintercalation methods used.[151] Observations vary for multiple phases of LCO (compressed powder pellets, single crystals, thin films), where multiple approaches are used for preparation and delithiation (chemical, EC-galvanostatic, EC-potentiostatic, ion exchange + chemical). The takeaway is that this anomaly is observed in a variety of experimental conditions, yet at times is not present when anticipated.

From our perspective, this ambiguity is in large part due to most previous investigation taking place on bulk systems using polycrystalline or compressed powders, instead of few-layer, single-crystal LCO. With bulk systems, galvanostatic and chemical delithiation typically occur radially inward, where outer layers delithiate to a greater extent than do inner layers. The degree of delithiation in such studies is typically assessed via measurement of surface potential, which masks the radial inhomogeneity of Li distribution.[151] In such cases, there is a large degree of variability permitted, which may explain the broad range of observations from previous studies. If charge ordering effects in LCO are to be investigated with any consistency, it becomes imperative to develop a method for isolating thin single-crystal LCO flakes. The dimensionality of such a mesoscopic systems is advantageous in this pursuit, with flake areas large enough to facilitate nanofabrication, yet small enough to minimize any radial delithitaion effects.

As previously detailed in Sec.II, the methods for LCO exfoliation first developed by Kim et al. have been improved upon, investigating electrostatic bonding between the transition metal oxide and alkali ion layers.[64, 65] Chemical exfoliation of LCO powder leads to large, swelled powder granules. Once dried, these can then be mechanically exfoliated, producing 10-100nm thick single-crystal flakes of $LiCoO_2$. It is this step of following chemical exfoliation by scotch-tape mechanical exfoliation which has led to the largest lateral area single-crystal flakes of $LiCoO_2$ yet observed. The size of these flakes enables the use of 2D electrical characterization techniques, such as 4-probe Hall measurements, to be utilized for $LiCoO_2$ for the first time. Our exploratory investigation has already provided much perspective between bulk and 2D transport, as well as some experimental insight on the complex correlated effects and phenomena detailed in section 5B.

In the 2D form, Li_xCoO_2 flakes are able to be masked, and metallic contacts deposited on the ends of the flake, as in Figure 16a. Perhaps the most obvious consequence of few layer LCO is the contact energy barrier formation for all tested conditions. Under a variety of metals and materials, Li_xCoO_2 nanoflakes exhibit a Schottky barrier in their IV curve (Figure 16b). When using divalent metals for electrodes, a doping effect with increased current magnitude is observed, seen here for the case of Ni. This is anticipated, and detailed in full elsewhere.[55, 212] The 2D LCO flakes of various lithium contents also reflect bulk transport characteristics, exhibiting lower resistivity as delithiation increases, and an insulator-metal transition below x=0.79 (figure 16c).[55]

Further experimentation is required to deduce the origin of the persistent Schottky barrier in Figure 16b. However, it is interesting to note that our exfoliation method discussed in Sec.II preferentially cleaves LCO along lithium planes, potentially leaving at least a partial exposed lithium layer on the surface of the flake. While at present we have no direct experimental confirmation of the Li termination of the surface or even less a qualitative determination of how much Li remains on the surface, the presence of Li on cleaved LCO single crystal surfaces has been observed by Iwaya *et al.* [75]. The consequence of a terminal lithium layer was the subject of discussion in Sec. VII B and [141] where a 2DEG was predicted to exist above the surface of the flake. We offer the speculation that if the electron gas were indeed present, it would certainly pose a large energy barrier needing to be overcome for hole-conduction between LCO and the contacting metal to take place, which could explain qualitatively the Schottky barrier behavior observed here.

As was mentioned previously, a unique advantage of using the delithiation technique presented in Sec. II is the low dimensionality of the resulting LCO flakes. In terms of electrical characterization, a bulk system may contain radial inhomogeneities of Li, spanning several hundreds of microns between electrodes, whereas a single-crystal nanoflake with a 5-10 micron conduction channel may have a higher likelihood of uniform Li distribution. Indeed, inhomogeneous Li distributions in LCO often lead to observation of a spinel phase, whereas our own nanoflakes were observed to be in the more stable $C2/m$ phase as discussed in Sec. III and [56]

The concept of charge ordering relies on Li ion distributions that are orderly enough to allow fluctuation and settling into a repeating pattern at low temperature. Curiously, to this effect, anomalies in the resistance-temperature curves were observed in prepared batches of

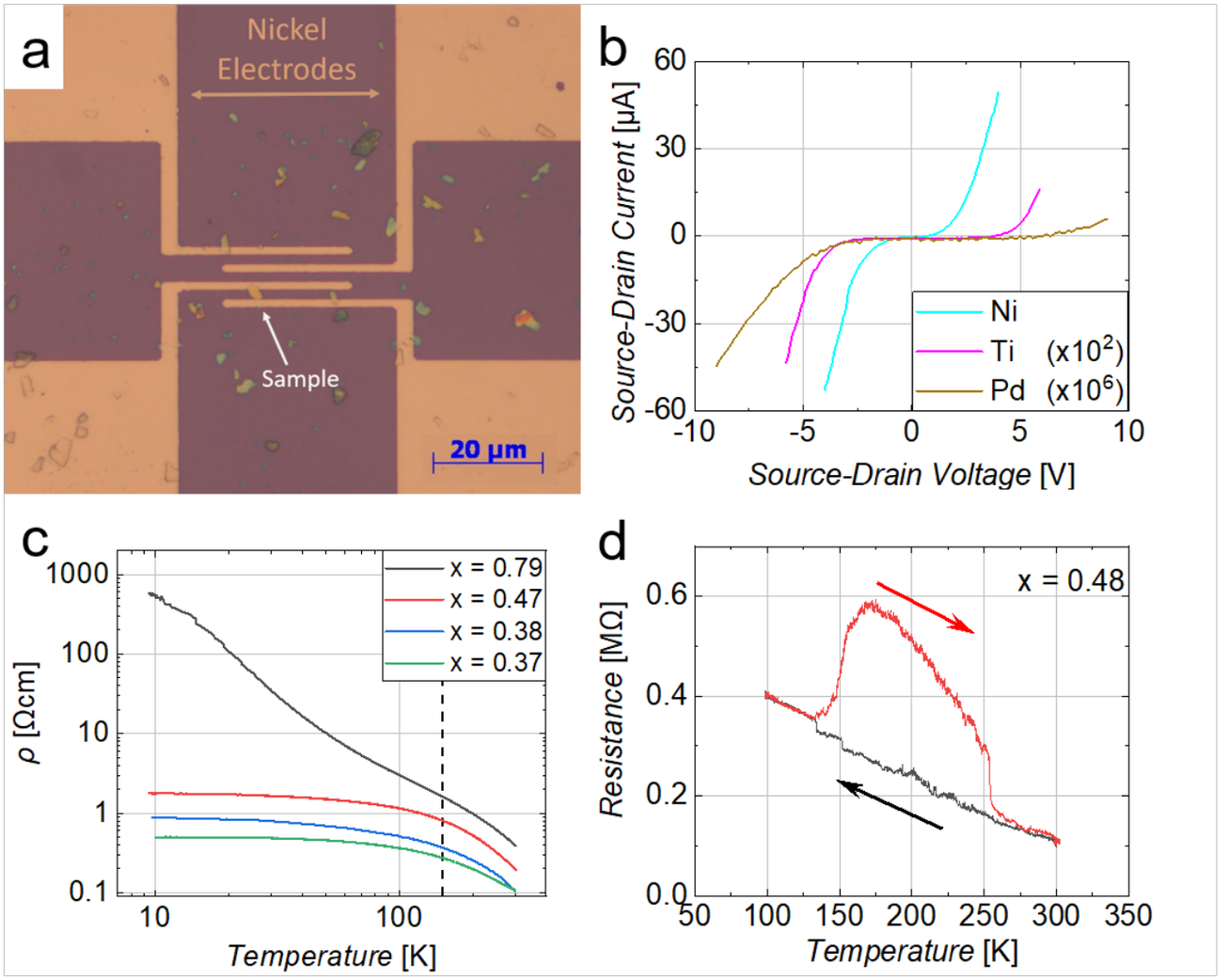

Fig. 16: a) Optical image of Li_xCoO_2 flakes with assembled source and drain electrodes. b) Source-drain curves of 2D Li_xCoO_2 flakes using various contact metals. Current magnitudes displayed here were multiplied by a factor for each metal, indicated at bottom-right; Ni has highest magnitude of current. c) Transport in Li_xCoO_2. Various lithium concentrations are indicated at top-right. Dashed line is inset at T_c=150K. d) Charge ordering effects in Li_xCoO_2 flakes. Anomalies in the resistance data were observed for 3-day prepared x=0.46 flakes upon warming up. The anomaly begins at around T$\sim$ 150K during the warm up. Figure adapted with permission from J. Phys. Chem. C **124**, 20693 (2020). Copyright 2020, American Chemical Society.

x=0.48 and 0.37 flakes which had been chemically delithiated over a 3 day period (figure 16d). Samples which had delithiated at a faster rate, over 1 day with stronger acid concentration, did not possess charge ordering phenomena despite having near-identical lithium content. Additionally, the anomalies in resistance for thin LCO flakes were markedly larger in magnitude than most previous bulk reports. In one case, a repeatable >1MΩ increase in resistance was observed near T_s. It is possible that the lower dimensionality of thin LCO flakes enables a greater switching control on electrical current, where a larger percentage of the conducting channel is influenced by charge ordering effects than in bulk systems.

It is apparent that being able to study LCO in a thin dimensionality is advantageous. In the initial explorational study, much insight has been gained on some of the fundamental aspects of LCO, among other predictions of a surface 2DEG finding its origin in topological band structure effects by Radha *et al.*[141] as dicussed in Sec. VII B. Other observations which still bear repeating and understanding, such as superconductivity in swollen LCO, have the potential to benefit from this new approach, to further our understanding of such correlated transition metal oxides.

IX. CONCLUSION

In this perspective paper, we have focused on three layered oxide materials, V_2O_5, MoO_3 and $LiCoO_2$, the first two examples of van der Waals bonded oxides and the latter exhibiting mostly ionic bonding between CoO_2^{-1} layers and Li^{+1} layers. The former can be exfoliated by means of mechanical exfoliation while the latter requires chemical exfoliation techniques to obtain atomically thin layers. By carrying out combined studies of their electronic, phonon and transport properties, insights were gained in how such two-dimensionality affects these oxide's fundamental properties. The effects of phase transitions and ordering were found to be important in $LiCoO_2$. As is always the case in oxides, point defects and their distribution may play a major role in the further development and control in such 2D oxides.

From the theory point of view, interesting effects were predicted, for example phonon frequency shifts, related to changes in 2D screening as well as the breaking of the weak van der Waals bonds. The electronic structure of oxides is a complex problem because even small changes may result in strong correlation effects. For instance in $LiCoO_2$, partial delithiation can break the non-magnetic band filling favored by perfect Li electron donation to the CoO_2 layers resulting in a perfect d^6 configuration. Such effects were observed to occur after annealing of the $LiCoO_2$ nanoflakes resulting in disordering of the remaining Li and Co and formation of more correlated and lower transport phases. It also leads to interesting magnetic anomalies due to the formation of magnetic moments upon delithiation, which had been previously observed in bulk but appear to be more prominent in ultrathin 2D $LiCoO_2$. In V_2O_5 and MoO_3 which are intrinsically relatively wide gap insulators, n-type conduction can be caused by oxygen vacancies or intentional intercalation with alkali or alkaline-earth atoms donating their electrons. This allows for the fabrication of nanoscale field gate transistor structures and measurements of their intrinsic transport properties. However, the intricate band structure of V_2O_5, which has 1D aspects related to the occurrence of chains within the layers can also lead to strong anisotropy of the conduction in the plane and intriguing magnetic effects. To fully understand how these differ in 2D versions, where reduced screening plays a major role, a better understanding of the electronic structure will be required as well as better control over defects and further refinements of the exfoliation techniques to obtain truly monolayer and large lateral area materials.

While standard DFT appears to provide reasonable band gaps and band structures, the for most semiconductors almost perfectly reliable *GW* method failed to predict the correct band gaps in V_2O_5 as well as in $LiCoO_2$ and the verdict is still out on MoO_3. It strongly overestimates the gaps by several eV. In $LiCoO_2$ surprisingly, one needs to invoke highly localized Frenkel type excitonic effects to understand the nature of the optical band gap and we expect that the same will be true in V_2O_5. Electron phonon coupling effects and in particular polaron formation is also expected to play a major role because of the large differences in static and high-frequency dielectric constants and the rather flat valence and conduction bands with high effective masses, which will tend to localize carriers in self-trapped polarons at low temperature. Since the self-energy that affects both one-particle spectra and two particle (*i.e.* optical) spectra is long-range both the fundamental quasiparticle gap and the optical gap will be strongly affected by 2D induced changes in screening. While realizing true monolayer 2D physics in these oxides remains challenging, the atomically thin nanostructures studied so far already hold surprises. The interplay between theory and experiment is important. The computational study of 2D Li-covered CoO_2 layers inspired by the exfoliation experiments revealed the presence of a spin-polarized 2DEG on their surface mediated by the Li bands coming down in energy and this in turn was shown to be evidence of at least partially covalent bonding between Li and CoO_2 layers which has topological consequences at the surface. In turn the bonding of Li (or Na) to CoO_2 layers in bulk undergoes a symmetry breaking transition when the layers are pulled apart beyond a critical distance and may lead to essentially a stack of monolayers still associated with Li or Na on one side and a Li or Na free surface on the other side. The presence of an electron gas formation under these circumstances may shed important new light on the superconductivity in hydrated (and hence layer expanded) Na_xCoO_2. Our detailed studies of the exfoliation process itself as well as the effects of annealing reveals that chemical exfoliation is a complex process with many still to be fully understood aspects. Many dots remain to be connected. As an outlook, we may expect much new and interesting physics from oxide systems when they finally break into the world of 2D monolayer materials. Their rich crystal structures and types of bonding and spin-dependent and correlated electronic structure will no doubt hold surprises for future research.

ACKNOWLEDGMENTS

This work was supported by the US Air Force Office of Scientific Research under grant No. Grant No. FA9550-18-1-0030. The calculations made use of the High Performance Computing Resource in the Core Facility for Advanced Research Computing at Case Western Reserve University. We would like to acknowledge Mourad Zeynalov for his experimental contributions throughout the α-$Na_{0.96}V_2O_5$ project. We thank Kenta Kimura and Tsuyoshi Kimura for providing NaV_2O_5 crystals.

Data Availability: The data that support the findings of this study are available from the corresponding author upon reasonable request.

[1] E. A. Abbott, *Flatland: A Romance in Many Dimensions* (New York: Dover Thrift Edition, 1884).
[2] K. S. Novoselov, A. K. Geim, S. V. Morozov, D. Jiang, Y. Zhang, S. V. Dubonos, I. V. Grigorieva, and A. A. Firsov, Electric Field Effect in Atomically Thin Carbon Films, Science **306**, 666 (2004).
[3] L. Li, Y. Yu, G. J. Ye, Q. Ge, X. Ou, H. Wu, D. Feng, X. H. Chen, and Y. Zhang, Black phosphorus field-effect transistors, Nature Nanotechnology **9**, 372 (2014).
[4] S. K. Radha and W. R. L. Lambrecht, Topological band structure transitions and goniopolar transport in honeycomb antimonene as a function of buckling, Phys. Rev. B **101**, 235111 (2020).
[5] P. Ares, J. J. Palacios, G. Abellán, J. Gómez-Herrero, and F. Zamora, Recent Progress on Antimonene: A New Bidimensional Material, Advanced Materials **30**, 1703771 (2018).
[6] J. Sone, T. Yamagami, Y. Aoki, K. Nakatsuji, and H. Hirayama, Epitaxial growth of silicene on ultrathin Ag(111) films, New Journal of Physics **16**, 095004 (2014).
[7] K. F. Mak, C. Lee, J. Hone, J. Shan, and T. F. Heinz, Atomically Thin MoS_2: A New Direct-Gap Semiconductor, Phys. Rev. Lett. **105**, 136805 (2010).
[8] B. Radisavljevic, A. Radenovic, J. Brivio, V. Giacometti, and A. Kis, Single-layer MoS2 transistors, Nature Nanotechnology **6**, 147 (2011).
[9] K. T. Faber, T. Asefa, M. Backhaus-Ricoult, R. Brow, J. Y. Chan, S. Dillon, W. G. Fahrenholtz, M. W. Finnis, J. E. Garay, R. E. García, Y. Gogotsi, S. M. Haile, J. Halloran, J. Hu, L. Huang, S. D. Jacobsen, E. Lara-Curzio, J. LeBeau, W. E. Lee, C. G. Levi, I. Levin, J. A. Lewis, D. M. Lipkin, K. Lu, J. Luo, J.-P. Maria, L. W. Martin, S. Martin, G. Messing, A. Navrotsky, N. P. Padture, C. Randall, G. S. Rohrer, A. Rosenflanz, T. A. Schaedler, D. G. Schlom, A. Sehirlioglu, A. J. Stevenson, T. Tani, V. Tikare, S. Trolier-McKinstry, H. Wang, and B. Yildiz, The role of ceramic and glass science research in meeting societal challenges: Report from an NSF-sponsored workshop, Journal of the American Ceramic Society **100**, 1777 (2017).
[10] C. Bhandari and W. R. L. Lambrecht, Electronic and magnetic properties of electron-doped V_2O_5 and NaV_2O_5, Phys. Rev. B **92**, 125133 (2015).
[11] R. Ma and T. Sasaki, Nanosheets of Oxides and Hydroxides: Ultimate 2D Charge-Bearing Functional Crystallites, Advanced Materials **22**, 5082 (2010).
[12] R. Ma and T. Sasaki, Two-Dimensional Oxide and Hydroxide Nanosheets: Controllable High-Quality Exfoliation, Molecular Assembly, and Exploration of Functionality, Accounts of Chemical Research **48**, 136 (2015), pMID: 25490186.
[13] R. Mas-Ballesté, C. Gómez-Navarro, J. Gómez-Herrero, and F. Zamora, 2D materials: to graphene and beyond, Nanoscale **3**, 20 (2011).
[14] R. Hinterding and A. Feldhoff, Two-Dimensional Oxides: Recent Progress in Nanosheets, Zeitschrift für Physikalische Chemie **233**, 117 (2019).
[15] R. Uppuluri, A. Sen Gupta, A. S. Rosas, and T. E. Mallouk, Soft chemistry of ion-exchangeable layered metal oxides, Chem. Soc. Rev. **47**, 2401 (2018).
[16] J. Liu and X.-W. Liu, Two-Dimensional Nanoarchitectures for Lithium Storage, Advanced Materials **24**, 4097 (2012).
[17] M. Osada and T. Sasaki, Two-Dimensional Dielectric Nanosheets: Novel Nanoelectronics From Nanocrystal Building Blocks, Advanced Materials **24**, 210 (2012).
[18] V. Nicolosi, M. Chhowalla, M. G. Kanatzidis, M. S. Strano, and J. N. Coleman, Liquid Exfoliation of Layered Materials, Science **340**, 10.1126/science.1226419 (2013).
[19] I. Y. Kim, Y. K. Jo, J. M. Lee, L. Wang, and S.-J. Hwang, Unique Advantages of Exfoliated 2D Nanosheets for Tailoring the Functionalities of Nanocomposites, The Journal of Physical Chemistry Letters **5**, 4149 (2014).
[20] E. Lee, Y. S. Yoon, and D.-J. Kim, Two-Dimensional Transition Metal Dichalcogenides and Metal Oxide Hybrids for Gas Sensing, ACS Sensors **3**, 2045 (2018).
[21] K. Kalantar-zadeh, J. Z. Ou, T. Daeneke, A. Mitchell, T. Sasaki, and M. S. Fuhrer, Two dimensional and layered transition metal oxides, Applied Materials Today **5**, 73 (2016).
[22] J. E. ten Elshof, H. Yuan, and P. Gonzalez Rodriguez, Two-Dimensional Metal Oxide and Metal Hydroxide Nanosheets: Synthesis, Controlled Assembly and Applications in Energy Conversion and Storage, Advanced Energy Materials **6**, 1600355 (2016).
[23] C. Tan, X. Cao, X.-J. Wu, Q. He, J. Yang, X. Zhang, J. Chen, W. Zhao, S. Han, G.-H. Nam, M. Sindoro, and H. Zhang, Recent Advances in Ultrathin Two-Dimensional Nanomaterials, Chemical Reviews **117**, 6225 (2017).
[24] P. Xiong, Y. Wu, Y. Liu, R. Ma, T. Sasaki, X. Wang, and J. Zhu, Two-dimensional organic–inorganic superlattice-like heterostructures for energy storage applications, Energy Environ. Sci. , (2020).
[25] N. Mahmood, I. A. De Castro, K. Pramoda, K. Khoshmanesh, S. K. Bhargava, and K. Kalantar-Zadeh, Atomically thin two-dimensional metal oxide nanosheets and their heterostructures for energy storage, Energy Storage Materials **16**, 455 (2019).
[26] H. Pang, X. Cao, L. Zhu, and M. Zheng, *Synthesis of Functional Nanomaterials for Electrochemical Energy Storage* (Springer, Singapore, 2020) pp. 59–66,201–205.
[27] F. Haque, T. Daeneke, K. Kalantar-zadeh, and J. Z. Ou, Two-Dimensional Transition Metal Oxide and Chalcogenide-Based Photocatalysts, Nano-Micro Letters **10**, 23 (2017).
[28] C. J. Heard, J. Čejka, M. Opanasenko, P. Nachtigall, G. Centi, and S. Perathoner, 2D Oxide Nanomaterials to Address the Energy Transition and Catalysis, Advanced Materials **31**, 1801712 (2019).
[29] Y. Zhang, L. Li, S.-X. Guo, X. Zhang, F. Li, A. M. Bond, and J. Zhang, Two-Dimensional Electrocatalysts for Efficient Reduction of Carbon Dioxide, ChemSusChem **13**, 59 (2020).
[30] M. Safarpour, S. Arefi-Oskoui, and A. Khataee, A review on two-dimensional metal oxide and metal hydroxide nanosheets for modification of polymeric membranes, Journal of Industrial and Engineering Chemistry **82**, 31 (2020).

[31] K. Shavanova, Y. Bakakina, I. Burkova, I. Shtepliuk, R. Viter, A. Ubelis, V. Beni, N. Starodub, R. Yakimova, and V. Khranovskyy, Application of 2d non-graphene materials and 2d oxide nanostructures for biosensing technology, Sensors **16**, 223 (2016).

[32] A. P. Dral and J. E. ten Elshof, 2D metal oxide nanoflakes for sensing applications: Review and perspective, Sensors and Actuators B: Chemical **272**, 369 (2018).

[33] Y. K. Jo, J. M. Lee, S. Son, and S.-J. Hwang, 2D inorganic nanosheet-based hybrid photocatalysts: Design, applications, and perspectives, Journal of Photochemistry and Photobiology C: Photochemistry Reviews **40**, 150 (2019).

[34] F. Yang, P. Song, M. Ruan, and W. Xu, Recent progress in two-dimensional nanomaterials: Synthesis, engineering, and applications, FlatChem **18**, 100133 (2019).

[35] T. Yang, T. T. Song, M. Callsen, J. Zhou, J. W. Chai, Y. P. Feng, S. J. Wang, and M. Yang, Atomically Thin 2D Transition Metal Oxides: Structural Reconstruction, Interaction with Substrates, and Potential Applications, Advanced Materials Interfaces **6**, 1801160 (2019).

[36] J. Yang, Z. Zeng, J. Kang, S. Betzler, C. Czarnik, X. Zhang, C. Ophus, C. Yu, K. Bustillo, M. Pan, J. Qiu, L.-W. Wang, and H. Zheng, Formation of two-dimensional transition metal oxide nanosheets with nanoparticles as intermediates, Nature Materials **18**, 970 (2019).

[37] Y. Xiao, N. M. Abbasi, Y.-F. Zhu, S. Li, S.-J. Tan, W. Ling, L. Peng, T. Yang, L. Wang, X.-D. Guo, Y.-X. Yin, H. Zhang, and Y.-G. Guo, Layered Oxide Cathodes Promoted by Structure Modulation Technology for Sodium-Ion Batteries, Advanced Functional Materials **30**, 2001334 (2020).

[38] G. Barcaro and A. Fortunelli, 2D oxides on metal materials: concepts, status, and perspectives, Phys. Chem. Chem. Phys. **21**, 11510 (2019).

[39] S. Sucharitakul, G. Ye, W. R. Lambrecht, C. Bhandari, A. Gross, R. He, H. Poelman, and X. P. Gao, V2O5: A 2D van der Waals Oxide with Strong In-Plane Electrical and Optical Anisotropy, ACS Applied Materials and Interfaces **9**, 23949 (2017).

[40] P. R. Reshma, P. Anees, K. Ganesan, P. Arun, and S. Dhara, Electronic and vibrational decoupling in chemically exfoliated bilayer 2D-V_2O_5 (2021), Research Square Preprint, DOI:10.21203/rs.3.rs-273236/v1.

[41] L. Seguin, M. Figlarz, R. Cavagnat, and J.-C. Lassègues, Infrared and Raman spectra of MoO3 molybdenum trioxides and MoO3 · xH2O molybdenum trioxide hydrates, Spectrochimica Acta Part A: Molecular and Biomolecular Spectroscopy **51**, 1323 (1995).

[42] W. B. Zhang, Q. Qu, and K. Lai, High-mobility transport anisotropy in few-layer MoO3 and its origin, ACS Applied Materials and Interfaces **9**, 1702 (2017).

[43] D. O. Scanlon, A. Walsh, B. J. Morgan, and G. W. Watson, An ab initio Study of Reduction of V2O5 through the Formation of Oxygen Vacancies and Li Intercalation, The Journal of Physical Chemistry C **112**, 9903 (2008).

[44] P. Watthaisong, S. Jungthawan, P. Hirunsit, and S. Suthirakun, Transport properties of electron small polarons in a V2O5 cathode of Li-ion batteries: a computational study, RSC Adv. **9**, 19483 (2019).

[45] L. Ngamwongwan, I. Fongkaew, S. Jungthawan, P. Hirunsit, S. Limpijumnong, and S. Suthirakun, Electronic and thermodynamic properties of native point defects in V2O5: a first-principles study, Phys. Chem. Chem. Phys. , (2021).

[46] A. Carpy, A. Casalot, M. Pouchard, J. Galy, and P. Hagenmuller, Propriétés electriques et magnétiques des bronzes oxyfluorés de vanadium de formule α'-NaV2O5-xFx ($0 \leq x \leq 1$) , Journal of Solid State Chemistry **5**, 229 (1972).

[47] C. Bhandari, W. R. L. Lambrecht, and M. van Schilfgaarde, Quasiparticle self-consistent *gw* calculations of the electronic band structure of bulk and monolayer v_2o_5, Phys. Rev. B **91**, 125116 (2015).

[48] M. Isobe and Y. Ueda, Magnetic Susceptibility of Quasi-One-Dimensional Compound α'- NaV2O5 - Possible Spin-Peierls Compound with High Critical Temperature of 34 K, Journal of the Physical Society of Japan **65**, 1178 (1996), http://dx.doi.org/10.1143/JPSJ.65.1178.

[49] J. Galy, Vanadium pentoxide and vanadium oxide bronzes—Structural chemistry of single (S) and double (D) layer MxV2O5 phases, Journal of Solid State Chemistry **100**, 229 (1992).

[50] A. Stavenhagen and E. Engels, Ueber Molybdänbronzen, Berichte der deutschen chemischen Gesellschaft **28**, 2280 (1895).

[51] M. S. Whittingham, Lithium Batteries and Cathode Materials, Chemical Reviews **104**, 4271 (2004), pMID: 15669156.

[52] L. R. De Jesus, G. A. Horrocks, Y. Liang, A. Parija, C. Jaye, L. Wangoh, J. Wang, D. A. Fischer, L. F. J. Piper, D. Prendergast, and S. Banerjee, Mapping polaronic states and lithiation gradients in individual V2O5 nanowires, Nature Communications **7**, 12022 (2016).

[53] S. Tepavcevic, Y. Liu, D. Zhou, B. Lai, J. Maser, X. Zuo, H. Chan, P. Král, C. S. Johnson, V. Stamenkovic, N. M. Markovic, and T. Rajh, Nanostructured Layered Cathode for Rechargeable Mg-Ion Batteries, ACS Nano **9**, 8194 (2015).

[54] M. Panagopoulou, D. Vernardou, E. Koudoumas, D. Tsoukalas, and Y. S. Raptis, Tungsten doping effect on V_2O_5 thin film electrochromic performance, Electrochimica Acta **321**, 134743 (2019).

[55] K. Crowley, K. Pachuta, S. K. Radha, H. Volkova, A. Sehirlioglu, E. Pentzer, M. H. Berger, W. R. Lambrecht, and X. P. Gao, Electrical characterization and charge transport in chemically exfoliated 2D Li_xCoO_2 nanoflakes, Journal of Physical Chemistry C **124**, 20693 (2020).

[56] H. Volkova, K. Pachuta, K. Crowley, S. K. Radha, E. Pentzer, X. P. A. Gao, W. R. L. Lambrecht, A. Sehirlioglu, and M.-H. Berger, Electron microscopy and spectroscopic study of structural changes, electronic properties, and conductivity in annealed Li_xCoO_2, Phys. Rev. Materials **5**, 015401 (2021).

[57] F. L. Ning and T. Imai, ^{17}O NMR Studies of a Triangular-Lattice Superconductor $Na_xCoO_2 \cdot yH_2O$, Phys. Rev. Lett. **94**, 227004 (2005).

[58] H. K. Yoshida, S. E. Dissanayake, A. D. Christianson, C. R. dela Cruz, Y.-Q. Cheng, S. Okamoto, K. Yamaura, M. Isobe, and M. Matsuda, Static and dynamic spin properties in the quantum triangular lattice antiferromagnet Ag_2CoO_2, Phys. Rev. B **102**, 024445 (2020).

[59] K. Takada, H. Sakurai, E. Takayama-Muromachi,

F. Izumi, R. A. Dilanian, and T. Sasaki, Superconductivity in two-dimensional coo2 layers, Nature **422**, 53 (2003).

[60] T. Sasaki and M. Watanabe, Osmotic swelling to exfoliation. exceptionally high degrees of hydration of a layered titanate, Journal of the American Chemical Society **120**, 4682 (1998).

[61] Y. Omomo, T. Sasaki, Wang, and M. Watanabe, Redoxable Nanosheet Crystallites of MnO2 Derived via Delamination of a Layered Manganese Oxide, Journal of the American Chemical Society **125**, 3568 (2003).

[62] T. Kim, E.-J. Oh, A.-Y. Jee, S. Lim, D. Park, M. Lee, S.-H. Hyun, J.-H. Choy, and S.-J. Hwang, Soft-Chemical Exfoliation Route to Layered Cobalt Oxide Monolayers and Its Application for Film Deposition and Nanoparticle Synthesis, Chemistry – A European Journal **15**, 10752 (2009).

[63] K. Edgehouse, M. Escamilla, L. Wang, R. Dent, K. Pachuta, L. Kendall, P. Wei, A. Sehirlioglu, and E. Pentzer, Stabilization of oil-in-water emulsions with graphene oxide and cobalt oxide nanosheets and preparation of armored polymer particles, Journal of Colloid and Interface Science **541**, 269 (2019).

[64] K. G. Pachuta, E. B. Pentzer, and A. Sehirlioglu, Cation deficiency associated with the chemical exfoliation of lithium cobalt oxide, Journal of the American Ceramic Society **102**, 5603 (2019).

[65] K. Pachuta, E. Pentzer, and A. Sehirlioglu, Evaluating the chemical exfoliation of lithium cobalt oxide using UV-Vis spectroscopy, Nanoscale Adv. **2**, 5362 (2020).

[66] J. Li, G. Li, J. Wang, C. Xue, Y. Zhang, X. Wu, L. Meng, and L. Li, Iron-Doped $LiCoO_2$ Nanosheets as Highly Efficient Electrocatalysts for Alkaline Water Oxidation, European Journal of Inorganic Chemistry **2019**, 2448 (2019).

[67] K. Adpakpang, S. M. Oh, X. Jin, and S.-J. Hwang, A Direct Hybridization between Isocharged Nanosheets of Layered Metal Oxide and Graphene through a Surface-Modification Assembly Process, Chemistry – A European Journal **20**, 15459 (2014).

[68] J.-Y. Kim, J.-I. Kim, S.-M. Choi, Y. Soo Lim, W.-S. Seo, and H. Jin Hwang, Nanostructured thermoelectric cobalt oxide by exfoliation/restacking route, Journal of Applied Physics **112**, 113705 (2012).

[69] X. Jin, K. Adpakpang, I. Young Kim, S. Mi Oh, N.-S. Lee, and S.-J. Hwang, An Effective Way to Optimize the Functionality of Graphene-Based Nanocomposite: Use of the Colloidal Mixture of Graphene and Inorganic Nanosheets, Scientific Reports **5**, 11057 (2015).

[70] R. Sasai, Y. Kato, W. Soontornchaiyakul, H. Usami, A. Masumori, W. Norimatsu, T. Fujimura, and S. Takagi, Photoinduced electron transfer in layer-by-layer thin solid films containing cobalt oxide nanosheets, porphyrin, and methyl viologen, Phys. Chem. Chem. Phys. **19**, 5611 (2017).

[71] X. Jin, J. Lim, N.-S. Lee, and S.-J. Hwang, A powerful role of exfoliated metal oxide 2D nanosheets as additives for improving electrocatalyst functionality of graphene, Electrochimica Acta **235**, 720 (2017).

[72] J.-S. Jang, S.-E. Lee, S.-J. Choi, W.-T. Koo, D.-H. Kim, H. Shin, H. J. Park, and I.-D. Kim, Heterogeneous, Porous 2D Oxide Sheets via Rapid Galvanic Replacement: Toward Superior HCHO Sensing Application, Advanced Functional Materials **29**, 1903012 (2019).

[73] A. Basch, L. de Campo, J. H. Albering, and J. W. White, Chemical delithiation and exfoliation of Li_xCoO_2, Journal of Solid State Chemistry **220**, 102 (2014).

[74] K. Miyoshi, K. Manami, R. Sasai, S. Nishigori, and J. Takeuchi, Electronic states realized by the interplay between Li diffusion and Co^{3+}/Co^{4+} charge ordering in Li_xCoO_2, Phys. Rev. B **98**, 195106 (2018).

[75] K. Iwaya, T. Ogawa, T. Minato, K. Miyoshi, J. Takeuchi, A. Kuwabara, H. Moriwake, Y. Kim, and T. Hitosugi, Impact of Lithium-Ion Ordering on Surface Electronic States of Li_xCoO_2, Phys. Rev. Lett. **111**, 126104 (2013).

[76] T. Motohashi, T. Ono, Y. Sugimoto, Y. Masubuchi, S. Kikkawa, R. Kanno, M. Karppinen, and H. Yamauchi, Electronic phase diagram of the layered cobalt oxide system Li_xCoO_2 ($0.0 \leq x \leq 1.0$), Phys. Rev. B **80**, 165114 (2009).

[77] C. Wolverton and A. Zunger, First-Principles Prediction of Vacancy Order-Disorder and Intercalation Battery Voltages in Li_xCoO_2, Phys. Rev. Lett. **81**, 606 (1998).

[78] R. Gummow, D. Liles, and M. Thackeray, Spinel versus layered structures for lithium cobalt oxide synthesised at 400°C, Materials Research Bulletin **28**, 235 (1993).

[79] H. Wang, Y.-I. Jang, B. Huang, D. R. Sadoway, and Y.-M. Chiang, TEM study of electrochemical cycling-induced damage and disorder in LiCoO2 cathodes for rechargeable lithium batteries, Journal of The Electrochemical Society **146**, 473 (1999).

[80] G. Trimarchi, Z. Wang, and A. Zunger, Polymorphous band structure model of gapping in the antiferromagnetic and paramagnetic phases of the Mott insulators MnO, FeO, CoO, and NiO, Phys. Rev. B **97**, 035107 (2018).

[81] F. Lei, Y. Sun, K. Liu, S. Gao, L. Liang, B. Pan, and Y. Xie, Oxygen Vacancies Confined in Ultrathin Indium Oxide Porous Sheets for Promoted Visible-Light Water Splitting, Journal of the American Chemical Society **136**, 6826 (2014).

[82] X. Chen, L. Liu, P. Y. Yu, and S. S. Mao, Increasing Solar Absorption for Photocatalysis with Black Hydrogenated Titanium Dioxide Nanocrystals, Science **331**, 746 (2011), https://science.sciencemag.org/content/331/6018/746.full.pdf.

[83] M. Guan, C. Xiao, J. Zhang, S. Fan, R. An, Q. Cheng, J. Xie, M. Zhou, B. Ye, and Y. Xie, Vacancy Associates Promoting Solar-Driven Photocatalytic Activity of Ultrathin Bismuth Oxychloride Nanosheets, Journal of the American Chemical Society **135**, 10411 (2013).

[84] K. Nakada, M. Fujita, G. Dresselhaus, and M. S. Dresselhaus, Edge state in graphene ribbons: Nanometer size effect and edge shape dependence, Phys. Rev. B **54**, 17954 (1996).

[85] X. Huang, C. Tan, Z. Yin, and H. Zhang, 25th Anniversary Article: Hybrid Nanostructures Based on Two-Dimensional Nanomaterials, Advanced Materials **26**, 2185 (2014).

[86] M. Chiesa and E. Giamello, Carbon Dioxide Activation by Surface Excess Electrons: An EPR Study of the CO_2- Radical Ion Adsorbed on the Surface of MgO, Chemistry – A European Journal **13**, 1261 (2007).

[87] F. Wang, J.-H. Seo, G. Luo, M. B. Starr, Z. Li, D. Geng, X. Yin, S. Wang, D. G. Fraser, D. Morgan, Z. Ma, and X. Wang, Nanometre-thick single-crystalline nanosheets

grown at the water–air interface, Nature Communications **7**, 10444 (2016).
[88] A. Zunger, Practical doping principles, Applied Physics Letters **83**, 57 (2003).
[89] A. Sehirlioglu, A. Sayir, and F. Dynys, Doping of $BiScO_3$–$PbTiO_3$ Ceramics for Enhanced Properties, Journal of the American Ceramic Society **93**, 1718 (2010).
[90] B. Luo, G. Liu, and L. Wang, Recent advances in 2D materials for photocatalysis, Nanoscale **8**, 6904 (2016).
[91] Y. Okamoto, S. Ida, J. Hyodo, H. Hagiwara, and T. Ishihara, Synthesis and Photocatalytic Activity of Rhodium-Doped Calcium Niobate Nanosheets for Hydrogen Production from a Water/Methanol System without Cocatalyst Loading, Journal of the American Chemical Society **133**, 18034 (2011).
[92] S. Ida, S. Koga, T. Daio, H. Hagiwara, and T. Ishihara, Direct Imaging of Light Emission Centers in Two-Dimensional Crystals and Their Luminescence and Photocatalytic Properties, Angewandte Chemie International Edition **53**, 13078 (2014).
[93] Z. Liu, A. Yu, and J. Y. Lee, Synthesis and characterization of $LiNi_{1-x-y}Co_xMn_yO_2$ as the cathode materials of secondary lithium batteries, Journal of Power Sources **81-82**, 416 (1999).
[94] W. Huddleston, F. Dynys, and A. Sehirlioglu, Effects of microstructure on fracture strength and conductivity of sintered NMC333, Journal of the American Ceramic Society **103**, 1527 (2020).
[95] Y. Sun, F. Lei, S. Gao, B. Pan, J. Zhou, and Y. Xie, Atomically Thin Tin Dioxide Sheets for Efficient Catalytic Oxidation of Carbon Monoxide, Angewandte Chemie International Edition **52**, 10569 (2013).
[96] S. Gao, X. Jiao, Z. Sun, W. Zhang, Y. Sun, C. Wang, Q. Hu, X. Zu, F. Yang, S. Yang, L. Liang, J. Wu, and Y. Xie, Ultrathin Co_3O_4 Layers Realizing Optimized CO_2 Electroreduction to Formate, Angewandte Chemie International Edition **55**, 698 (2016).
[97] M. C. Sarahan, E. C. Carroll, M. Allen, D. S. Larsen, N. D. Browning, and F. E. Osterloh, $K_4Nb_6O_{17}$-derived photocatalysts for hydrogen evolution from water: Nanoscrolls versus nanosheets, Journal of Solid State Chemistry **181**, 1678 (2008), solid State Chemistry on the Nanoscale: Achievements, Challenges, and Opportunities.
[98] Z. Geng, X. Kong, W. Chen, H. Su, Y. Liu, F. Cai, G. Wang, and J. Zeng, Oxygen Vacancies in ZnO Nanosheets Enhance CO_2 Electrochemical Reduction to CO, Angewandte Chemie International Edition **57**, 6054 (2018).
[99] K. Suriye, B. Jongsomjit, C. Satayaprasert, and P. Praserthdam, Surface defect (Ti^{3+}) controlling in the first step on the anatase TiO_2 nanocrystal by using sol–gel technique, Applied Surface Science **255**, 2759 (2008).
[100] S. Gao, Z. Sun, W. Liu, X. Jiao, X. Zu, Q. Hu, Y. Sun, T. Yao, W. Zhang, S. Wei, and Y. Xie, Atomic layer confined vacancies for atomic-level insights into carbon dioxide electroreduction, Nature Communications **8**, 14503 (2017).
[101] F. Lei, Y. Sun, K. Liu, S. Gao, L. Liang, B. Pan, and Y. Xie, Oxygen Vacancies Confined in Ultrathin Indium Oxide Porous Sheets for Promoted Visible-Light Water Splitting, Journal of the American Chemical Society **136**, 6826 (2014), pMID: 24773473.
[102] L. Liu, Y. Jiang, H. Zhao, J. Chen, J. Cheng, K. Yang, and Y. Li, Engineering Coexposed {001} and {101} Facets in Oxygen-Deficient TiO_2 Nanocrystals for Enhanced CO_2 Photoreduction under Visible Light, ACS Catalysis **6**, 1097 (2016).
[103] Y.-L. Lee, J. Kleis, J. Rossmeisl, and D. Morgan, Ab initio energetics of $LaBO_3$(001) (B = Mn, Fe, Co, and Ni) for solid oxide fuel cell cathodes, Phys. Rev. B **80**, 224101 (2009).
[104] P. Zhao, D. Kiriya, A. Azcatl, C. Zhang, M. Tosun, Y.-S. Liu, M. Hettick, J. S. Kang, S. McDonnell, S. KC, J. Guo, K. Cho, R. M. Wallace, and A. Javey, Air Stable p-Doping of WSe2 by Covalent Functionalization, ACS Nano **8**, 10808 (2014).
[105] Y. Abghoui, A. L. Garden, J. G. Howalt, T. Vegge, and E. Skúlason, Electroreduction of N_2 to Ammonia at Ambient Conditions on Mononitrides of Zr, Nb, Cr, and V: A DFT Guide for Experiments, ACS Catalysis **6**, 635 (2016).
[106] H. Tan, Z. Zhao, M. Niu, C. Mao, D. Cao, D. Cheng, P. Feng, and Z. Sun, A facile and versatile method for preparation of colored TiO_2 with enhanced solar-driven photocatalytic activity, Nanoscale **6**, 10216 (2014).
[107] Q. Zhu, Y. Peng, L. Lin, C.-M. Fan, G.-Q. Gao, R.-X. Wang, and A.-W. Xu, Stable blue TiO2−x nanoparticles for efficient visible light photocatalysts, J. Mater. Chem. A **2**, 4429 (2014).
[108] A. Sinhamahapatra, J.-P. Jeon, and J.-S. Yu, A new approach to prepare highly active and stable black titania for visible light-assisted hydrogen production, Energy Environ. Sci. **8**, 3539 (2015).
[109] A. Naldoni, M. Allieta, S. Santangelo, M. Marelli, F. Fabbri, S. Cappelli, C. L. Bianchi, R. Psaro, and V. Dal Santo, Effect of Nature and Location of Defects on Bandgap Narrowing in Black TiO_2 Nanoparticles, Journal of the American Chemical Society **134**, 7600 (2012).
[110] X. Han, Q. Kuang, M. Jin, Z. Xie, and L. Zheng, Synthesis of Titania Nanosheets with a High Percentage of Exposed (001) Facets and Related Photocatalytic Properties, Journal of the American Chemical Society **131**, 3152 (2009).
[111] M. Parras, A. Varela, R. Cortés-Gil, K. Boulahya, A. Hernando, and J. M. González-Calbet, Room-Temperature Ferromagnetism in Reduced Rutile $TiO_{2-\delta}$ Nanoparticles, The Journal of Physical Chemistry Letters **4**, 2171 (2013).
[112] W. Bi, C. Ye, C. Xiao, W. Tong, X. Zhang, W. Shao, and Y. Xie, Spatial Location Engineering of Oxygen Vacancies for Optimized Photocatalytic H_2 Evolution Activity, Small **10**, 2820 (2014).
[113] H. He, P. Zapol, and L. A. Curtiss, A Theoretical Study of CO_2 Anions on Anatase (101) Surface, The Journal of Physical Chemistry C **114**, 21474 (2010).
[114] J. Green, E. Carter, and D. M. Murphy, Interaction of molecular oxygen with oxygen vacancies on reduced TiO_2: Site specific blocking by probe molecules, Chemical Physics Letters **477**, 340 (2009).
[115] R. Schaub, P. Thostrup, N. Lopez, E. Lægsgaard, I. Stensgaard, J. K. Nørskov, and F. Besenbacher, Oxygen Vacancies as Active Sites for Water Dissociation on Rutile TiO_2(110), Phys. Rev. Lett. **87**, 266104 (2001).
[116] Materials Project: `https://materialsproject.org/`,

doi:10.1038/sdata.2018.65.

[117] A. Molina-Sánchez and L. Wirtz, Phonons in single-layer and few-layer MoS_2 and WS_2, Phys. Rev. B **84**, 155413 (2011).

[118] C. Bhandari and W. R. L. Lambrecht, Phonons and related spectra in bulk and monolayer V_2o_5, Phys. Rev. B **89**, 045109 (2014).

[119] A. Ratnaparkhe, S. K. Radha, and W. R. L. Lambrecht, Calculated phonon modes, infrared and Raman spectra in orthorhombic α-MoO_3 and monolayer MoO_3 (2021), arXiv:2103.00043 [cond-mat.mtrl-sci].

[120] T. Sohier, M. Gibertini, M. Calandra, F. Mauri, and N. Marzari, Breakdown of Optical Phonons' Splitting in Two-Dimensional Materials, Nano Letters **17**, 3758 (2017), pMID: 28517939.

[121] P. Cudazzo, I. V. Tokatly, and A. Rubio, Dielectric screening in two-dimensional insulators: Implications for excitonic and impurity states in graphane, Phys. Rev. B **84**, 085406 (2011).

[122] S. Dixit, N. R. Sahoo, A. Mall, and A. Kumar, Mid infrared polarization engineering via sub-wavelength biaxial hyperbolic van der Waals crystals, Scientific Reports **11**, 6612 (2021).

[123] Taboada-Gutiérrez, Javier and Álvarez-Pérez, Gonzalo and Duan, Jiahua and Ma, Weiliang and Crowley, Kyle and Prieto, Iván and Bylinkin, Andrei and Autore, Marta and Volkova, Halyna and Kimura, Kenta and Kimura, Tsuyoshi and Berger, M. H. and Li, Shaojuan and Bao, Qiaoliang and Gao, Xuan P.A. and Errea, Ion and Nikitin, Alexey Y. and Hillenbrand, Rainer and Martín-Sánchez, Javier and Alonso-González, Pablo, Broad spectral tuning of ultra-low-loss polaritons in a van der Waals crystal by intercalation, Nature Materials **19**, 964 (2020).

[124] M. van Schilfgaarde, T. Kotani, and S. Faleev, Quasiparticle Self-Consistent *GW* Theory, Phys. Rev. Lett. **96**, 226402 (2006).

[125] T. Kotani, M. van Schilfgaarde, and S. V. Faleev, Quasiparticle self-consistent GW method: A basis for the independent-particle approximation, Phys.Rev. B **76**, 165106 (2007).

[126] L. Hedin, New method for calculating the one-particle green's function with application to the electron-gas problem, Phys. Rev. **139**, A796 (1965).

[127] L. Hedin and S. Lundqvist, Effects of electron-electron and electron-phonon interactions on the one-electron states of solids, in *Solid State Physics, Advanced in Research and Applications*, Vol. 23, edited by F. Seitz, D. Turnbull, and H. Ehrenreich (Academic Press, New York, 1969) pp. 1–181.

[128] C. Bhandari, M. van Schilfgaarde, T. Kotani, and W. R. L. Lambrecht, All-electron quasiparticle self-consistent *GW* band structures for $SrTiO_3$ including lattice polarization corrections in different phases, Phys. Rev. Materials **2**, 013807 (2018).

[129] B. Cunningham, M. Grüning, P. Azarhoosh, D. Pashov, and M. van Schilfgaarde, Effect of ladder diagrams on optical absorption spectra in a quasiparticle self-consistent *GW* framework, Phys. Rev. Materials **2**, 034603 (2018).

[130] M. Shishkin, M. Marsman, and G. Kresse, Accurate quasiparticle spectra from self-consistent gw calculations with vertex corrections, Phys. Rev. Lett. **99**, 246403 (2007).

[131] W. Chen and A. Pasquarello, Accurate band gaps of extended systems via efficient vertex corrections in *GW*, Phys. Rev. B **92**, 041115 (2015).

[132] H.-P. Komsa and A. V. Krasheninnikov, Effects of confinement and environment on the electronic structure and exciton binding energy of MoS_2 from first principles, Phys. Rev. B **86**, 241201 (2012).

[133] J. Meyer, K. Zilberberg, T. Riedl, and A. Kahn, Electronic structure of vanadium pentoxide: An efficient hole injector for organic electronic materials, Journal of Applied Physics **110**, 033710 (2011).

[134] S. Botti and M. A. L. Marques, Strong Renormalization of the Electronic Band Gap due to Lattice Polarization in the *GW* Formalism, Phys. Rev. Lett. **110**, 226404 (2013).

[135] T. Kotani, Quasiparticle self-consistent gw method based on the augmented plane-wave and muffin-tin orbital method, Journal of the Physical Society of Japan **83**, 094711 (2014), http://dx.doi.org/10.7566/JPSJ.83.094711.

[136] C. Friedrich, S. Blügel, and A. Schindlmayr, Efficient implementation of the *GW* approximation within the all-electron FLAPW method, Phys. Rev. B **81**, 125102 (2010).

[137] C. Bhandari, *First-principles study of electronic and vibrational properties of bulk and monolayer* V_2O_5, Ph.D. thesis, Case Western Reserve University (2016).

[138] W. R. L. Lambrecht, C. Bhandari, and M. van Schilfgaarde, Lattice polarization effects on the screened Coulomb interaction W of the *GW* approximation, Phys. Rev. Materials **1**, 043802 (2017).

[139] A. Miglio, V. Brousseau-Couture, E. Godbout, G. Antonius, Y.-H. Chan, S. G. Louie, M. Côté, M. Giantomassi, and X. Gonze, Predominance of non-adiabatic effects in zero-point renormalization of the electronic band gap, npj Computational Materials **6**, 10.1038/s41524-020-00434-z (2020).

[140] S. K. Radha, W. R. L. Lambrecht, D. Pashov, M. van Schilfgaarde, B. Cunningham, and M. Grüning, Optical response and band structure of $LiCoO_2$ including electron-hole interaction effects (2020), in prepaeration.

[141] S. K. Radha and W. R. L. Lambrecht, Spin-polarized two-dimensional electron/hole gases on $LiCoO_2$ layers., SciPost Phys. **10**, 57 (2021).

[142] R. E. Schaak, T. Klimczuk, M. L. Foo, and R. J. Cava, Superconductivity phase diagram of NaxCoO2·1.3H2O, Nature **424**, 527 (2003).

[143] H. J. Zeiger, Unified model of the insulator-metal transition in Ti_2O_3 and the high-temperature transitions in V_2O_3, Physical Review B **11**, 5132 (1975).

[144] V. Eyert, VO_2: A novel view from band theory, Physical Review Letters **107**, 016401 (2011).

[145] S. Beke, A review of the growth of {V2O5} films from 1885 to 2010, Thin Solid Films **519**, 1761 (2011).

[146] L. Fiermans, P. Clauws, W. Lambrecht, V. L., and V. J., Single crystal V_2O_5 and Lower Oxides, A survey of Their Elecronic, Optical, Structural and Surface Properties, Phys. Stat. Solidi (a) **59** (1980).

[147] R. Gopinath and B. K. Patel, A Catalytic Oxidative Esterification of Aldehydes Using $V_2O_5-H_2O_2$, Organic Letters **2**, 577 (2000).

[148] S. Velusamy and T. Punniyamurthy, Novel Vanadium-Catalyzed Oxidation of Alcohols to Aldehydes and Ke-

tones under Atmospheric Oxygen, Organic Letters **6**, 217 (2003).

[149] N. Jiang and A. J. Ragauskas, Selective Aerobic Oxidation of Activated Alcohols into Acids or Aldehydes in Ionic Liquids, The Journal of Organic Chemistry **72**, 7030 (2007).

[150] G. Micocci, A. Serra, A. Tepore, S. Capone, R. Rella, and P. Siciliano, Properties of vanadium oxide thin films for ethanol sensor, Journal of Vacuum Science & Technology A: Vacuum, Surfaces, and Films **15**, 34 (1997).

[151] T. Y. Ou-Yang, F. T. Huang, G. J. Shu, W. L. Lee, M. W. Chu, H. L. Liu, and F. C. Chou, Electronic phase diagram of Li_xCoO_2 revisited with potentiostatically deintercalated single crystals, Physical Review B - Condensed Matter and Materials Physics **85**, 035120 (2012).

[152] H. Smolinski, C. Gros, W. Weber, U. Peuchert, G. Roth, M. Weiden, and C. Geibel, NaV_2O_5 as a quarter-filled ladder compound, Physical Review Letters **80**, 5164 (1998).

[153] D. O. Scanlon, A. Walsh, B. J. Morgan, and G. W. Watson, An ab initio Study of Reduction of V_2O_5 through the Formation of Oxygen Vacancies and Li Intercalation, The Journal of Physical Chemistry C **112**, 9903 (2008).

[154] A. Yosikawa, F. Terasakli, N. Takano, and M. Ohara, An explanation of anisotropy in electrical conductivity of V2O5 due to overlap integrals, Journal of Materials Science Letters **16**, 632 (1997).

[155] Y. Ueda and M. Isobe, Magnetic properties of AV_2O_5 (A = Li, Na, Cs, Ca and Mg), Journal of Magnetism and Magnetic Materials **177-181**, 741 (1998).

[156] W. G. Mumme and J. A. Watts, The crystal structure of reduced cesium vanadate, CsV_2O_5, Journal of Solid State Chemistry **3**, 319 (1971).

[157] M. Willinger, N. Pinna, D. S. Su, and R. Schlögl, Geometric and electronic structure of $\gamma - V_2O_5$: Comparison between $\alpha - V_2O_5$ and $\gamma - V_2O_5$, Phys. Rev. B **69**, 155114 (2004).

[158] A. Jarry, M. Walker, S. Theodoru, L. J. Brillson, and G. W. Rubloff, Elucidating Structural Transformations in $Li_xV_2O_5$ Electrochromic Thin Films by Multimodal Spectroscopies, Chemistry of Materials **32**, 7226 (2020).

[159] M. J. Walker, A. Jarry, N. Pronin, J. Ballard, G. W. Rubloff, and L. J. Brillson, Nanoscale depth and lithiation dependence of V2O5 band structure by cathodoluminescence spectroscopy, J. Mater. Chem. A **8**, 11800 (2020).

[160] V. P. Filonenko, M. Sundberg, P.-E. Werner, and I. P. Zibrov, Structure of a high-pressure phase of vanadium pentoxide, β-V_2O_5, Acta Crystallographica Section B **60**, 375 (2004).

[161] Y. Kanke, K. Kato, E. Takayama-Muromachi, and M. Isobe, Acta Crystallographica Section C **46**, 1590 (1990).

[162] R. Enjalbert and J. Galy, A refinement of the structure of vanadium pentoxide, Acta Crystallogr., Sect. C: Cryst. Struct. Commun. **C42**, 1467 (1986).

[163] D. K. Chakrabarty, D. Guha, and A. B. Biswas, Electrical properties of vanadium pentoxide doped with lithium and sodium in the α-phase range, Journal of Materials Science **11**, 1347 (1976).

[164] D. McNulty, D. Noel Buckley, and C. O'Dwyer, NaV_2O_5 from sodium ion-exchanged vanadium oxide nanotubes and its efficient reversible lithiation as a li-ion anode material, ACS Applied Energy Materials **2**, 822 (2019).

[165] M. Lohmann, J. Hemberger, M. Nicklas, A. Loidl, M. Klemm, G. Obermeier, and S. Horn, Thermodynamic, transport and magnetic properties of α'-NaV_2O_5, Physica B: Condensed Matter **259-261**, 983 (1999).

[166] W. Lambrecht, B. Djafari-Rouahni, and J. Vennik, On the origin of the split-off conduction bands in V_2O_5., J. Phys.C: Solid State Phys. **14** (1981).

[167] J. N. Yao, , Y. A. Yang, and B. H. Loo, Enhancement of Photochromism and Electrochromism in MoO3/Au and MoO3/Pt Thin Films 10.1021/JP972217U (1998).

[168] B. W. Faughnan and R. S. Crandall, Optical properties of mixed-oxide WO_3/MoO_3 electrochromic films, Applied Physics Letters **31**, 834 (1977).

[169] M. Rahmani, S. Keshmiri, J. Yu, A. Sadek, L. Al-Mashat, A. Moafi, K. Latham, Y. Li, W. Wlodarski, and K. Kalantar-zadeh, Gas sensing properties of thermally evaporated lamellar MoO3", journal = "Sensors and Actuators B: Chemical, **145**, 13 (2010).

[170] E. Comini, L. Yubao, Y. Brando, and G. Sberveglieri, Gas sensing properties of MoO_3 nanorods to CO and CH_3OH, Chemical Physics Letters **407**, 368 (2005).

[171] C. Girotto, E. Voroshazi, D. Cheyns, P. Heremans, and B. P. Rand, Solution-Processed MoO_3 Thin Films As a Hole-Injection Layer for Organic Solar Cells, ACS Applied Materials & Interfaces **3**, 3244 (2011).

[172] I. Hancox, K. V. Chauhan, P. Sullivan, R. A. Hatton, A. Moshar, C. P. A. Mulcahy, and T. S. Jones, Increased efficiency of small molecule photovoltaic cells by insertion of a MoO_3 hole-extracting layer, Energy Environ. Sci. **3**, 107 (2010).

[173] H. Peelaers, M. L. Chabinyc, and C. G. Van de Walle, Controlling n-Type Doping in MoO_3, Chemistry of Materials **29**, 2563 (2017).

[174] K. Crowley, G. Ye, R. He, K. Abbasi, and X. P. A. Gao, α-MoO_3 as a Conductive 2D Oxide: Tunable n-Type Electrical Transport via Oxygen Vacancy and Fluorine Doping, ACS Applied Nano Materials **1**, 6407 (2018).

[175] B. A. Holler, K. Crowley, M. Berger, and X. P. A. Gao, 2D Semiconductor Transistors with Van der Waals Oxide MoO_3 as Integrated High-κ Gate Dielectric, Advanced Electronic Materials **6**, 2000635 (2020).

[176] A. Chithambararaj, N. Rajeswari Yogamalar, and A. C. Bose, Hydrothermally Synthesized h-MoO_3 and α-MoO_3 Nanocrystals: New Findings on Crystal-Structure-Dependent Charge Transport, Crystal Growth and Design **16**, 1984 (2016).

[177] Y. Guo and J. Robertson, Origin of the high work function and high conductivity of MoO_3, Applied Physics Letters **105**, 222110 (2014).

[178] J. Meyer, P. R. Kidambi, B. C. Bayer, C. Weijtens, A. Kuhn, A. Centeno, A. Pesquera, A. Zurutuza, J. Robertson, and S. Hofmann, Metal Oxide Induced Charge Transfer Doping and Band Alignment of Graphene Electrodes for Efficient Organic Light Emitting Diodes, Scientific Reports **4**, 5380 (2015).

[179] S. Balendhran, J. Deng, J. Z. Ou, S. Walia, J. Scott, J. Tang, K. L. Wang, M. R. Field, S. Russo, S. Zhuiykov, M. S. Strano, N. Medhekar, S. Sriram, M. Bhaskaran, and K. Kalantar-zadeh, Enhanced Charge Carrier Mobility in Two-Dimensional High Dielectric Molybdenum Oxide, Advanced Materials **25**, 109 (2013).

[180] M. M. Alsaif, A. F. Chrimes, T. Daeneke, S. Balendhran, D. O. Bellisario, Y. Son, M. R. Field, W. Zhang, H. Nili, E. P. Nguyen, K. Latham, J. Van Embden, M. S. Strano, J. Z. Ou, and K. Kalantar-Zadeh, High-Performance Field Effect Transistors Using Electronic Inks of 2D Molybdenum Oxide Nanoflakes, Advanced Functional Materials **26**, 91 (2016).

[181] S. Balendhran, S. Walia, M. Alsaif, E. P. Nguyen, J. Z. Ou, S. Zhuiykov, S. Sriram, M. Bhaskaran, and K. Kalantar-zadeh, Field Effect Biosensing Platform Based on 2D α-MoO3, ACS Nano **7**, 9753 (2013).

[182] L. F. Wan, J. T. Incorvati, K. R. Poeppelmeier, and D. Prendergast, Building a Fast Lane for Mg Diffusion in α-MoO_3 by Fluorine Doping, Chemistry of Materials **28**, 6900 (2016).

[183] R. Naouel, H. Dhaouadi, F. Touati, and N. Gharbi, Synthesis and Electrical Properties of Well-Ordered Layered α-MoO3 Nanosheets, Nano-Micro Letters **3**, 242 (2011).

[184] A.-F. I. Saad, Dielectric Properties of Molybdenum Oxide Thin Films, Journal of optoelectronics and Advanced Materials **7**, 2743 (2005).

[185] M. Sayer, A. Mansingh, J. B. Webb, and J. Noad, Long-range potential centres in disordered solids, Journal of Physics C: Solid State Physics **11**, 315 (1978).

[186] Z. Ren, J. Zhang, J. Zhang, C. Zhang, S. Xu, Y. Li, and Y. Hao, Diamond Field Effect Transistors With MoO_3 Gate Dielectric, IEEE Electron Device Letters **38**, 786 (2017).

[187] A. Liu, H. Zhu, H. Sun, Y. Xu, and Y.-Y. Noh, Solution Processed Metal Oxide High-κ Dielectrics for Emerging Transistors and Circuits, Advanced Materials **30**, 1706364 (2018).

[188] J. Robertson, High dielectric constant gate oxides for metal oxide Si transistors, Reports on Progress in Physics **69**, 327 (2006).

[189] L. Manchanda, M. Morris, M. Green, R. van Dover, F. Klemens, T. Sorsch, P. Silverman, G. Wilk, B. Busch, and S. Aravamudhan, Multi-component high-K gate dielectrics for the silicon industry, Microelectronic Engineering **59**, 351 (2001).

[190] J. S. Park, W.-J. Maeng, H.-S. Kim, and J.-S. Park, Review of recent developments in amorphous oxide semiconductor thin-film transistor devices, Thin Solid Films **520**, 1679 (2012).

[191] J. Meyer, S. Hamwi, M. Kröger, W. Kowalsky, T. Riedl, and A. Kahn, Transition Metal Oxides for Organic Electronics: Energetics, Device Physics and Applications, Advanced Materials **24**, 5408 (2012).

[192] Q. Peng, Z. Wang, B. Sa, B. Wu, and Z. Sun, Electronic structures and enhanced optical properties of blue phosphorene/transition metal dichalcogenides van der Waals heterostructures, Scientific Reports **6**, 1 (2016).

[193] S. Levasseur, M. Ménétrier, and C. Delmas, Combined effects of Ni and Li doping on the phase transitions in Li_xCoO_2 electrochemical and ^{7}Li nuclear magnetic resonance studies, Journal of the Electrochemical Society **149**, A1533 (2002).

[194] H. J. Orman and P. J. Wiseman, Cobalt(III) lithium oxide, $CoLiO_2$: structure refinement by powder neutron diffraction, Acta Crystallographica Section C Crystal Structure Communications **40**, 12 (1984).

[195] K. Miyoshi, K. Manami, J. Takeuchi, R. Sasai, and S. Nishigori, Enhanced Electrical Resistivity after Rapid Cool of the Specimen in Layered Oxide Li_xCoO_2, Physics Procedia **75**, 278 (2015).

[196] J. T. Hertz, Q. Huang, T. McQueen, T. Klimczuk, J. W. Bos, L. Viciu, and R. J. Cava, Magnetism and structure of Li_xCoO_2 and comparison to Na_xCoO_2, Physical Review B - Condensed Matter and Materials Physics **77**, 075119 (2008).

[197] D. Mohanty and H. Gabrisch, Comparison of magnetic properties in Li_xCoO_2 and its decomposition products $LiCo_2O_4$ and Co_3O_4, Solid State Ionics **194**, 41 (2011).

[198] N. Imanishi, M. Fujiyoshi, Y. Takeda, O. Yamamoto, and M. Tabuchi, Preparation and ^{7}Li-NMR study of chemically delithiated $Li_{1-x}CoO_2$ (0<x<0.5), Solid State Ionics **118**, 121 (1999).

[199] T. Motohashi, T. Ono, Y. Sugimoto, Y. Masubuchi, S. Kikkawa, R. Kanno, M. Karppinen, and H. Yamauchi, Electronic phase diagram of the layered cobalt oxide system Li_xCoO_2 ($0.0 \leq x \leq 1.0$), Physical Review B **80**, 165114 (2009).

[200] T. Mizokawa, Y. Wakisaka, T. Sudayama, C. Iwai, K. Miyoshi, J. Takeuchi, H. Wadati, D. G. Hawthorn, T. Z. Regier, and G. A. Sawatzky, Role of oxygen holes in Li_xCoO_2 revealed by soft X-ray spectroscopy, Physical Review Letters **111**, 056404 (2013).

[201] Y. Ishida, A. Mizutani, K. Sugiura, H. Ohta, and K. Koumoto, Metal-nonmetal transition in Li_xCoO_2 thin films and thermopower enhancement at high Li concentration, Physical Review B - Condensed Matter and Materials Physics **82**, 075325 (2010).

[202] M. Ménétrier, I. Saadoune, S. Levasseur, and C. Delmas, The insulator-metal transition upon lithium deintercalation from $LiCoO_2$: electronic properties and ^{7}Li NMR study, Journal of Materials Chemistry **9**, 1135 (1999).

[203] K. Miyoshi, C. Iwai, H. Kondo, M. Miura, S. Nishigori, and J. Takeuchi, Magnetic and electronic properties of Li_xCoO_2 single crystals, Physical Review B - Condensed Matter and Materials Physics **82**, 075113 (2010).

[204] K. Miyoshi, K. Manami, R. Sasai, S. Nishigori, and J. Takeuchi, Electronic states realized by the interplay between Li diffusion and Co^{3+}/Co^{4+} charge ordering in Li_xCoO_2, Physical Review B **98**, 195106 (2018).

[205] J. Molenda, A. Stokłosa, and T. Bąk, Modification in the electronic structure of cobalt bronze Li_xCoO_2 and the resulting electrochemical properties, Solid State Ionics **36**, 53 (1989).

[206] B. H. Savitzky, I. El Baggari, A. S. Admasu, J. Kim, S. W. Cheong, R. Hovden, and L. F. Kourkoutis, Bending and breaking of stripes in a charge ordered manganite, Nature Communications **8**, 10.1038/s41467-017-02156-1 (2017).

[207] M. S. Senn, J. P. Wright, and J. P. Attfield, Charge order and three-site distortions in the Verwey structure of magnetite, Nature **481**, 173 (2012).

[208] S. Kikkawa, S. Miyazaki, and M. Koizumi, Deintercalated $NaCoO_2$ and $LiCoO_2$, Journal of Solid State Chemistry **62**, 35 (1986).

[209] H. L. Liu, T. Y. Ou-Yang, H. H. Tsai, P. A. Lin, H. T. Jeng, G. J. Shu, and F. C. Chou, Electronic structure and lattice dynamics of Li_xCoO_2 single crystals, New Journal of Physics **17**, 103004 (2015).

[210] K. Mukai, Y. Ikedo, H. Nozaki, J. Sugiyama, K. Nishiyama, D. Andreica, A. Amato, P. L. Russo, E. J. Ansaldo, J. H. Brewer, K. H. Chow, K. Ariyoshi, and T. Ohzuku, Magnetic phase diagram of layered cobalt dioxide Li_xCoO_2, Physical Review Letters **99**,

087601 (2007).

[211] J. Sugiyama, K. Mukai, Y. Ikedo, H. Nozaki, M. Månsson, and I. Watanabe, Li Diffusion in LixCoO2 Probed by Muon-Spin Spectroscopy, Physical Review Letters **103**, 147601 (2009).

[212] H. Tukamoto and A. R. West, Electronic conductivity of $LiCoO_2$ and its enhancement by magnesium doping, Journal of the Electrochemical Society **144**, 3164 (1997).

AIP Publishing

Journal of Applied Physics

ACCEPTED MANUSCRIPT

PLEASE CITE THIS ARTICLE AS DOI: 10.1063/5.0051093

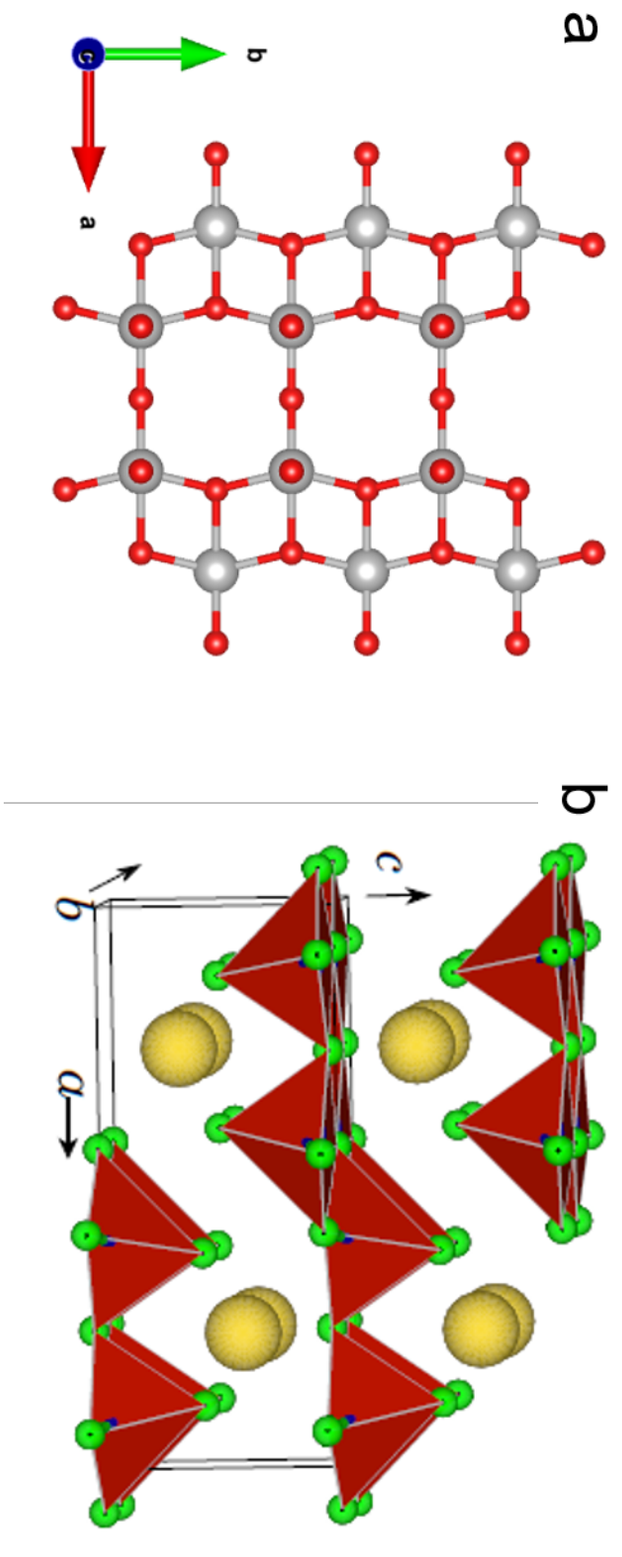

AIP Publishing

Journal of Applied Physics

ACCEPTED MANUSCRIPT

PLEASE CITE THIS ARTICLE AS DOI: 10.1063/5.0051093

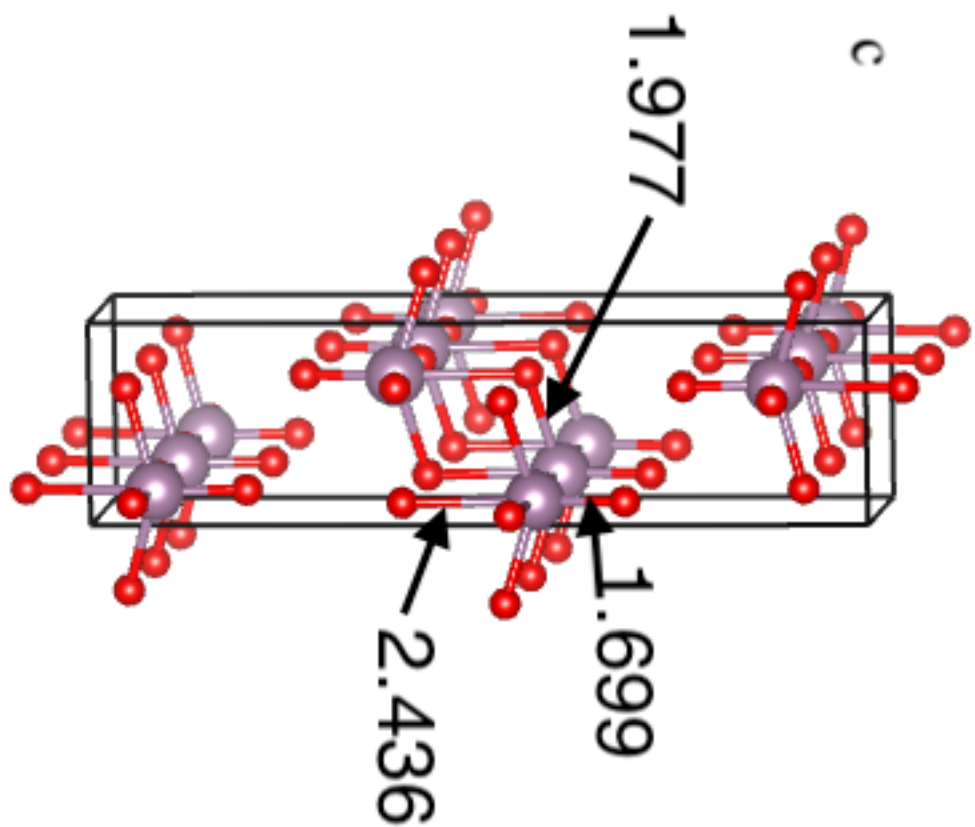

AIP Publishing

Journal of Applied Physics

ACCEPTED MANUSCRIPT

PLEASE CITE THIS ARTICLE AS DOI: 10.1063/5.0051093

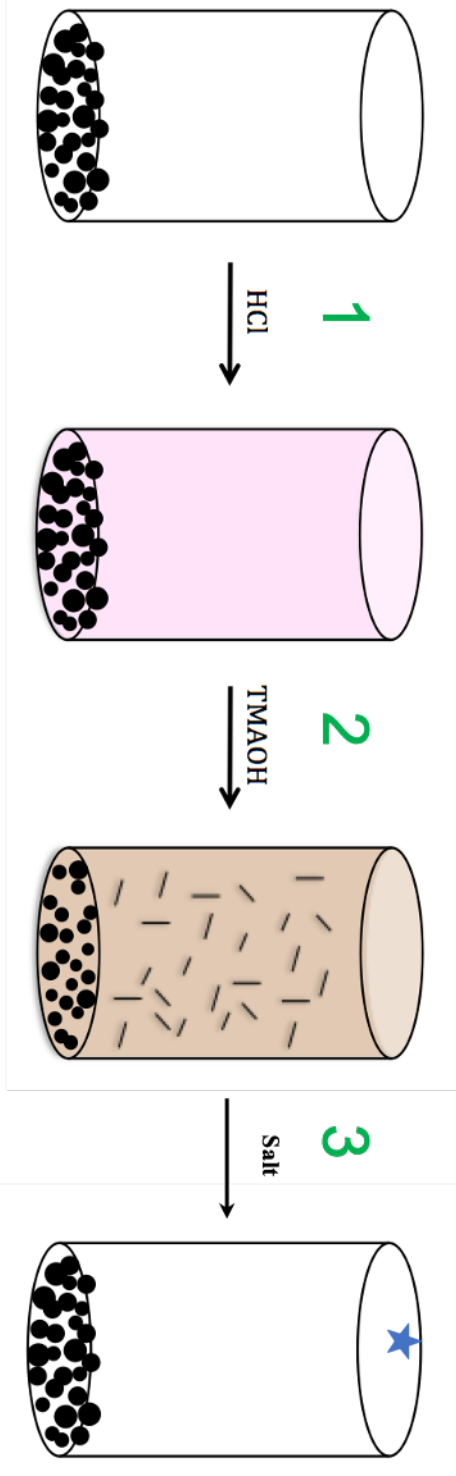

AIP Publishing

Journal of Applied Physics

PLEASE CITE THIS ARTICLE AS DOI: 10.1063/5.0051093

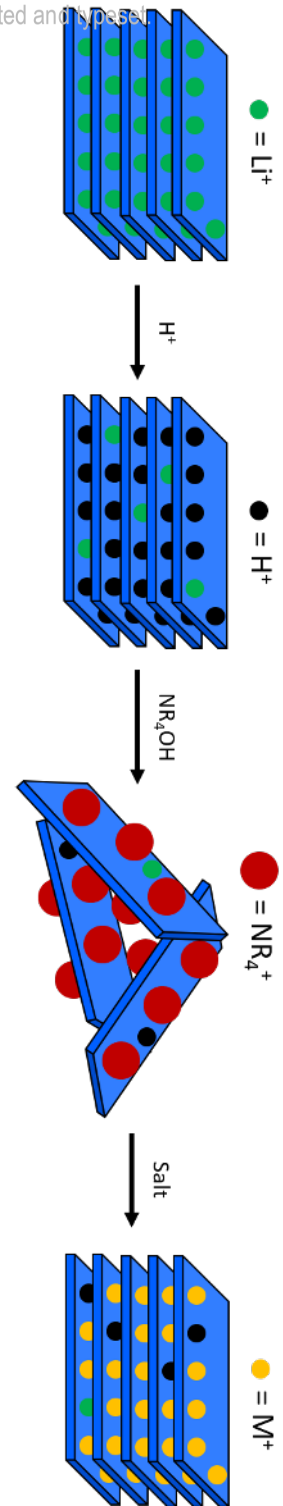

AIP Publishing

Journal of Applied Physics

ACCEPTED MANUSCRIPT

This is the author's peer reviewed, accepted manuscript. However, the online version of record will be different from this version once it has been copyedited and typeset.
PLEASE CITE THIS ARTICLE AS DOI: 10.1063/5.0051093

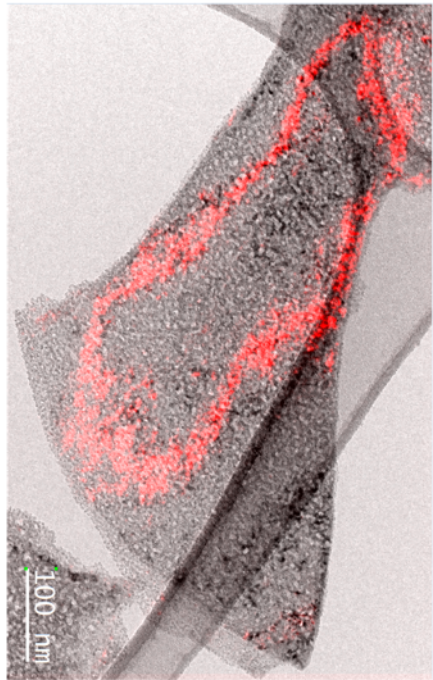

AIP Publishing

Journal of Applied Physics

ACCEPTED MANUSCRIPT

PLEASE CITE THIS ARTICLE AS DOI: 10.1063/5.0051093

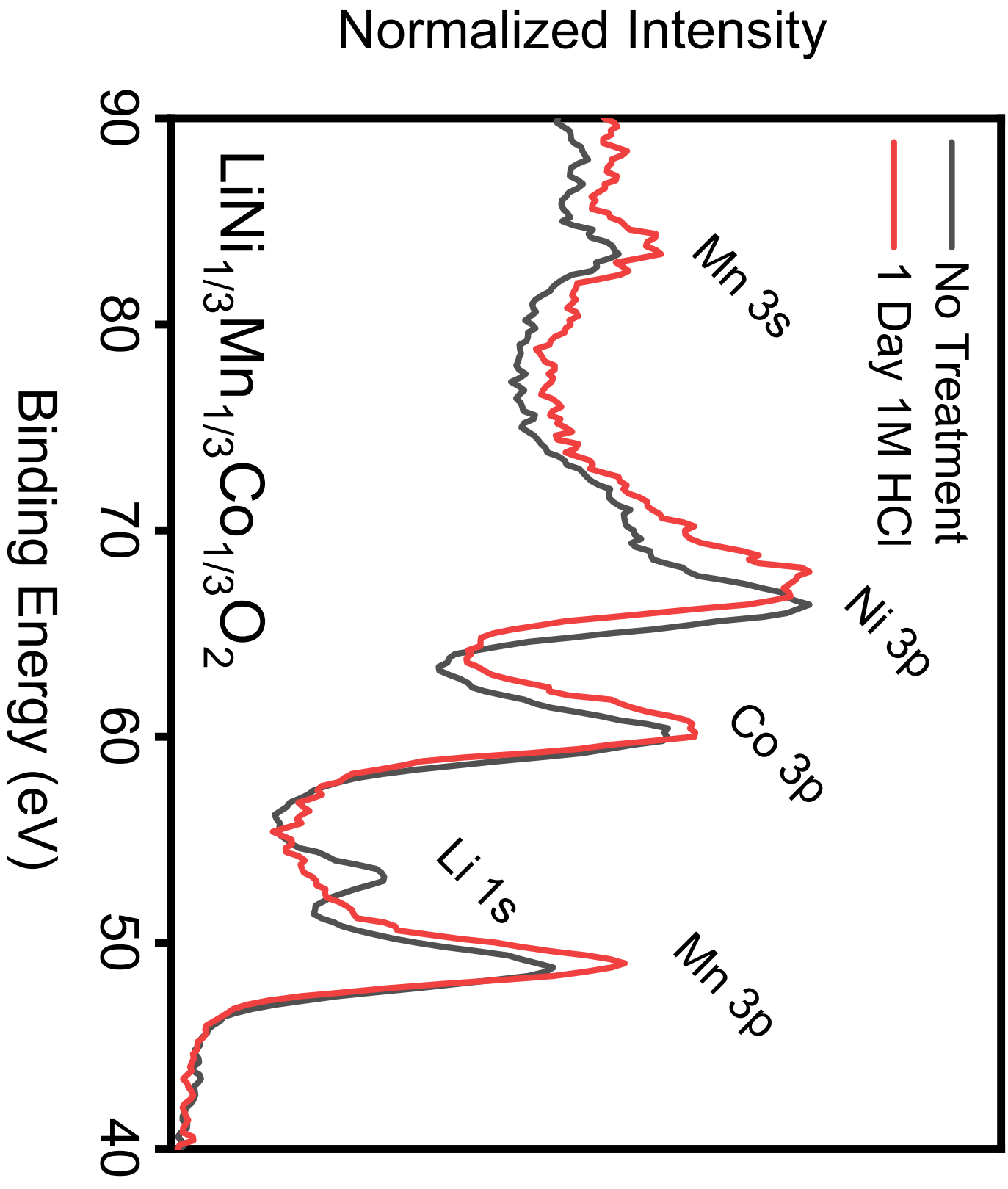

Journal of Applied Physics

ACCEPTED MANUSCRIPT

This is the author's peer reviewed, accepted manuscript. However, the online version of record will be different from this version once it has been copyedited and typeset.
PLEASE CITE THIS ARTICLE AS DOI: 10.1063/5.0051093

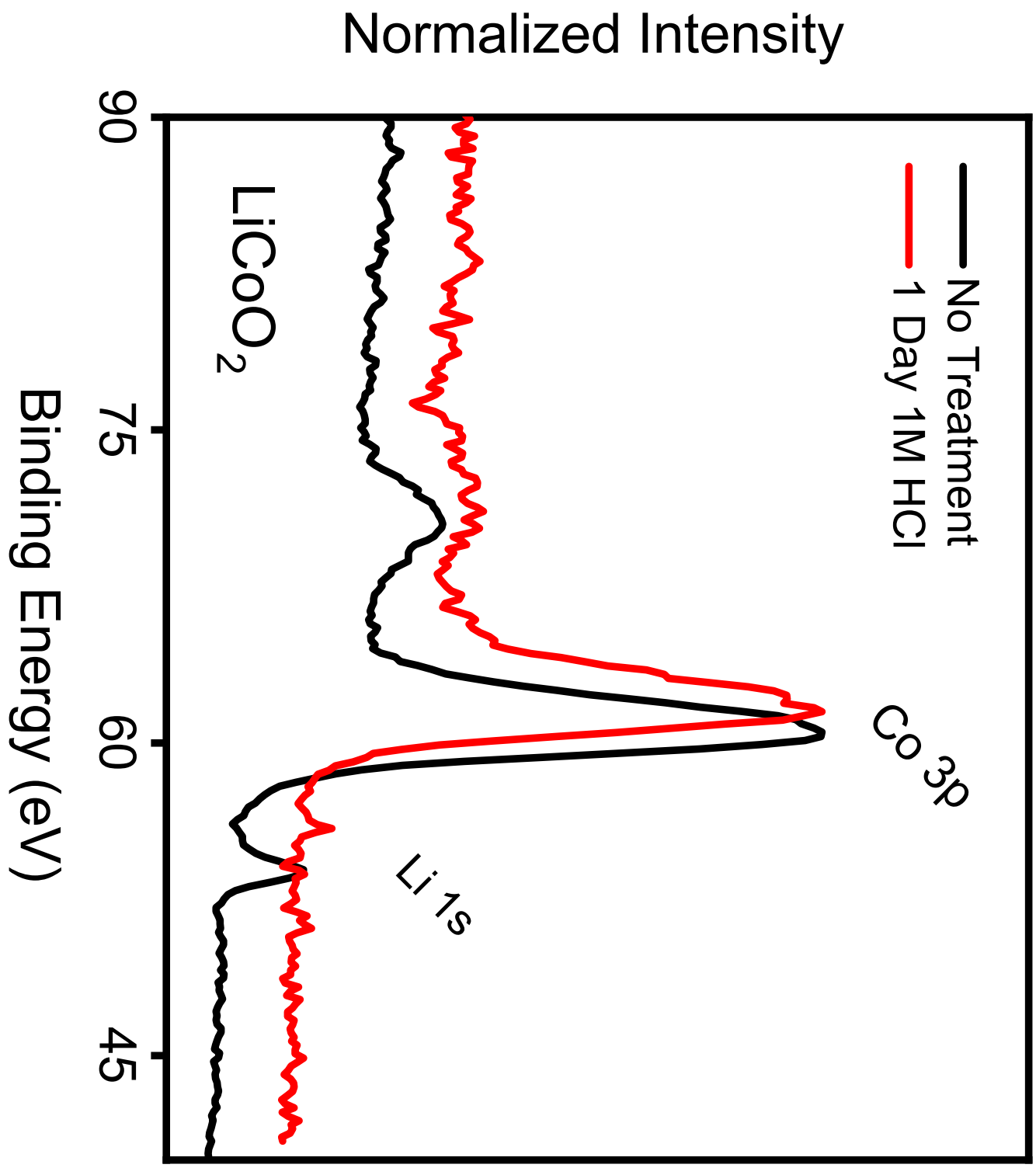

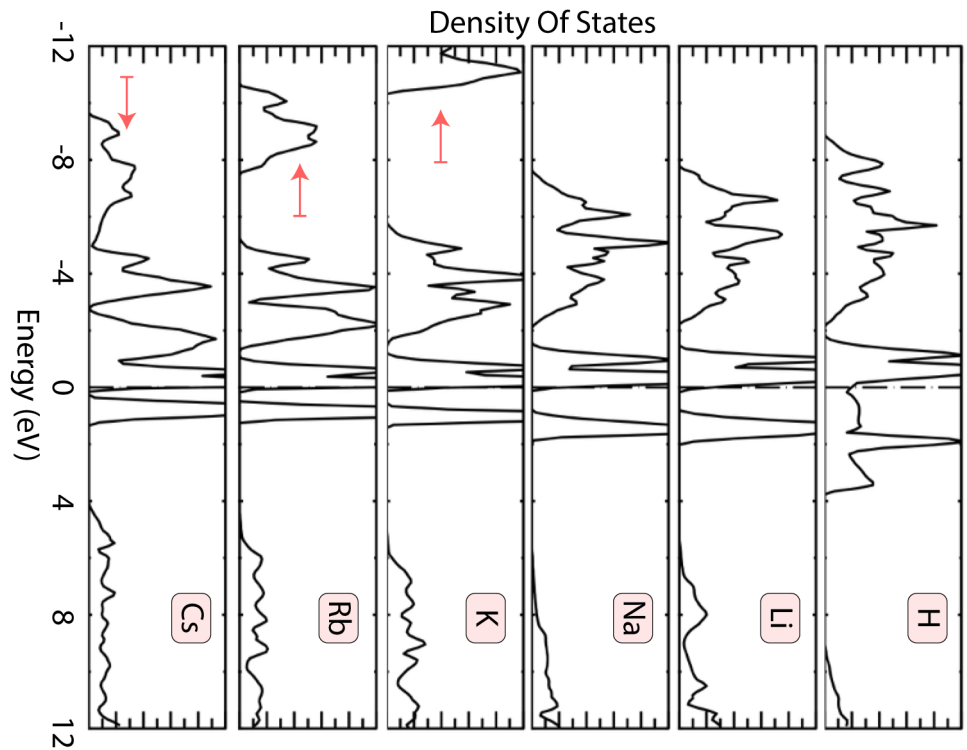

AIP Publishing Journal of Applied Physics ACCEPTED MANUSCRIPT

This is the author's peer reviewed, accepted manuscript. However, the online version of record will be different from this version once it has been copyedited and typeset.
PLEASE CITE THIS ARTICLE AS DOI: 10.1063/5.0051093

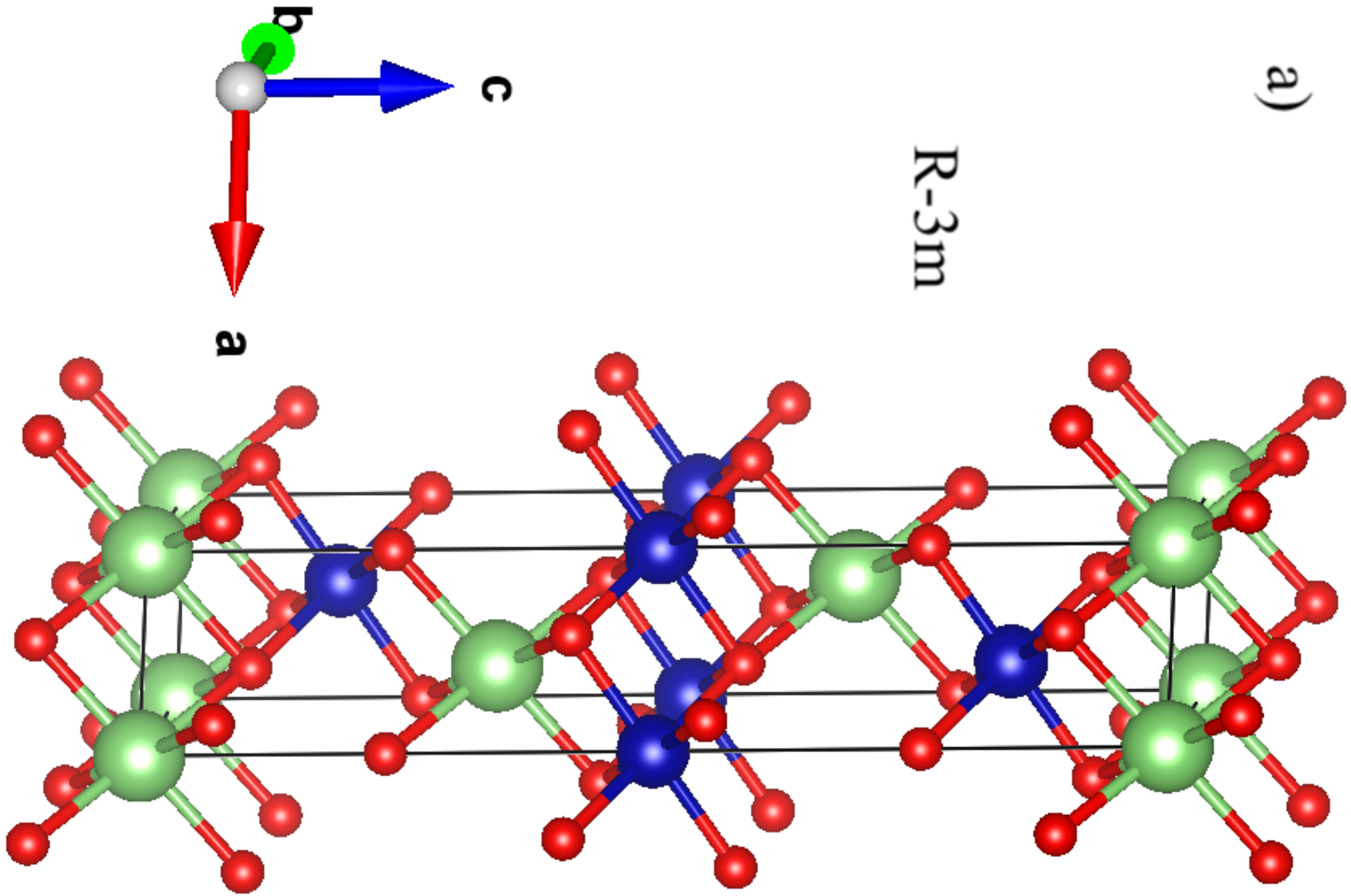

b)

P4/nmm

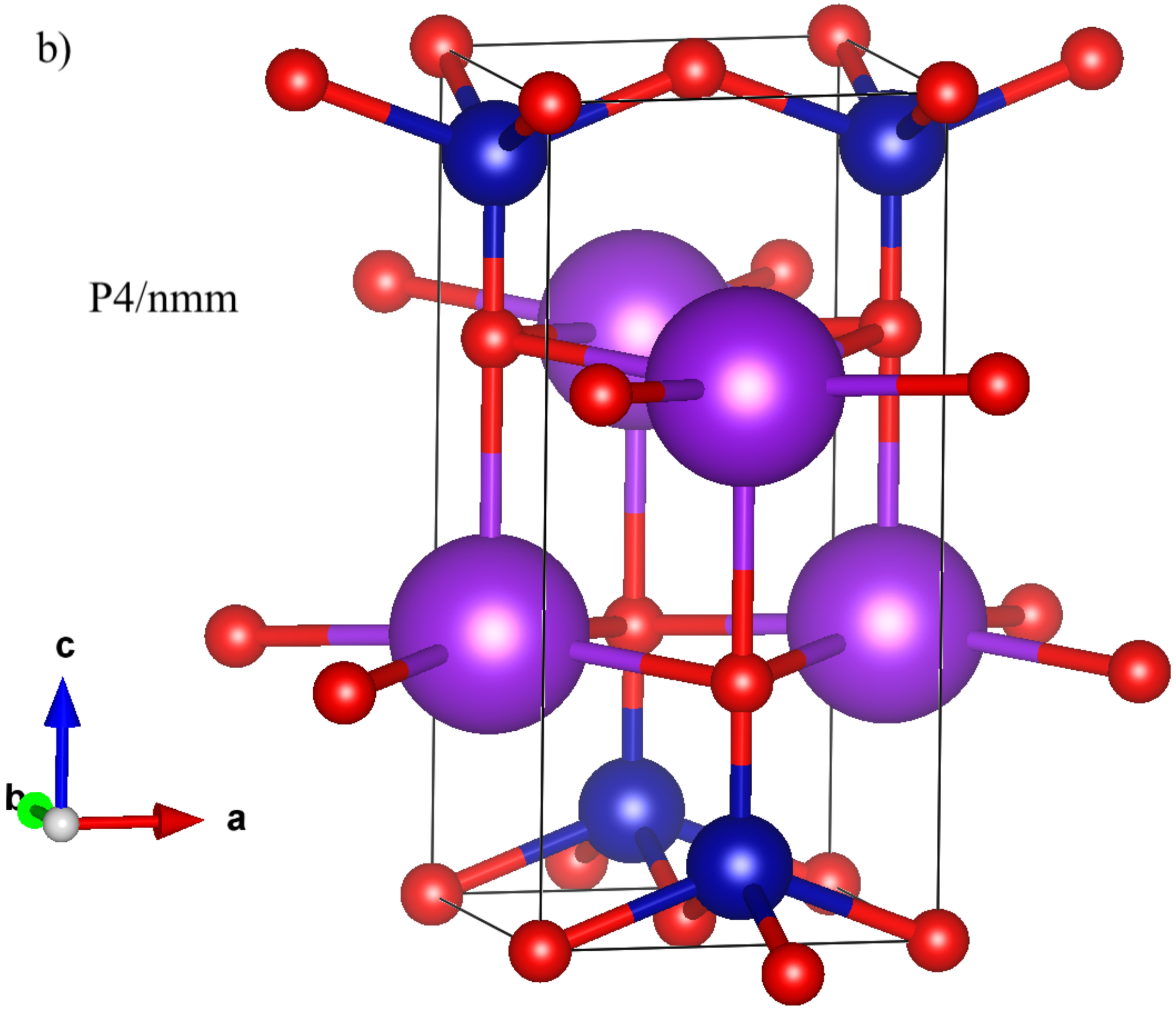

c)

I-4

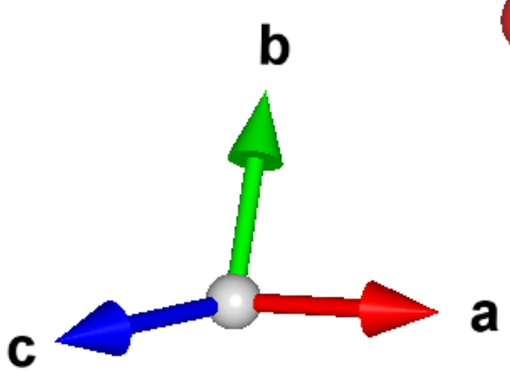

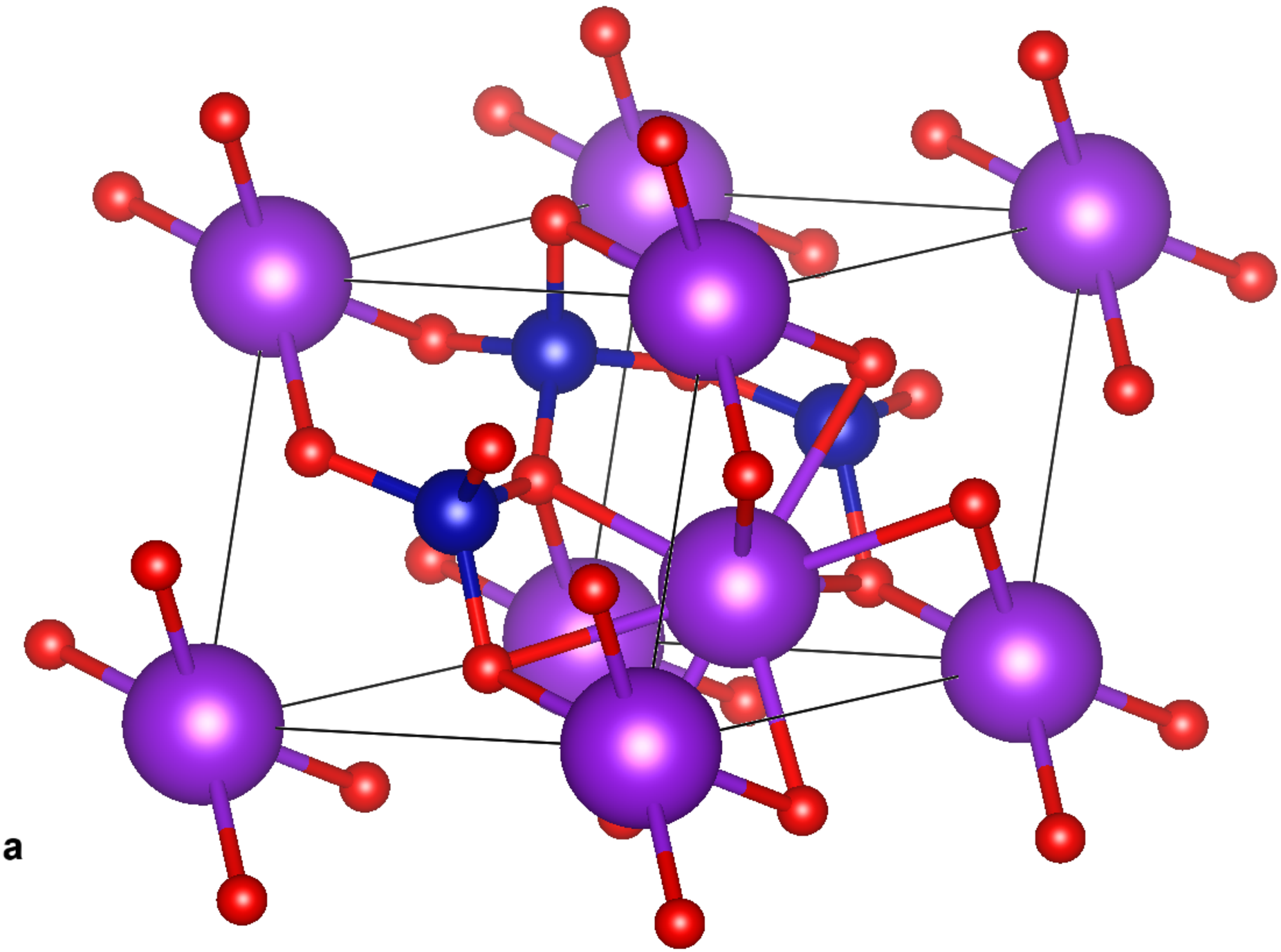

Journal of Applied Physics

AIP Publishing

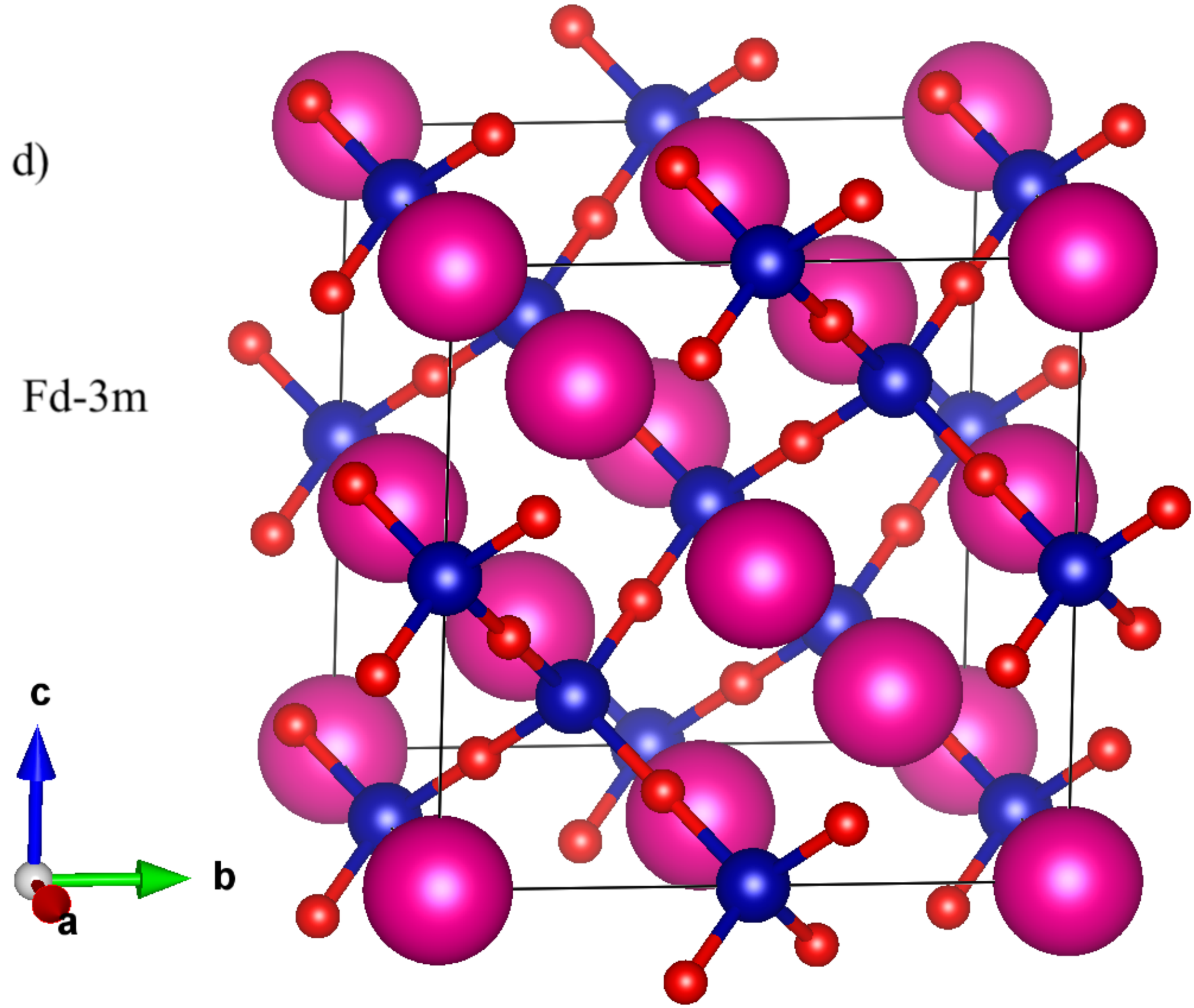

Journal of Applied Physics

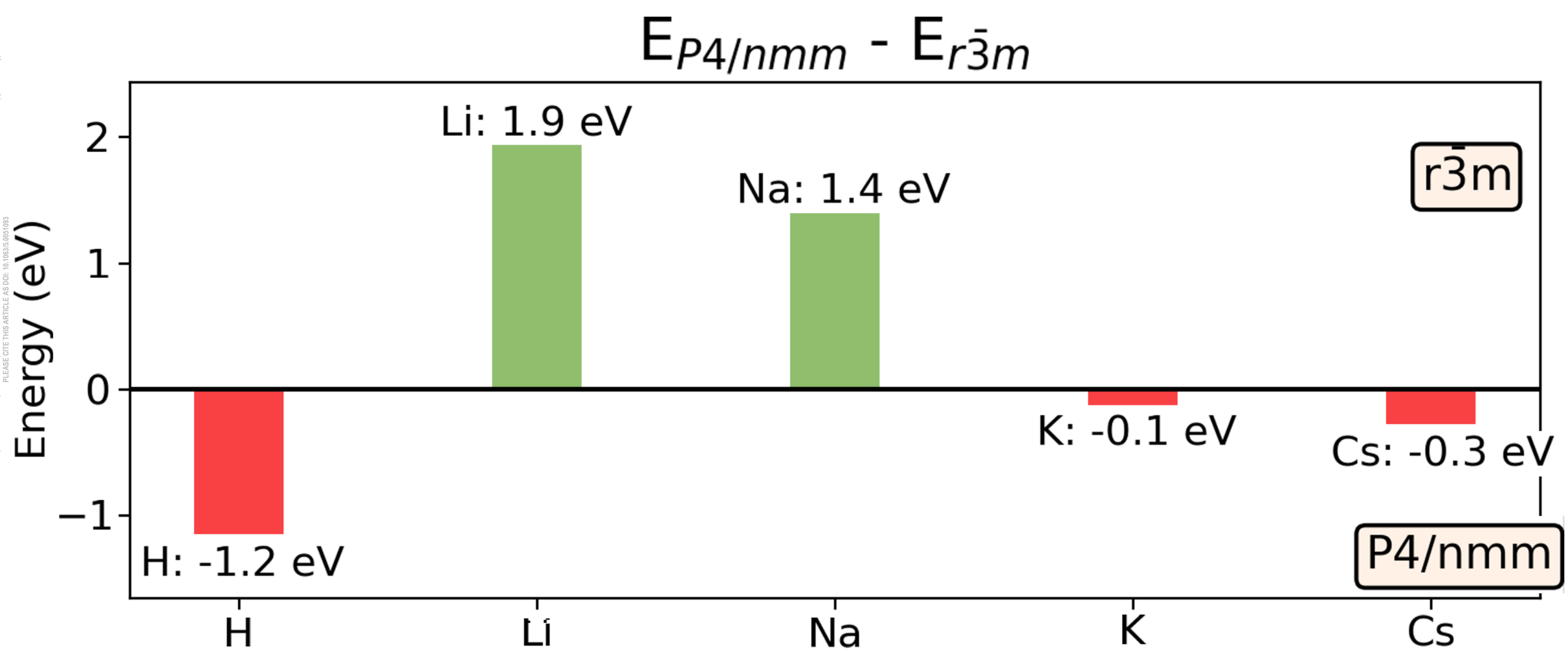

AIP Publishing

Journal of Applied Physics

ACCEPTED MANUSCRIPT

PLEASE CITE THIS ARTICLE AS DOI: 10.1063/5.0051093

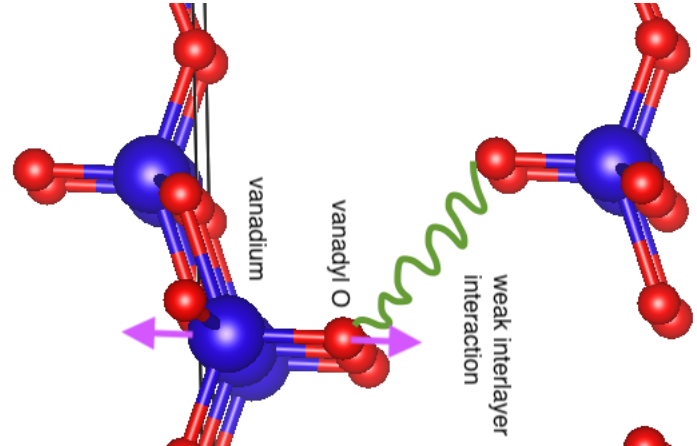

AIP Publishing

Journal of Applied Physics

ACCEPTED MANUSCRIPT

This is the author's peer reviewed, accepted manuscript. However, the online version of record will be different from this version once it has been copyedited and typeset.
PLEASE CITE THIS ARTICLE AS DOI: 10.1063/5.0051093

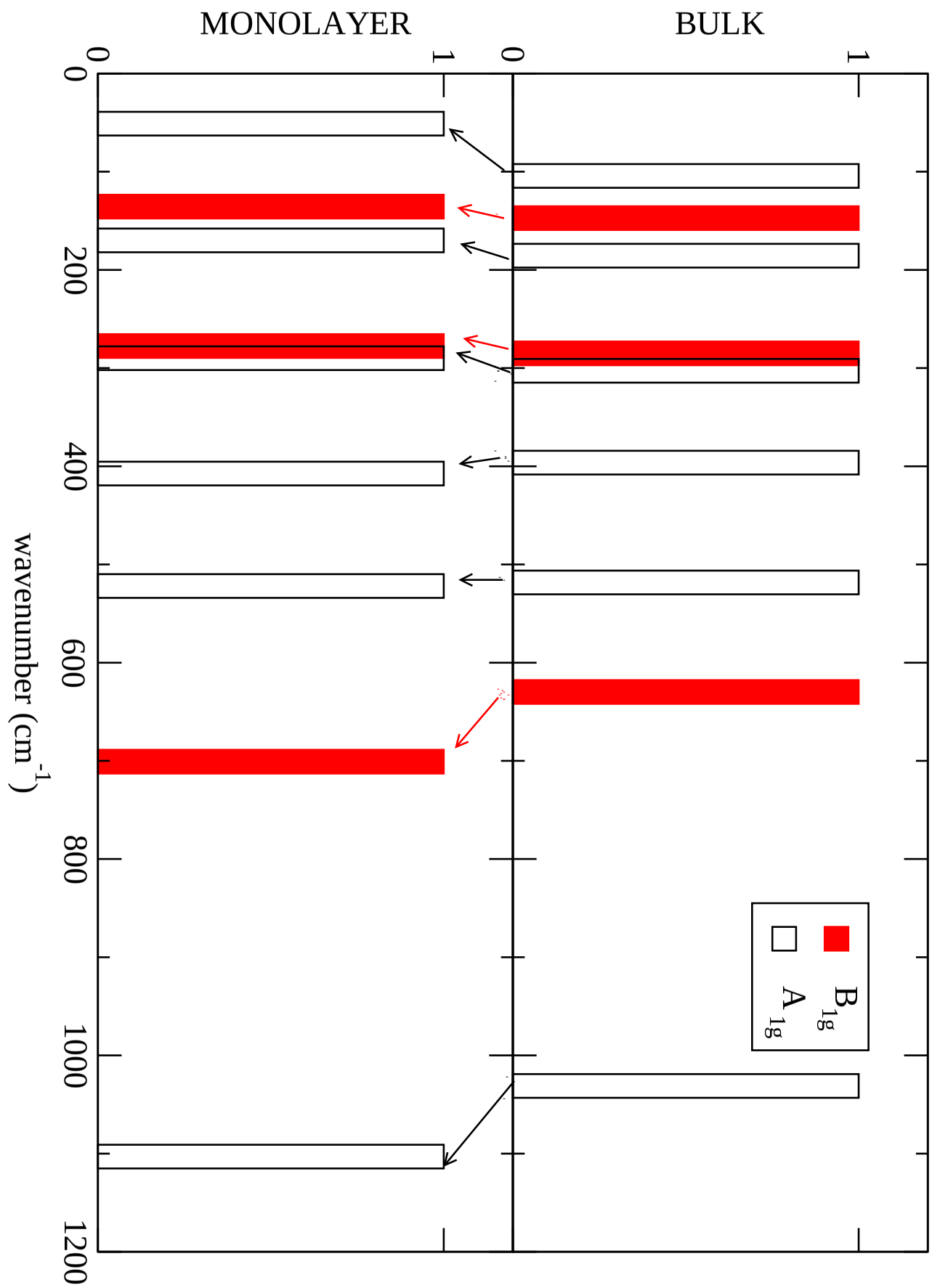

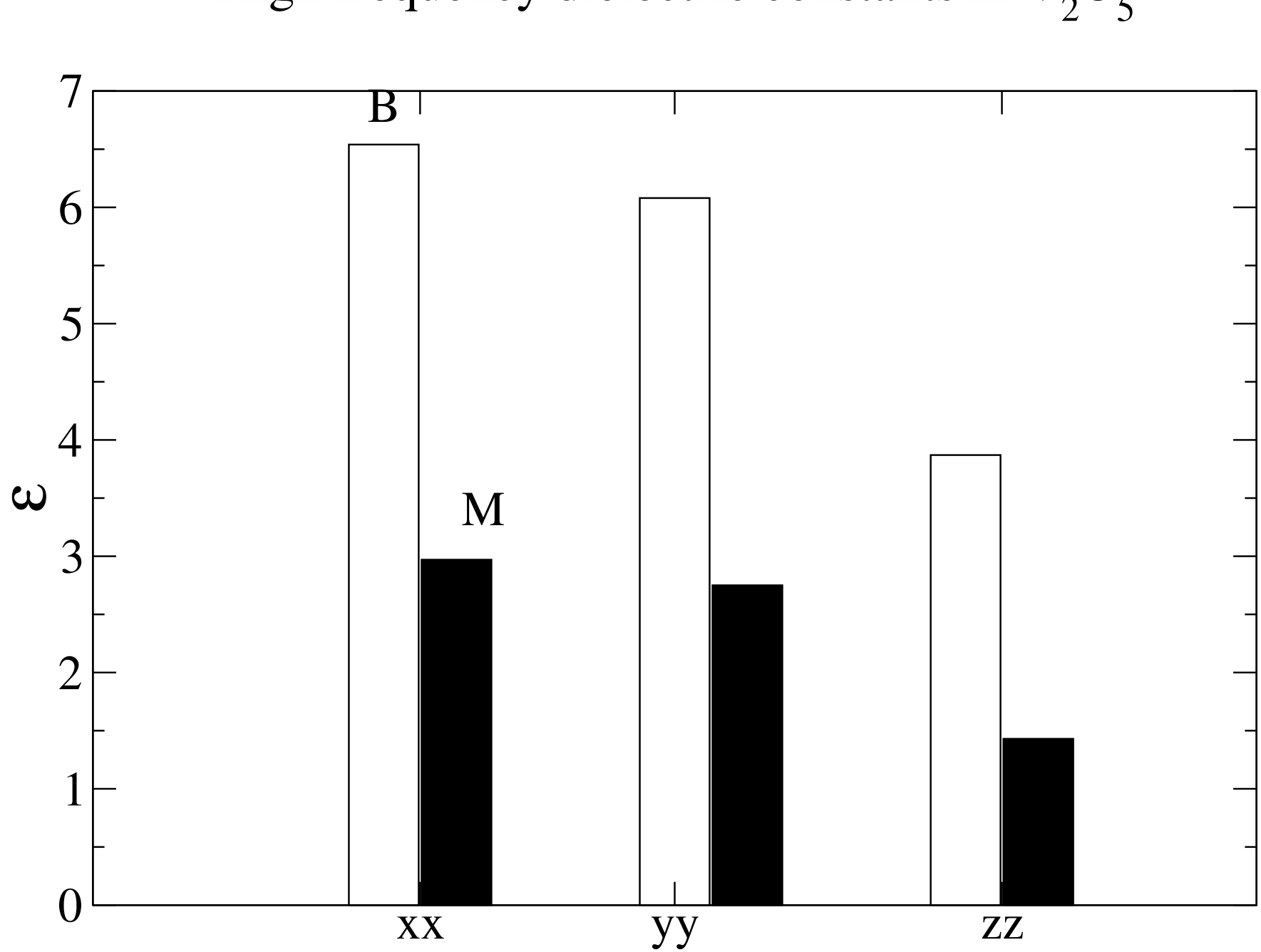

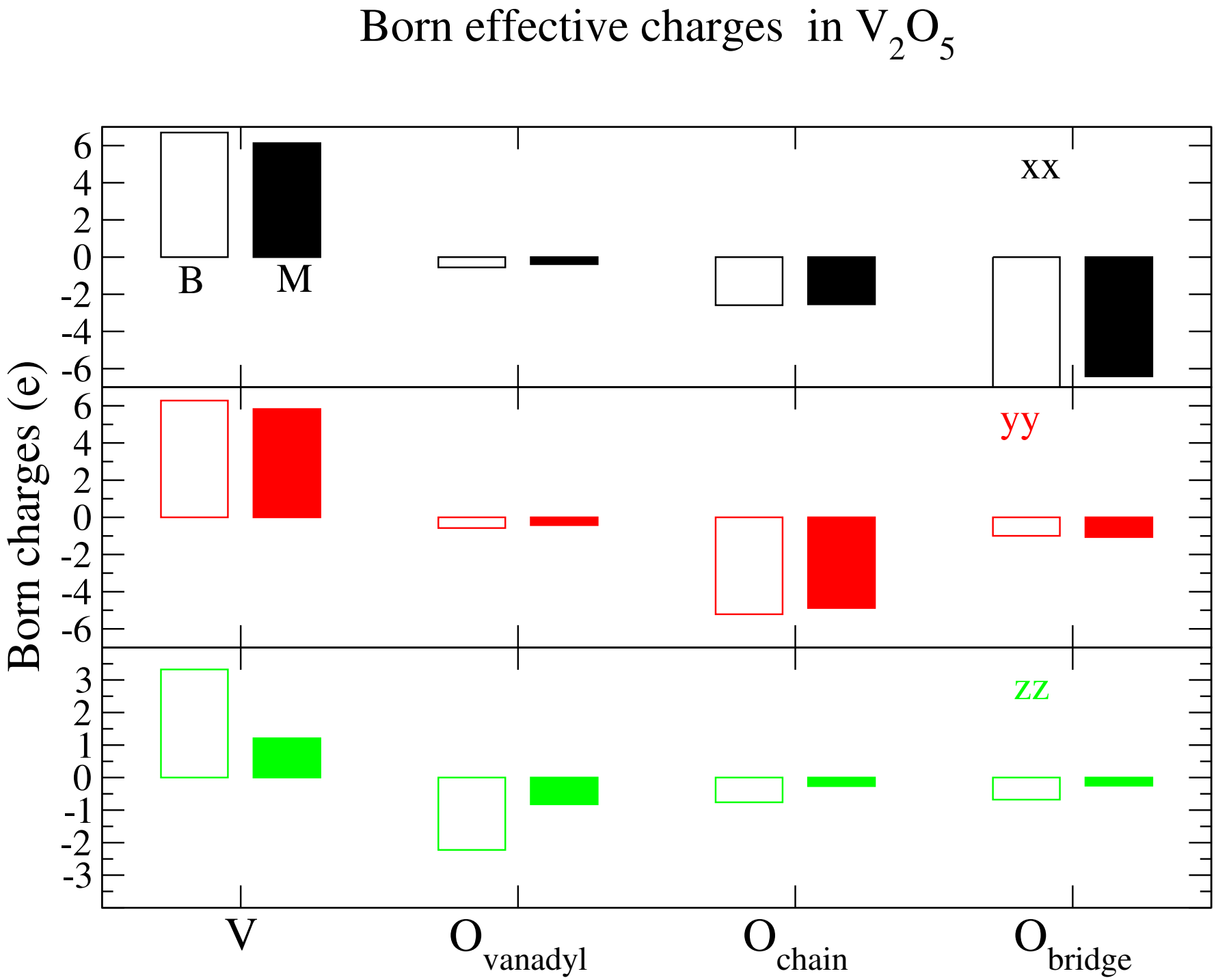

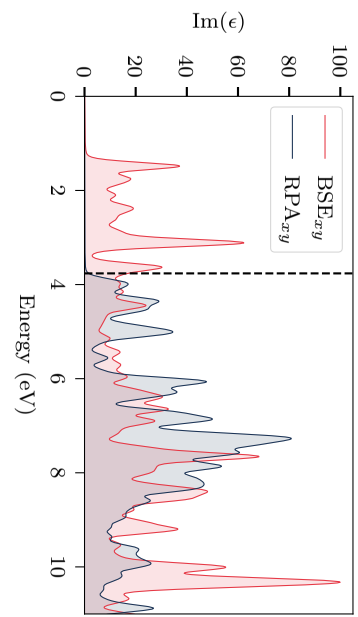

Journal of Applied Physics

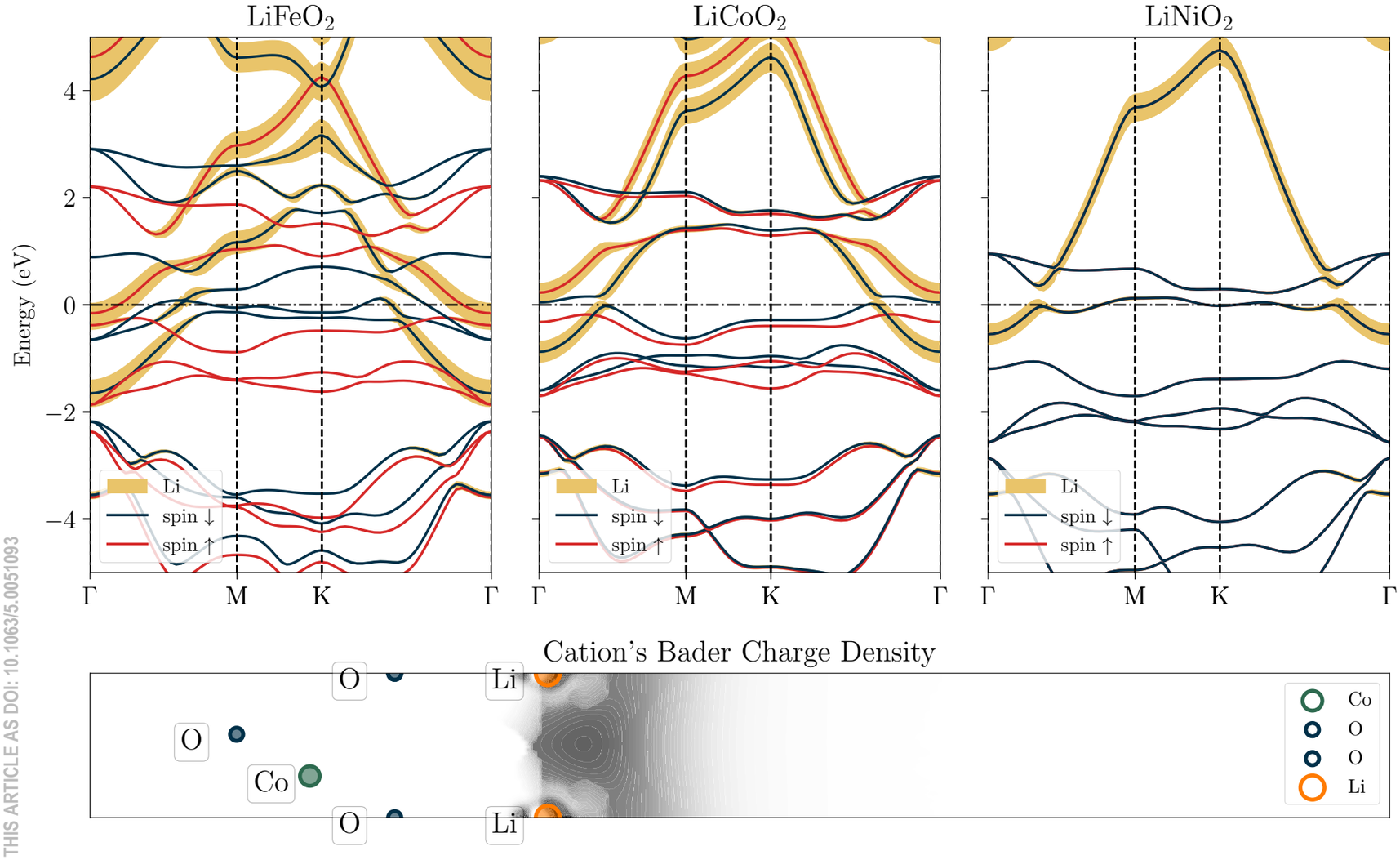

AIP Publishing

Journal of Applied Physics

ACCEPTED MANUSCRIPT

This is the author's peer reviewed, accepted manuscript. However, the online version of record will be different from this version once it has been copyedited and typeset.
PLEASE CITE THIS ARTICLE AS DOI: 10.1063/5.0051093

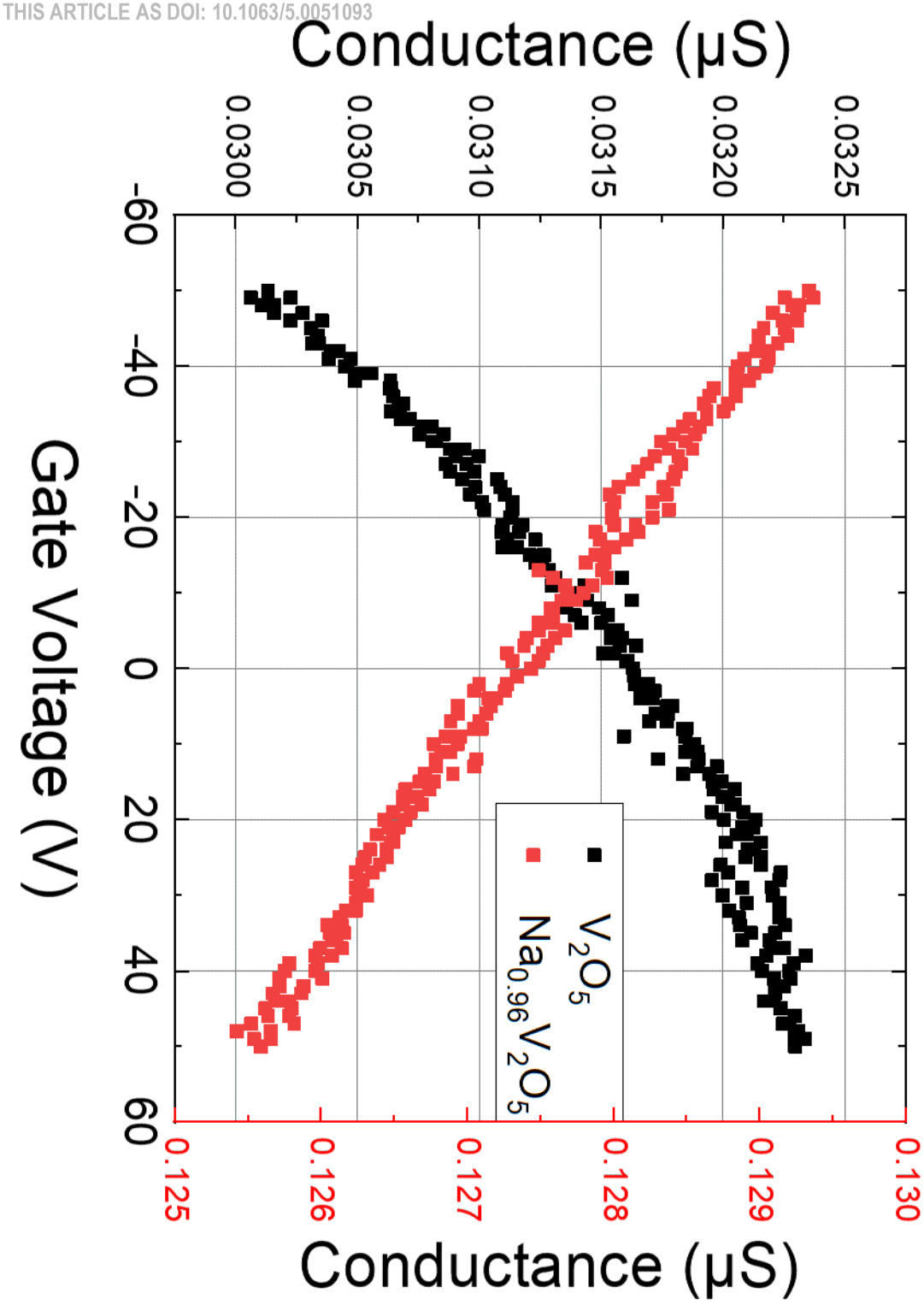

Journal of Applied Physics